Assessing the feasibility of the installation method of screwing for monopiles for offshore wind turbines

E. Jongkees

TU Delft

Huisman
Equipped for impact.

Assessing the feasibility of the installation method of screwing for monopiles for offshore wind turbines

By

E.P. Jongkees

Master Thesis

in partial fulfilment of the requirements for the degree of

Master of Science
in Mechanical Engineering

at the Department Maritime and Transport Technology of Faculty Mechanical, Maritime and Materials Engineering of Delft University of Technology
to be defended publicly on Wednesday July 5, 2023 at 15:00

Student number:	4237730	
MSc track:	Multi-Machine Engineering	
Report number:	2023.MME.8823	
Thesis committee:	Dr. ir. H. Polinder	TU Delft committee Chair, 3me
	Dr. J. Jovanova	TU Delft daily supervisor, 3me
	Dr. ir. G. Keetels	TU Delft committee member
	Ir. E. Romeijn	Company Supervisor, Huisman Equipment
Date:	July 5, 2023	

TU Delft

Preface

With this report I finish the master Multi-Machine Engineering of the faculty Mechanical Engineering and my time at the TU Delft. It has been a long road but finally we are here. The result is a thesis which is about an important and increasingly relevant subject; wind energy at sea. I hope it will be valuable for further research, even if the contribution might be small.

I would like to take this opportunity to express my gratitude to the supervisors from the TU Delft, Jovana Jovanova and Henk Polinder. Their guidance and support have brought me to this subject and helped me to finish the thesis.

I also want to express a special thanks to Eric Romeijn, who was the supervisor at Huisman Equipment. His never ending knowledge and experience helped me to find the research topic of the thesis and to fulfill it in the best way possible.

Lastly, I want to thanks my family and girlfriend for their support, not only during the graduation assignment, but also throughout the entire study time. In the end they all made this possible in the first place.

Eduard Jongkees

Leiden, July 2023

Abstract

The demand of offshore wind energy has increased enormously in the last decade, and continues to do so in the foreseeable future. The monopile will remain the most important foundation structure. There is however not yet a durable solution for its main disadvantage; the under water sound radiation during installation. In this report a new installation method is therefore explored: screwing monopile into the ground.

The proposed design is based on a actual wind turbine location at the coast of the Netherlands. Given these soil conditions which are obtained with a CPT, a model is build to approximate the resistance during installation. Then a model is developed to determine the soil-pile interaction including a screw thread. The outcome of this analysis is a design of the screw thread and driving requirements. The screw thread is build out of helicals, which are 0.6 m wide and 80 mm thick. They run from the bottom of the monopile, to 20 m from the bottom, with an angle of 15 degree. There are six helicals that run parallel of each other and have a vertical spacing of 1.68 m. Furthermore, the helicals have a slight bank angle of 20 degree, to prevent the soil around the monopile to disturb. The required tangential driving force is 500 MN at 6 m diameter, or 3000 MNm. In order to cope with the extreme forces, the monopile is redesigned such, that the upper part is minimal 10 m in diameter. The wall thickness is also changed to 80 mm over the entire length, since shock waves do not have to be taken into account anymore.

For the driving mechanism firstly is looked at the required driving power. This is a function of the endeavored driving time. With a driving power of 10 MW, the driving time is 1.3 hour, with 10 MW 1.1 hour and with 20 MW 0.9 h. For the connection between the ship and the monopile two types are proposed. The first type is the pile driver lead, which is a common type for onshore piling. With this type the driving equipment can be directly connected to the pile because they it follow the vertical displacement. It does however requires a massive structure at the ship, something that is not beneficial for the deck space. The second type is the gripper type. This uses a similar gripper as currently is common, and the driving equipment is placed directly on the gripper. To allow for freedom in the vertical direction, but still be able to deliver the torque, a spline with roller bearings is proposed. These splines can be welded directly onto the monopile, or onto a sleeve which is mounted over the monopile and connected to the flange. The (dis)advantages of both are obvious: the splines directly on the monopile avoid an extra tool and step in the installation process. They do require a monopile that has a upper diameter equal to the lower diameter since the driving equipment can not compensate for different diameters. With a sleeve the proposed monopile design can be used. It is however an extra step in the installation process and the tool requires valuable deck space.

To drive the monopile two main types are looked at: a geared rack and pinion type and driving with hydraulic cylinders. It turn out the the teeth of the rack and pinion are not strong enough to apply the required force if a double layer of gear assemblies all around the monopile is considered. The hydraulic cylinder however are able to apply the force. With a variable hydraulic system the speed can also be changed over the depth for a faster installation time. Lastly the reaction on the ship is considered, both for a DP-vessel and a jack-up vessel. The thrusters of the DP-vessel are not able to hold the ship in place. The jack-up vessel however, is able to cope with the extra forces on the legs.

Lastly, the implication on the logistics of the monopile are described. The helicals have an enormous impact on the efficiency of the manufacturing of the monopile, while that is one of the reasons that a monopile is comparatively cheap. Also conditions are stated for the support points during storage and transshipment. The support stands and pads in the upending must avoid the appendages, but there is enough space to do so.

Contents

List of Figures

List of Tables

List of Abbreviations

API	American petroleum institute
AR	Advance ratio
CPT	Cone penetration test
DP	Dynamic positioning
FBD	Free body diagram
GWEC	Global wind energy council
HKW	Hollandse kust west
IEA	International energy agency
OWT	Offshore wind turbine
RVO	Rijksdienst voor ondernemend Nederland
SDP	Screw displacement pile
SPMT	Self propelled modular transporter
TP	Transistion piece

1. Introduction

1.1 Problem description

Wind energy has become an ever-increasing market. Due to climate agreements, there is a growing demand for electricity produced by wind turbines. In table 1.1 it is shown that the worldwide wind power capacity will multiple in size the coming decades. Furthermore, it is expected by the global wind energy council (GWEC) that most wind power capacity will be installed in the second half of the decade [9]. Although these numbers are an estimation, the trend of an increase in installed wind power is obvious. Offshore wind energy has a large share in this increase. While at the moment responsible for no more than 13 per cent of the total wind energy capacity, it does see the biggest growth with a potential annual installation of 40 GW in 2030 according to the GWEC.

Year	2020		2021 - 2025		2026 - 2030	
	Cumulative	Commissioned	Cumulative expected	Commissioned expected	Cumulative expected	Commissioned expected
Onshore [GW]	708	87	1107	399	2107	1000
Offshore [GW]	35	6.1	105	70	270	165
Percentage offshore	4.7%	7%	9%	18%	13%	17%
Total [GW]	743	93	1212	4469	2377	1165

Table 1.1: Worldwide wind power capacity [9]

The international energy agency, IEA, estimates the technical potential of offshore wind power at 36.000 TWh per year for installations in water less than 60 m deep and within 60 km from shore [11]. These water depths and distances to shore are ideal for bottom fixed wind turbines, such as monopile based wind turbines. In fig. 1.1a the demand and potential of offshore wind energy per region is depicted while fig. 1.1b shows the offshore wind power capacity in 2018, and as planned for 2040. It is clear that particularly Europe and China have great ambitions for offshore wind power. Although China has less technical potential, they still are the country with the most planned wind energy. The big potential in Europe is mainly due to the North Sea. Therefore countries as England, Denmark, Germany and Norway are planning to build large wind farms in the coming decades, as can be seen in fig. 1.1c. This figure gives an overview of the current and planned wind farm sites.

Despite all the potential and plans however, exploiting offshore wind energy is a major challenge. The easy locations at sea were used at first, causing every next location to be more challenging to install offshore wind turbines (OWTs). The difficulty herein is mainly due to water depth, soil condition and the distance to shore, which make them economically less feasible to exploit. These challenges arise for example from difficulties with the ever growing weight and dimensions of the equipment and components, the logistics, sound production under water caused by pile driving and the connection to the main grid.

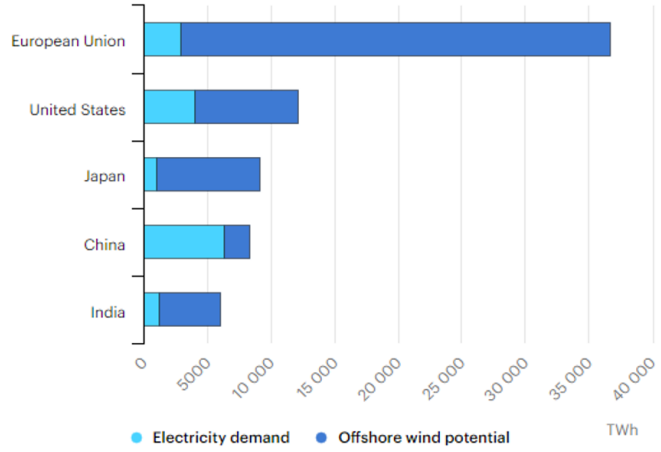

(a) Offshore electricity demand in 2018 and the technical potential [12]

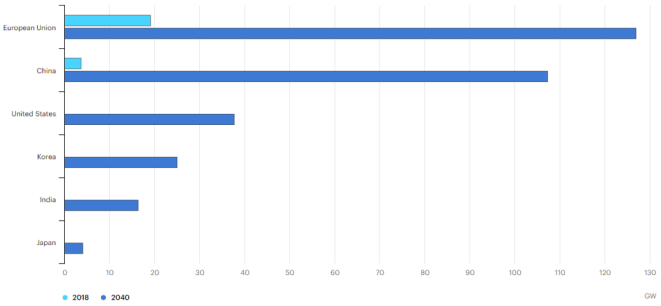

(b) Installed offshore wind capacity in 2018 and planned for 2040 [12]

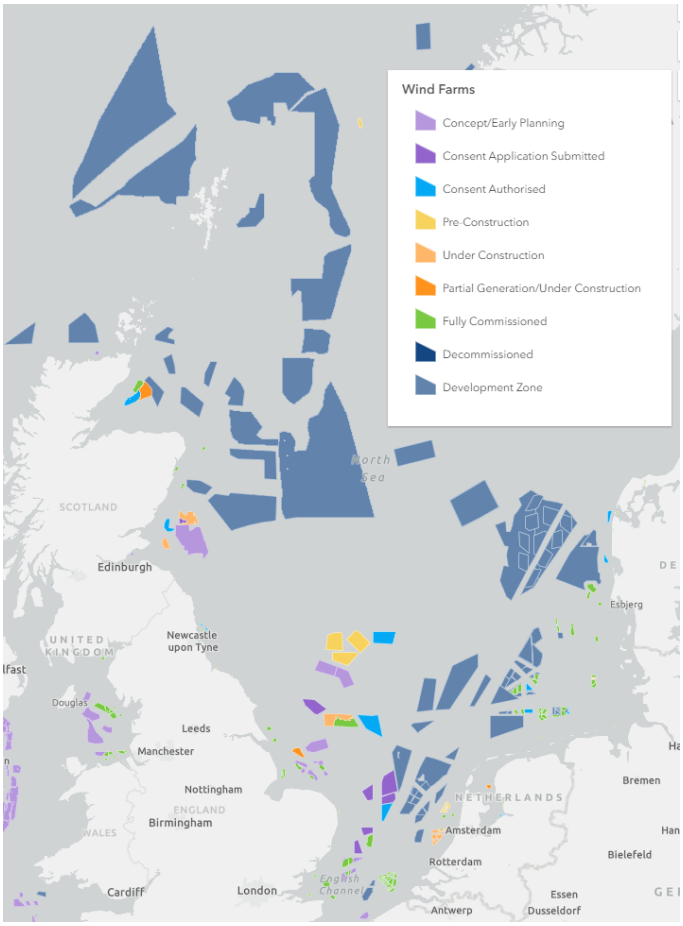

(c) Geographical overview of wind farms at the North Sea in different stages of development [13]

Figure 1.1: Future prospect for wind energy at sea

1.2 Research objective and questions

In industry one of the biggest foreseen challenges is the sound radiation under water caused by impact piling of the monopile. Legislation forbids exceeding certain sound levels. Currently sound mitigation measures have to be taken to stay under the sound limits. However, as monopiles become larger, the radiated sound levels increase as well. There is therefore a strive to develop low noise methods to install monopiles.

In this thesis we will discover the installation method of screwing monopiles into the ground.

In the search for a silent method to install monopiles, we find that screwing is a method which is not yet explored, but has great potential. We think so, because on smaller scale it is a widely used method for pile driving which avoids the vibration induced nuisance. We reckon that the same principles hold when this method is scaled up, even to the size of monopiles. As a result of the literature study we come to the following research objective and questions:

Assessing the feasibility of the installation method of screwing for monopiles for offshore wind turbines

To answer the objective, the following research questions are composed:

1 **How does the soil interact with the monopile?**

When a monopile is driven into the ground, the soil is affected by the wall of the monopile. To determine the resistance, and ultimately the force required to drive the pile, a model of the soil-pile interaction need to be set up.

2 **What should the design of the screw thread look like?**

The goal is to screw the monopile into the ground with a low risk of refusal and as fast as possible with the least amount of energy consumption. To achieve this, the screw thread, made out of helicals, should be designed to minimize the resistance, while providing enough downward force to drive the monopile into the sea bed. Secondary aspects to take into account are manufacturability and durability of the helicals. Subsequently, with an optimal screw thread design, the energy requirements can be determined which are needed for the design of the driving mechanism.

3 **What driving mechanism could be used?**

For applying the required torque, different driving mechanisms are examined. The monopile could be either driven by equipment on the pile, or by equipment fastened to the installation ship. Also there is a difference between jack-up vessels and dynamically positioned vessels. Both options are to be explored, and, based on the required torque, basis specifications are set up. From these specifications a design principle can be chosen.

4 **How does the modified monopile fit in the entire installation process?**

The helicals that form the screw thread are placed at the outside of the monopile. Since the monopile is frequently transported, from production to installation, it must be examined whether the helicals interfere with the production process as is common now.

1.3 Report structure

To answer the research questions, first an introduction is presented of the state of art of offshore wind turbine's, which also gives a scope in which the research is conducted. Then in the following chapters the research questions are discussed. Chapter 3 considers the interaction between the soil and the monopile, while chapter 4 expends this topic with the addition of the helicals. With the obtained information chapter 5 examines possibles driving mechanisms. Chapter 6 considers the implications that the helicals might have on the installation process. Finally in chapter 7 the research questions are concluded and a vision on the research objective and recommendations for further research are given.

2. State of the art

In this chapter a brief introduction is given into the offshore wind energy. First the general installation process is described. Then background information about noise and the impact on aquatic life is given. Lastly, the choice for the monopile is explained and the dimensions of the monopile as used in this research is presented.

2.1 Installation of offshore wind turbines

To give an idea of how this research fits into the real world, an introduction of the installation process of offshore wind farms at a high level is presented in this section. Before a wind farm can be exploited, the following steps must have been taken:

- Determining the location
- Manufacturing of components
- Transportation to location
- Installing foundations
- Installing OWT
- Installing the transformer station
- Laying the cable array
- Connection to the main grid
- Testing and commissioning
- Essential maintenance

It must be noted that the above numeration is very brief and only addressing the technical steps. In reality an extensive political, economical, administrative and commercial process precedes the actual commissioning. This varies from political points of view with respect to the energy mix, the national and international energy need, the decision making and execution, to the interest of commercial parties willing to participate in related projects. This process can take up to several years before the actual building takes place.

Location determining Based on political and geological interests, locations for wind farms are determined. The first wind farms were located where the ground conditions were optimal and the distance to shore the smallest. This has the implication that every newer location is becoming more challenging to build. The main reason for this is the increasing water depth and the more difficult soil to pile in. Furthermore, although space at sea seems fairly unlimited, every area has its own designated destination plan. Certain areas are designated for e.g. nature, fishing, anchoring or shipping lanes. It is therefore a challenge to fit wind farms while minding other destinations and interests as well.

Production, transport and installation Due to the sheer size, the production of the foundation and wind turbine parts takes place at locations accessible by large ships. First the foundations, in this case the monopiles, are transported to the designated wind farm location. For monopile foundations, dedicated ships are designed for both the transport and installation. Three types of ships can be used: jack-up, moored and dynamic positioned vessels. Jack-up vessels provide a rigid platform to work from. The main advantage is that the positioning of the monopiles is easily controlled, as a result of which, a fixed pile gripper frame can by used as can been seen in fig. 2.1. Moored and dynamically

positioned ships need a motion compensating pile gripper frame because they vary slightly in their position during operation.

Before the installation, a layer of scour protection is added to the seabed. By dumping rocks erosion around the foundation is prevented. The installation of the monopiles generally follows the same steps regardless of the vessel and pile driving type. The monopile has been transported horizontally and has to be up-ended first. This is done by lifting the top side of the monopile while letting the bottom side rest on the up-ending tool. The pile is lifted using a lifting tool. This tool clamps the upper side of the pile and can be removed again in a later stage. In fig. 2.1a an installation ship is shown on which a monopile is resting in the up-ending tool. After up-ending, the monopile fully hangs on the crane and is lowered into the gripper frame and onto the seabed, as is shown in fig. 2.1b. Depending on the local conditions, the pile sinks about 1 m into the soil due to its own weight after it hits the sea bed. Due to the small footprint relative to the seabed the frame needs to keep the pile perfectly upright, to guarantee a perfect installation. As described above, for a jack-up vessel this can be done by a fixed pile gripper frame. It is also mainly for this reason that the weather window in which the operation can take place is limited. This limitation is even bigger with moored or dynamic positioned vessels. The main advantage of those however, is that no costly time is consumed for jacking the vessel up or installing the mooring lines, which can take up to 4 hours for a jack-up vessel.

(a) Typical lay out of an installation ship. One monopile is resting in the up-end tool. The yellow transition pieces are standing on the deck.

(b) A fully jacked-up installation ship. The monopile is seen just before it gets lowered into the fixed pile gripper frame

Figure 2.1: A jack-up vessel for installation of monopiles and transition pieces with a fixed pile gripper frame [1]

The next step is to drive the monopile into the ground. This is also the step which is focused on in this thesis. For the pile driving, the lifting tool is changed for the pile driving machine, while the gripper keeps the monopile in place. An impact hammer is the most common method for pile driving. Other methods are vibratory driving or drilling. Generally, it takes in the ordes of four hours to drive the pile into the ground, depending on the dimensions and soil conditions. In most operations a noise mitigation system will be used to mitigate the sound. The so called bubble curtain is the most common method to achieve this. After the piling the transition piece (TP) is placed over the monopile. It is fixed to the monopile because the top of the monopile and the inner side of the TP are slightly tapered, ensuring a tight, frictional fit. Furthermore, it is secured to the monopile by bolting and using grout, which is a material very similar to concrete. The TP's function is to link the wind turbine to the foundation, for connection of the electricity cables and to provide a platform for servicing. Also, the TP is used to correct any misalignment of the pile. In practice a maximum tilt angle of 0.25° for the OWT is used as a limit. With a TP, a misalignment can be corrected within certain limits [14]. The maximum tilt angle of 0.25° originates from limits of the equipment of the turbines themselves, and is since kept in place

as a standard. It can be noted that a tilt angle more than 0.5° can be seen with the naked eye. At this stage the activities for the installation ship are done for this particular monopile. The procedure for the entire field is follows the same steps. In the next stage another ship will install the wind turbine components.

The turbine components compose of the tower, nacelle, hub and blades. There are three major manufacturers of OWTs; General Electric, Siemens and Vestas. Currently the largest turbine presented is the Vestas V236-15MW. It has an output of 15 MW and will be expected to be produced in 2024. It has a rotor diameter of 236 m with 115 m blades weighing 35 tons each, a 135 m tower weighing 860 tons, and a nacelle weighing 600 tons at a height of 150 m. Although this is the most powerful turbine yet presented, the dimensions are in the same order of magnitude as the other manufacturers models. It is not straightforward to scale the dimensions up. It comes with several drawbacks as for example larger blade tip deflection, which makes it harder to keep the required distance between the tower and the blades. Also it will create challenges for manufacturing, transportation and installation. The height of the rotor hub also needs to increase with longer blades. Furthermore the increase of both the weight and height of the nacelle will push the cranes to the limit. Despite these challenges current market developments indicate that the OWT's power rating will increase to 20 MW at the end of this decade [15].

Commissioning After installing the OWTs a substation is placed near the wind farm. This substation connects all OWTs via a cable array and transforms the voltage such that it can be transported to the mainland efficiently. In fig. 2.2a a schematic overview is given of the route the electricity takes from the OWT to the mainland. The cable array is laid by a separate ship. This part of the process turns out the be rather challenging. It has been said that although the cable array installation is roughly 10% of the total costs, it accounts for 80% of the unforeseen costs. The reason is that the cables are vulnerable and sensitive to damages. fig. 2.2b shows what a cable array actually looks like, in this case at the Borssele wind farm. Prior to commissioning several tests are carried out to ensure proper functionality of all systems. These systems are, among others, the function of power generating itself, the connection to the grid and communication systems [16].

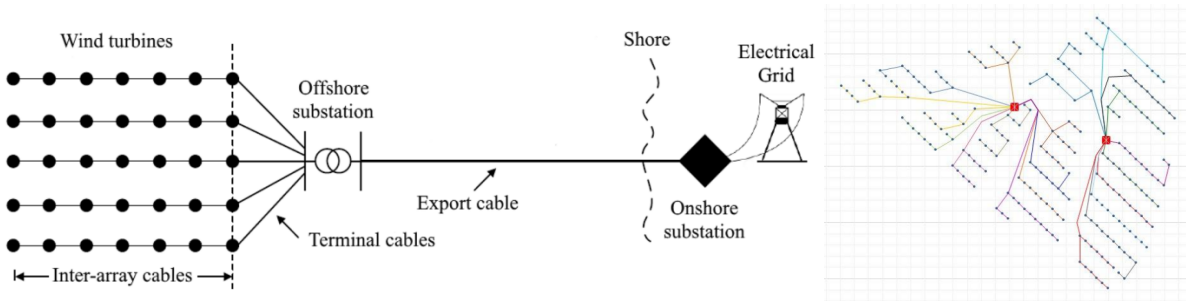

(a) Schematic overview of a cable array and connection to the mainland [17]

(b) Actual cable array of the Borssele wind farm. The black dots are OWTs and the red dots are the substations [18]

Figure 2.2: Overview of the connection between OWTs and the mainland

2.2 Sound

Sound is a form of energy that propagates through a medium by waves [19]. Sound waves can differ in frequency, wavelength and intensity. The absolute sound wave strength is defined by intensity. In

practice a logarithmic scale is used for the convenience of capturing the wide range of intensity levels. For the logarithmic scale, the unit decibel [dB] is used. The decibel scale indicates the ratio between the measured value and a reference value [20]. Noise is considered as an unwanted sound. Generally with noise, ambient background sound is meant. Ambient background noise can be caused by for example waves and distant ships. For impact piling 'sound' is used to make the distinction between the offshore activities and unrelated background noises.

There are multiple definitions to describe sound. Decibel (dB) is a relative scale and must therefore be referenced to a reference pressure. Note that in air and water different reference pressures are used, dB re 20 µPa and dB re 1 µPa respectively.

The sound pressure level (SPL) is given by the standard equation

$$SPL = 20log_{10}(P_{rms}/P_0) \tag{2.1}$$

where P_0 is the preference pressure of 1 µPa for underwater acoustics, and P_{rms} is the sound pressure in µPa, and is expressed as the root mean square pressure

$$P_{rms} = \sqrt{\frac{1}{T_0}\int_{t_0}^{t_1} p(t)^2 dt} \tag{2.2}$$

The SPL is therefore given in units of dB re 1 µPa [21]. Note that the SPL is sometimes described with the squared power inside the logarithm and the multiplier 10 rather than 20 and units dB re 1 µPa^2 [22]. The SPL does not account for inconsistent sound levels. For the description of sound over a longer period of time the equivalent continuous sound level L_{eq} is better suited. The L_{eq} gives the sound level of a steady-state sound that has the same total energy as the time-varying sound and is given by

$$L_{eq}(T) = SEL + 10log(N/T) \tag{2.3}$$

where T is the time period in seconds, SEL is the sound exposure level as described in 2.4 and N is the number of events during the time period, thus in this case the number of hammer blows [23]. The sound exposure level (SEL) is the acoustic pressure during a time period

$$SEL = 20log_{10}(E/E_0) \tag{2.4}$$

where E_0 is the reference sound exposure and E is the sound exposure expressed as

$$E = \int_{t_0}^{t_1} p(t)^2 dt \tag{2.5}$$

where t_0 and t_1 indicate the time interval and $p(t)$ is the measured pressure. The SEL is a measure that averages the sound intensity and is widely used in legislation.

For approximating the SEL at an arbitrary distance from the piling activities several numerical models have been developed which have very similar predictions for simplified cases [24]. However, while numerical models are efficient for complex problems, they are computationally slow for vibroacoustic situations. Therefore analytical and empirical approximations are also widely used since they offer considerable insight into the system [25]. A common approximation for the SEL with a point source is

$$SEL(r) = SEL(r_1) - 15log_{10}(r/r_1) \tag{2.6}$$

where $SEL(r)$ is the SEL at an arbitrary distance from the source in dB and $SEL(r_1)$ is the known SEL at a distance r_1 from the source. With eq. (2.6) an approximation can be made for the SEL when

only $SEL(r_1)$ is known. Some authorities use this approximation to evaluate the impact of pile driving on the environment [26]. A disadvantage of this method is that the approximation assumes a point source, while the noise source from piling activities covers the entire length of the pile. Therefore the damped cylindrical spreading decay formula

$$SEL(r) = SEL(r_1) - 10log_{10}(r/r_1) - \alpha(r - r_1) \tag{2.7}$$

is proposed, where r_1 is the reference distance and α the decay factor in decibels per meter [27]. The decay factor is

$$\alpha = \frac{-10log_{10}(|R|^2)}{2Hcotan(\theta) + \Delta l} \tag{2.8}$$

where R is the reflection factor between water and sea bottom, H the depth of the water and θ the angle of the radiated Mach cone. eq. (2.7) is applicable when moderate wave heights can be assumed, and therefore perfect reflection. In this case, energy is only lost through the bottom interaction [28]. For eq. (2.8) the assumption is made that for the relatively low frequencies emitted from piling, namely below 2kHz with the main energy content around 400Hz, the decay factor can be considered as frequency independent.

Sound therefore, can be interpreted in different ways, depending on the definition and the perception. It is not only depending on the pressure and amplitude, but also on the frequency and duration of the vibrations. Although the principle of sound is rather well understood, it is still difficult to give an accurate estimation of the sound radiation at off shore activities. Not only the driving methods, but also the water depth, soil conditions and the characteristics of the surface waves influence the sound propagation. Of all driving methods, impact piling can be modelled the most accurate, since it is a short energy pulse. Vibratory piling however, creates a continuous source of sound with a wider range of frequencies which result in less precise predictions. It is however evident that the peak sound levels created by vibratory piling are much lower compared with those created by impact piling.

2.3 Impact on aquatic life and legislation

Impact on aquatic life It is well known that underwater noise has an impact on aquatic life [29–31]. Every animal has its own frequencies for which it is susceptible to noise pollution. Whales for example are most sensitive for frequencies below 10 kHz, with some even below 100 Hz [19]. Dolphins and porpoises have sensitive hearing above 500 Hz [32]. Also, the frequencies below 10 kHz tend to travel farther in water and therefore have a larger impact on sea life [33]. Since the 1950s reports conclude that offshore shipping has raised the background noise with 10 to 16 dB. It is found that noise produced by offshore operations are mainly below 1000 Hz [34].

Anthropogenic sound from ships, sonar, dredging, piling and other offshore activities has increased dramatically in the last century. This noise pollution impacts sea life in multiple ways, such as changing individual and social behaviour, communication, reproduction. Noise pollution is therefore also a threat to the entire ecosystem rather than only individual species [35, 36].

Auditory masking is one of the main effects of noise pollution on marine animals. It occurs when the perception of a sound is distorted by background noise [37]. Anthropogenic noise can constrain communication between marine animals. It is found that noise can cause fish to swim fast to the bottom of the water in groups and increase their alarms responses. Furthermore fish can show avoidance behaviour because of underwater sound, possibly leading to failing reproduction and thus decreasing population of certain species. For example the occurrence of harbor porpoises and dolphins declined after the commencement of the installation of OWTs [38].

Methodologically it is found very challenging to assess the influence the construction of a wind farm has on the marine life. The volumes around the pile activities are so vast that it is practically impossible to obtain very accurate facts of the numbers and behaviour of marine life. Furthermore, the pile-driving noise is just one of the many anthropological sounds in the water, especially during pile driving itself. It is known that propellers, mainly the relatively small propellers of azimuth thrusters with which installations ships are equipped, account for a significant portion of underwater noise. This already present background noise makes it difficult to draw hard conclusions on the influence of pile driving alone. Nevertheless, it is clear that offshore activities, and especially pile driving, has a huge impact on sea life around the wind farms [39].

Noise also makes some marine species more vulnerable to predation because they are distracted. Experiments have shown that, for example, crabs allowed their predator to approach closer before fleeing than in the case without ship noise playback [40]. Other research has conducted that harbour seals are very susceptible to very low received sound levels. They use this ability to distinguish between different kinds of killer whales, depending on whether they pose a threat or not. Acoustic masking can cause disturbance in these observations and thus have a major influence on the behaviour of the animals, ultimately leading to influences on the survival rate of certain animals [41].

Legislation Based on the Marine Strategy Framework Directive, European member states are free to determine their legislation considering underwater noise [42]. The result is that countries have slightly different regulations and boundaries. In the Dutch waters, noise is seasonal bounded. In this case the harbor porpoise is taken as a reference since it appears to be the most sensitive to noise. From January till May, when more porpoises live in the North Sea, legislation dictates that a limited amount of pile can be installed [43]. In German and Belgian waters, however, an absolute maximum of 160 SEL at 750 m distance from the pile driving activities [44]. In the industry, the limit of 160 SEL at 750 m is considered as the general limit that they must be able to reach.

Since the legislation differs per country, the abidance is different as well. Directives are put out to describe how to cope with underwater noise [45]. Common is that operators should take into account the presence of marine mammals during the piling activities. Marine mammal observers can be present during offshore activities to ensure the following of the mitigation measures. They will look out for the use of bubble curtains and the presence of marine mammals. They can also oversee the measurement of underwater sound according to the mitigation zone. Furthermore, marine mammal observers can give advice about midnight piling activities, as there is a greater risk of failing to detect the presence of marine life.

Anthropogenic sound is widely common in the sea water since decades. The installation of OWT's however, causes an extreme rises of the under water sound. To cope with this, governments introduced legislation to limit the sound levels. The legislation differs per country, but a widely used limit is 160 SEL at 750 m.

2.4 Foundations

Since easier parts of the shallow waters were exploited at first, there is a growing market for deeper locations at sea. Floating OWTs could be a solution for this. At this time, however, floating OWTs are still in the experimental phase and conceptionally not relevant for this survey. Therefore we will focus on bottom fixed foundations, which are feasible for depths up to 60 m. In 2019 70% of all foundations were monopiles and 29% were jackets [46]. Up to date, monopiles remain the most used installation method with 81%, jackets remain the second most with 9%, while gravity-based and tripods are accountable for

10%. Therefore this research will focus on monopiles.

The monopile foundation is the most used in the current market. This is mainly because it is a relatively simple product and it is cheap in production and installation. Numbers vary depending on definitions and boundaries, but generally, the cost of the assembly and installation of a monopiles is in the order of 20% of the total cost [47]. The production takes place in several steps. Steel slabs are rolled according to the desired diameter after which the ends are welded together to form a ring. Then subsequent rings are welded together to form essentially a large, hollow tube, which is the monopile. These production steps are shown in fig. 2.3.

Figure 2.3: Overview of a monopile production process. At first slabs of a specified thickness are rolled into a ring. Then multiple rings are welded together to create the monopile [2–4]

Monopiles have grown spectacularly in size in the last decade and will become even larger in the future. It is expected that they will grow up to a length of 120 m, a diameter of 12 m and 2.500 tons in the short term, and even 130 m by 15 m and 3.500 tons at the end of the decade [48]. In fig. 2.4e a schematic cross-section of a typical monopile is shown. The upper half of the pile is tapered with a wider bottom than the top, and it varies in thickness along its length. It should be noted that even within one wind farm the dimensions vary, depending on the conditions such as the soil and water depth. In this research, we will take the monopile as shown in fig. 2.4e as a basis for the calculations. The typical piling depth of a monopile is, again depending on the size, in the range of 20 to 50 m.

Since there is a continuous strive to develop more economically efficient wind farms, the turbines are increasing in power output. This results in heavier blades, nacelles and towers, which in return necessitates bigger monopiles as well. As said, it is therefore expected that monopiles will reach weights of even 3.500 tons at the end of this decade. Weight reduction is thus one of the main topics in monopile design. This can be done by either using high strength steel or increasing the ratio between diameter and thickness, resulting in more slender monopiles. However, high strength steel is expensive and

nullifies the the main advantage of monopiles; its low cost. Thinner walls do have as a consequence, that insufficient support points can damage the monopile, since local bending and hoop stresses increase with thinner walls. Especially during transshipment this can cause damages [49]. Furthermore, extra thickness is required to cope with the shock waves that travel through the monopile by the impact hammer. In this research we will initially consider a simplified, large monopile. In fig. 2.4e the dimensions of this monopile are shown. These dimensions are based on monopile that are actually manufactured. For simplification the the wall thickness variations are kept to a minimum. In reality a monopile has many small differences in the wall thickness over the length. fig. 2.4a to fig. 2.4d show multiple monopiles in storage, transshipment and transport.

Although more and more research is done for different foundation methods, monopiles still are the main foundation type for OWT's, and are expected to remain so in the next decades. They will however increase significantly in size, up to 130 m by 15 m and 3.500 tons. This size increase creates issues with respect to the manufacturing, handling and installation. From this follows the necessity for further research into advanced installation methods for monopiles.

(a) Production site of monopiles and transition pieces at SIF on the Maasvlakte [3]

(b) Monopiles rolled out on SPMT's [49]

(c) Monopile loaded onto support points [50]

(d) Monopiles loaded longitudinally on a transport vessel. [51]

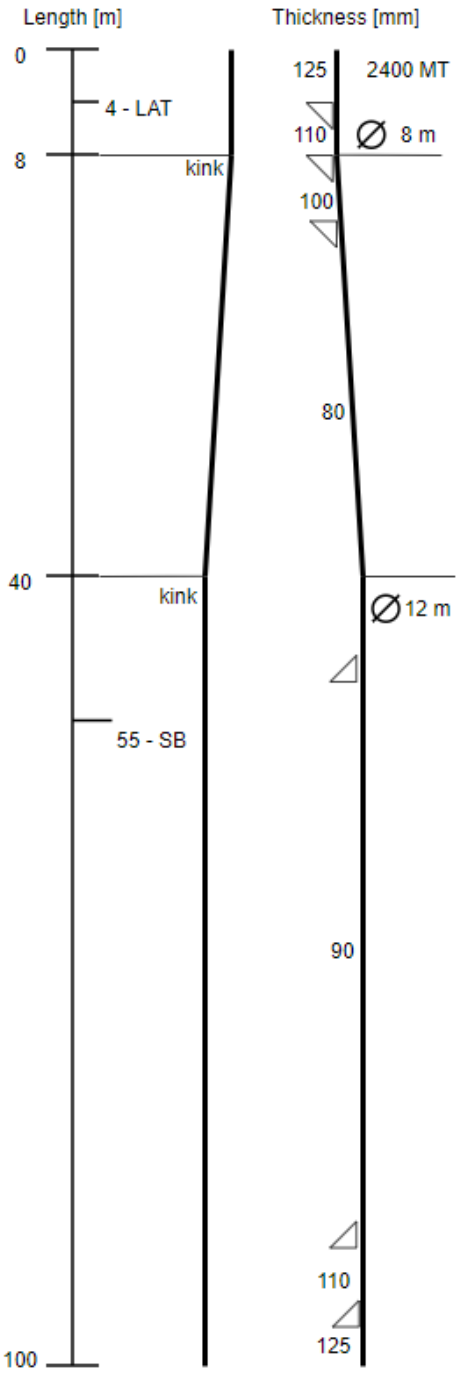

(e) Typical dimensions of a monopile as recently installed on the North Sea.

Figure 2.4: Indication of dimensions of monopiles

2.5 Conclusion

It is evident that there will be more and more demand for wind energy at sea; governments have repeatedly made there plans even more ambitious. These increased ambitions push manufacturers to produce larger wind turbines, with the result that the foundations need to become larger as well. The monopile is the type foundation currently used the most. It is namely relatively cheap and robust, and the industry has good experience with it. Their design however is also quite inefficient for handling the load of the wind turbines. This means that they become extremely large and heavy, expected even up to 3.600 tons. A consequence of this increase in size, is that with the currently most used installation method, namely impact piling, the radiated sound also increases such, that the sound limits will be exceeded. However, the monopile is also the foundation type that has a lot of potential for the wind farms that are being planned, due to their geological environments. It is therefore essential to keep the noise levels as low as possible.

To keep the noise levels under the legislation limits, noise suppression methods are being used. However, with the growing size of the monopiles, noise suppression alone is not enough. As a method, vibratory driving is used to prevent exceeding the noise limits. The downside is that it is also a method with a large probability of refusals. One principle that is not yet been utilized in the off shore industry is torque driven pile driving. However, screwing piles for the foundations of small buildings is a common technique. In place where limited vibrations are allowed, screw driven piles good be a solution. This technique however, only exists for small dimensions, with diameter less than 0.5 m. The main advantage of the method is that it is relatively silent, but still has great penetration ability. This is therefore also the technique we will examine in this research, by means of answering the research questions as stated in section 1.2.

3. Soil-monopile interaction

What is the interaction of the monopile and the soil?

In this chapter the interaction between the pile and the soil is discussed. The theory regarding the soil-pile interaction is extensively described in literature. However, it is a fuzzy science due to the uncertainty of the soil conditions and mostly empirical theories. This chapter therefore provides a theory which is the basis of the model for the particular soil-pile interaction for the research. Later, in chapter 4, the screw thread is also taken into account. The ultimate goal of chapter 3 and 4 is to obtain a torque figure, which subsequently can be used to set up requirements for the driving mechanism.

Approach In order to analyse the interaction of the soil and the monopile, the following points are addressed.

- Soil conditions
- Skin resistance
- Base resistance
- Self penetration

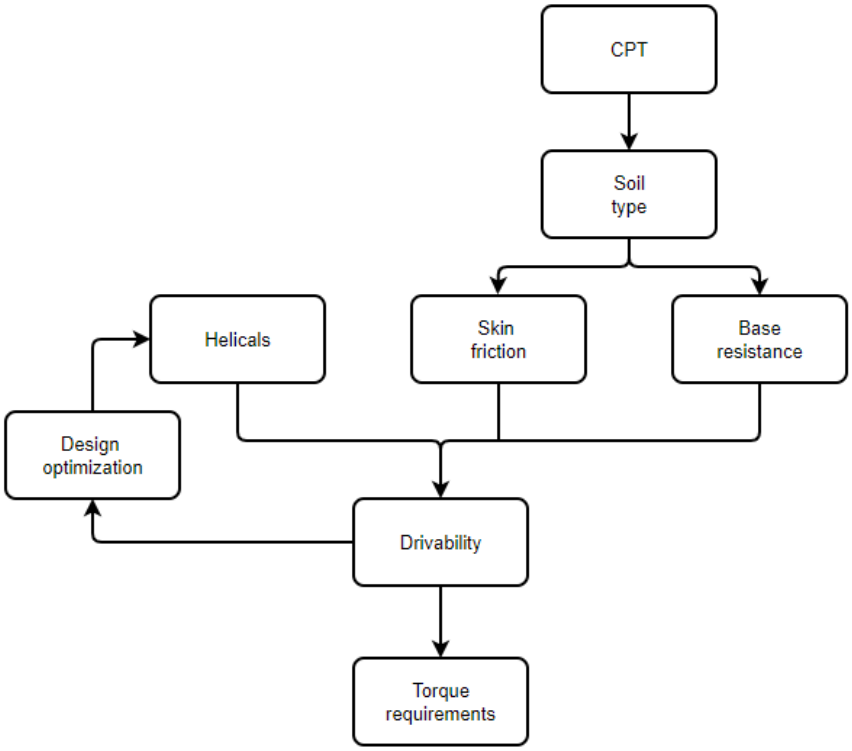

Figure 3.1: Flowchart of the analysis of the drivability of the monopile to ultimately obtain the torque requirements.

At first the soil properties are determined, based on CPT-data. With the soil properties the skin and base resistance can be calculated for a monopile without a screw thread. Then the force balance around

the helicals is discussed. These aspects can then be combined to calculate the drivability, and consequently the torque requirements. In fig. 3.1 this process is shown in a block diagram. Since the skin and base resistance follow directly from the monopile dimensions and the soil properties, these are calculated in this chapter, based on the monopile as shown in fig. 2.4e without the screw thread. The resistance and driving force of the helicals however, is the aspect we want to optimize for the best drivability of the monopile. The analysis of the helicals and the optimization process is described in chapter 4.

3.1 Soil conditions

Soil characteristics are inherently challenging to accurately obtain. Even with proper soil monsters and CPT's, ultimately only a fraction of the soil the monopile will interact with is analysed. However, it does give a broad idea of the composition of the relevant ground layers. This section describes the soil conditions as assumed in this research.

Cone penetration test To further specify the soil condition, data from a cone penetration test (CPT) is used. During a CPT a device is pushed into the ground, while measuring the resistance it encounters. In fig. 3.2 a CPT is schematically shown. The penetrometer is pushed downward with a continuous rate of typically 2 cm/s. It is driven by 1 m long rods with the same diameter, which are screwed to each other at the top. The penetrometer is equipped with sensors to measure the tip resistance, sleeve friction and the porewater pressure [52]. The measurements are subsequently shown in a graph such as in fig. 3.3.

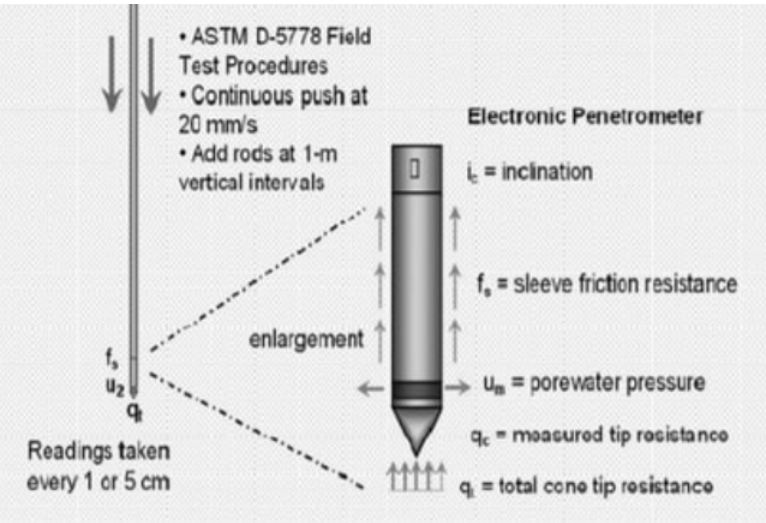

Figure 3.2: A schematic depiction of a cone penetration test [5]

The CPT chosen for this research is from the wind farm Hollandse Kust West (HKW), specifically at the location of wind turbine 11. In industry it has been said that this location is generally challenging for installation. Because it can therefore be seen as an upper bound in terms of driving resistance, it is a representative starting point for soil conditions. The CPT-data is obtained from the geotechnical investigations commissioned by the RVO [6]. In appendix B the original CPT-data are presented. For this research the CPT-data has been discretized by taking one data point per meter. With this resolution the data keeps its characteristics, while it takes less computational power. In fig. 3.3 the discretized data is shown. Since the CPT covers only a small area, unforeseen fluctuations in soil conditions for the entire monopile can always occur. Therefore an approximation of the CPT-data will be sufficient and accurate enough for the goal of this research. The used CPT-data is already corrected for the pore pressure.

From the CPT the soil type can be obtained. The ratio of the cone resistance and the sleeve friction is decisive for particular soil types [53]. In fig. 3.3 the friction ratio is shown in the third graph. In color the soil type given. For a friction ratio between 0.5 and 1 percent, the soil type is sand. For a ratio above 4 percent the soil type is clay. Between 1 and 4 percent the type shift from sand, silty sand, sandy silt to clay. As seen in fig. 3.3 the soil type for this research is sand to silty sand.

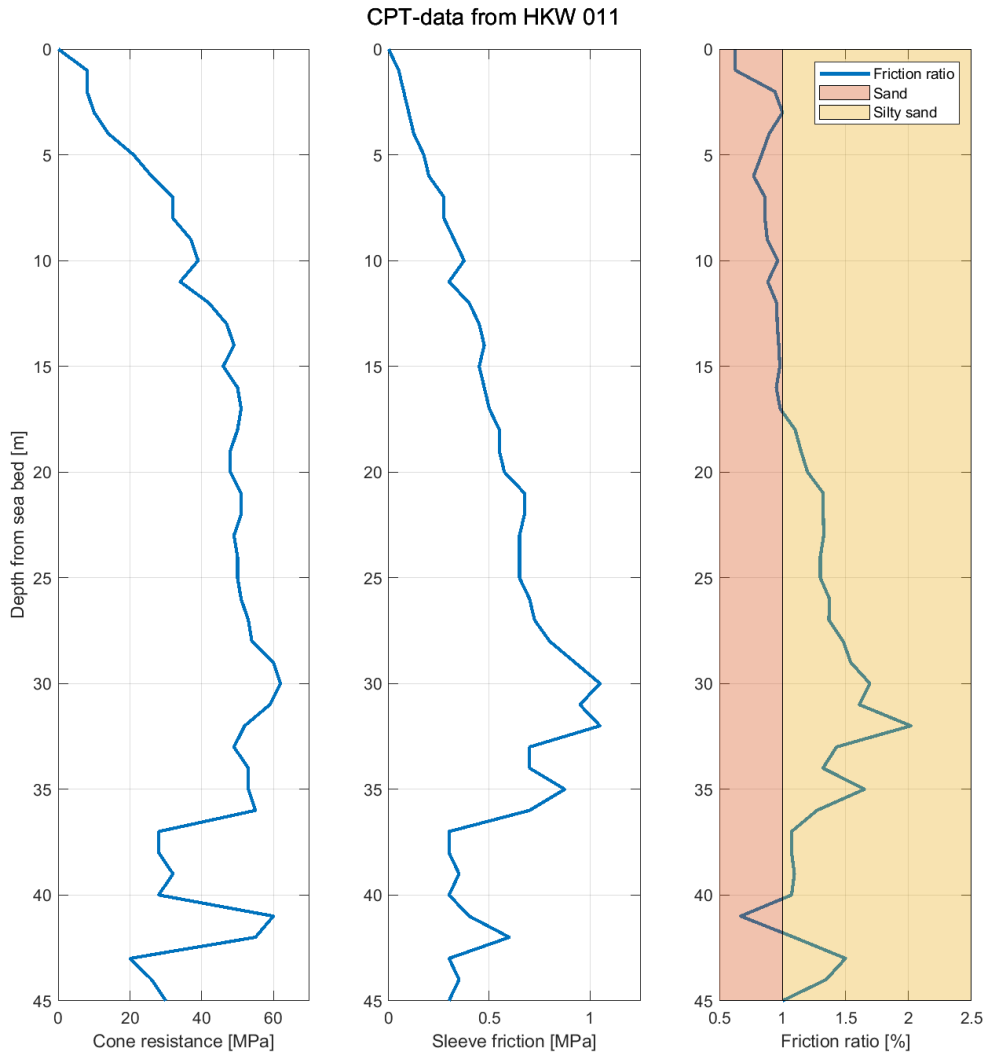

Figure 3.3: The CPT-data as used in the research [6].

Vertical pressure In the ground two pressures are relevant for the monopile: the vertical and horizontal pressure. The vertical pressure is obtained with the sum of all the above layers. For the soil under the sea bed holds therefore

$$p_{ver} = p_{atm} + p_{water} + p_{soil} \tag{3.1}$$

where p_{atm} is the atmospheric pressure, p_{water} the pressure due to the sea water and p_{soil} the soil pressure. The soil pressure is obtained by

$$p_{soil} = d\gamma g \tag{3.2}$$

with d the depth below seabed, γ the effective soil density obtained by subtracting the water density from the ground density, and g the gravity. The effective soil density in this research is $2000 kg/m^3$. In

fig. 3.4 the pressures mentioned in 3.1 are depicted. In this research both the water depth and the sea depth are 45 m. This follows from the standardized monopile as described in 2.4.

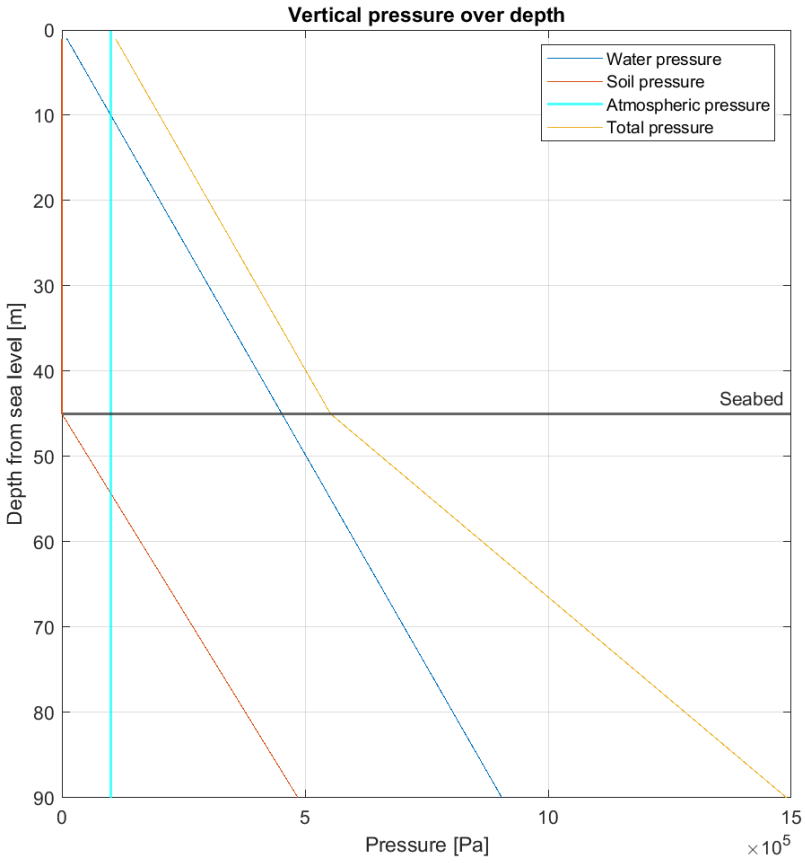

Figure 3.4: The vertical pressure from sea level to monopile depth.

Horizontal pressure Unlike in water, the vertical earth pressure in soil is different than the horizontal pressure. The horizontal pressure can be obtained as a function of the vertical pressure and the soil type. The soil type dictates the angle of repose. This is the maximum angle of a the slope the material makes when it gets piled. For sandy soils this value is $\theta = 35°$. With the angle of repose the lateral earth pressure can be calculated. In literature several methods are found. Some methods are more detailed than other, but all are essentially using the angle of repose as input variable. In this research we use the well known method of Jaky

$$K_0 = 1 - sin\theta \tag{3.3}$$

where K_0 is the neutral earth pressure coefficient, and θ is the angle of repose in radians [54]. Subsequently the horizontal earth pressure can be obtained by

$$p_{hor} = K_0 p_{ver} \tag{3.4}$$

where p_{ver} is derived in 3.4. This formula is widely accepted as a valid approximation, since other formula's improve the approximation only within the expected uncertainty one finds while working with soils.

When the soil around the helicals is considered however, one would have to work with the active and passive earth pressures. These are different because the object moving through the soil effects the soil itself. The passive soil pressure is located at the side to which the object is moving, while the active pressure is located at the other side. The active and passive earth pressure coefficients can be derived by

$$K_a = tan^2(45° - \frac{\theta}{2}) \tag{3.5}$$

$$K_p = tan^2(45° + \frac{\theta}{2}) \tag{3.6}$$

where K_a is the active and K_p is the passive earth pressure coefficient, and θ is again the angle of repose. In chapter 4 the principle active and passive is used to determine the interaction between the soil and the helicals.

3.2 Skin resistance of the monopile

Based on the soil conditions the resistance the monopile encounters can be determined. The resistance essentially consists of three parts: the outer and inner skin friction and base resistance. Furthermore, it depends whether the monopile is stationary or moving. The total resistance is to be exceeded by the driving force of the monopile in order to penetrate the ground. In this section we analyse the contributions to the total resistance and eventually obtain the self penetration depth of the monopile. With this information we can specify the desired performance of the helicals.

Free body diagram of the monopile and soil The monopile encounters friction from the soil it eventually needs to penetrate. In order to determine all the relevant force, we start with a free body diagram, FBD, of the monopile inserted in the soil. In fig. 3.5 the FBD is shown and in table 3.1 the various components are described. In the following paragraphs and chapter 4 we will regularly refer to the FBD and table. For convenience, the signs of the driving forces are given with an F, while the resistances are referred to with an R. Ultimately, all the components listed in 3.1 need to be analysed to determine whether the principle of screwing works, and what the torque requirements are.

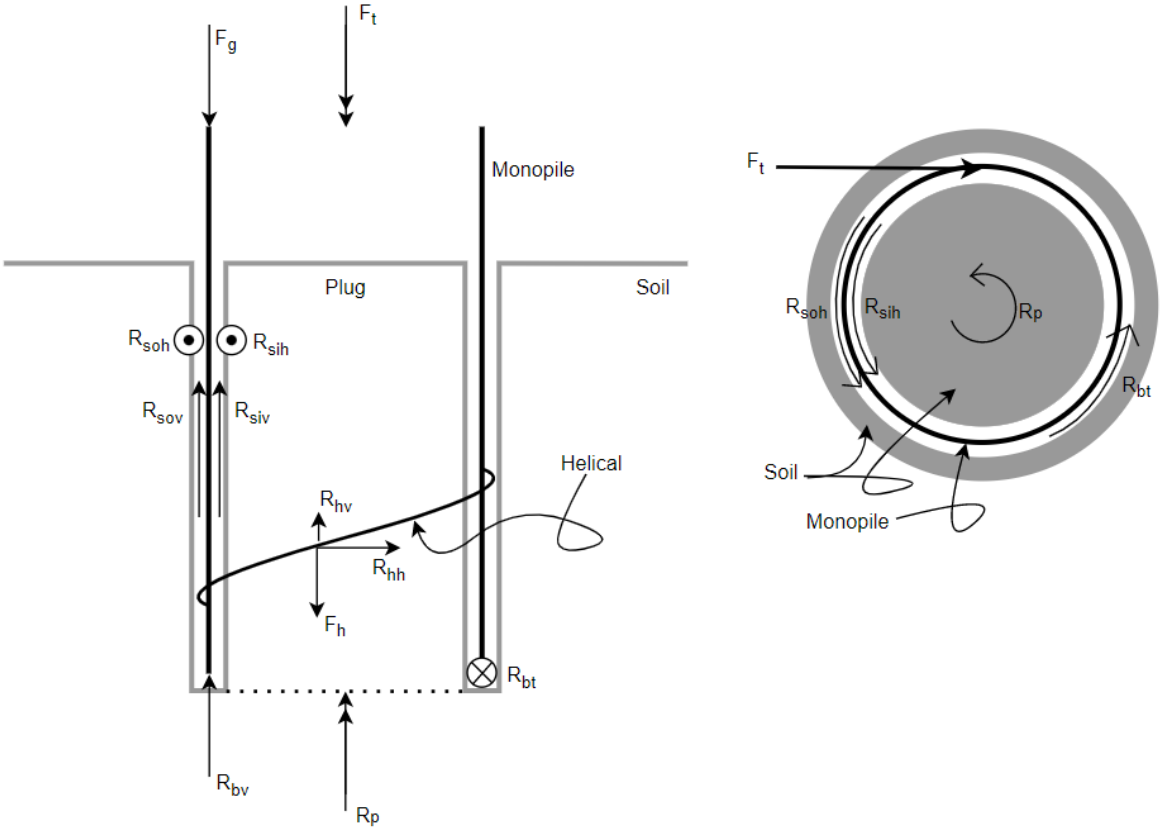

Figure 3.5: Free body diagram of the monopile as it is inserted into the ground. At the left the side view and on the right the top view. In table 3.1 the drawn components are described.

	Description	Sign
Independent on helicals	Own weight	F_g
	Tangential driving force	F_t
	Outside horizontal skin resistance	R_{soh}
	Outside vertical skin resistance	R_{sov}
	Inside horizontal skin resistance	R_{sih}
	Inside vertical skin resistance	R_{siv}
	Vertical base resistance	R_{bv}
	Tangential base resistance	R_{bt}
	Rotational resistance plug	R_p
Dependent on helicals	Helical driving force	F_h
	Horizontal helical resistance	R_{hh}
	Vertical helical resistance	R_{hv}

Table 3.1: Description of the forces acting at the monopile and their signs as used in fig. 3.5

Static skin resistance The skin resistance depends on the soil conditions as stipulated above. Based on the soil type the friction can be determined. As established in section 3.1, the soil consists of sand and silty sand which means that for determining the skin resistance, a method for non-cohesive soils can be used. There are multiple methods to achieve this [10]. Within the API standard four new methods were introduced that analyse the axial static capacity of a monopile. These methods were calibrated based on pile field tests for certain soil conditions. That means that the parameters are determined such, that the model is curve fitted onto the actual piling results. The accuracy of these methods can be described by the model error, which is defined as the ratio of the calculated bearing capacity to the measured bearing capacity, denoted by

$$\epsilon_R = \frac{Q_c}{Q_m} \tag{3.7}$$

where Q_c is the calculated bearing capacity and the Q_m the measured bearing capacity [55].

For determining the skin friction, the four methods share the same general formula $f(z)$, which gives the skin friction as a function of the depth z in $[Pa]$. $f(z)$ is denoted by

$$f(z) = uq_c(\frac{\sigma'_v}{p_a})^a A_r^b[max(\frac{L-z}{D_0}, v)]^{-c}(tan\varphi)^d \tag{3.8}$$

with q_c the measured cone tip resistance, σ'_v the vertical pressure, p_a the atmospheric pressure, φ the angle of repose and A_r the pile displacement ratio, defined by

$$A_r = 1 - (\frac{D_i}{D_0})^2 \tag{3.9}$$

where D_i is the inner diameter and D_o the outer diameter. Furthermore, L is the length of the monopile and z the penetration depth. Lastly, u, a, b, c, d and v are parameters, which differ for each of the four methods. If we take the model error as denoted in 3.7 into account, the so called 'simplified ICP-05'-method proves to be reliable and accurate for sandy soil conditions and, crucially, does not underestimate the skin friction. Since safety is a top priority this method is used in this research [10]. The difference between the methods are the parameters, the ICP-05 parameters are listed in table 3.2. The resulting skin friction is shown in fig. 3.6.

With the skin friction f as described in equation eq. (3.8) the force that the monopile encounters due

Parameter	Value
u	0.023
a	0.1
b	0.2
c	0.4
d	1
v	$A_r^{0.25}$

Table 3.2: Parameters for the Simplified ICP-05-method for determining the skin friction [10]

to skin friction can be calculated with

$$R_s = \sum_{z=1}^{d} f(z) A_{mp} \tag{3.10}$$

where z is the depth the monopile is inserted in the sea bed and A_{mp} the area of the monopile per meter height. The circumference can be considered a constant over the depth, since only the lower part is inserted into the sea bed, and thus the area A_{mp} is also a constant. At $z = d$ the monopile is at its maximum depth, in this research 45 m. Furthermore in this research, all the results are based on the CPT-data of HKW as described in 3.1 and with the monopile as shown in fig. 2.4e, with a lower diameter of 12 meter and a base thickness of 80 mm.

Since the monopile has skin friction on the outside and inside, two values for R_s are calculated. The outside skin resistance R_{so} and inside skin resistance R_{si}. Using eq. (3.10) R_{so} is calculated with the outside area per meter height, while for R_{si} the inner area is used. With those data the total cumulative skin resistance is $R_s = R_{so} + R_{si}$ and is depicted in fig. 3.6.

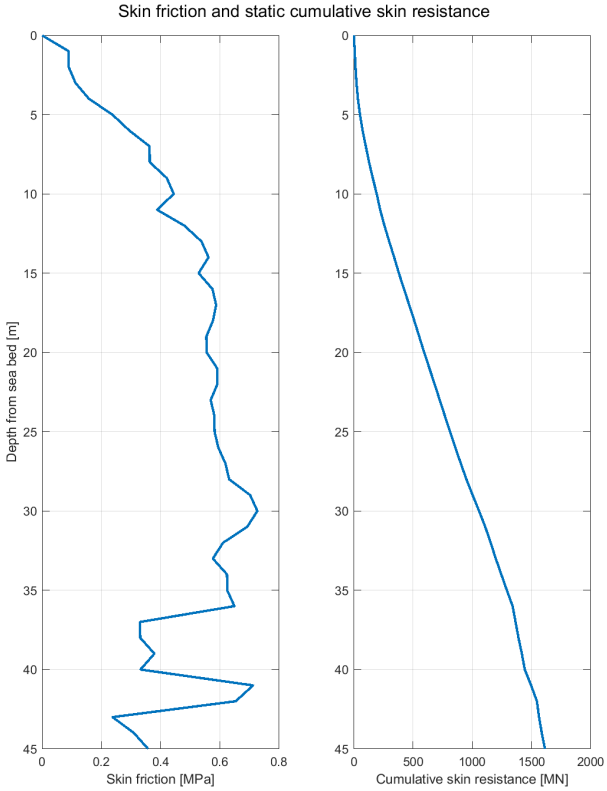

Figure 3.6: The absolute skin friction in MPa as calculated with eq. (3.8) and the cumulative skin resistance R_s in MN as determined with eq. (3.10).

Dynamic skin resistance In the above paragraph the static skin friction is obtained. In reality however, there is a difference between the static and dynamic resistance. In industry the dynamic resistance is derived by multiplying the static friction with a β-factor. The β-factor is calculated by

$$\beta = tan\delta \tag{3.11}$$

where δ represents the friction angle between sand and steel, and is equal to $\delta = \theta - 5$ with θ the angle of repose 35°. This makes $\beta = 0.58$. The dynamic cumulative skin resistance is shown in fig. 3.7. It must be noted that this principle and its values are based on experience in the field. The mechanics behind this principle must be sought in the change of the soil consolidation due to the movement of the monopile. It is therefore a time depended principle. In the research we assume that the consolidation of the soil takes longer than the interval time of movements of the monopile, meaning that the beta factor is valid, also when the monopile briefly stops moving.

It is important to note that the outside skin resistance is omnidirectional; it does not depend on the rotation of the monopile. However, the inside skin resistance, and therefore the total resistance as well, does depend on the direction the wall of the monopile is moving with respect to the soil. This is because the plug inside the soil will rotate along with the monopile, as will be discussed in the next paragraph.

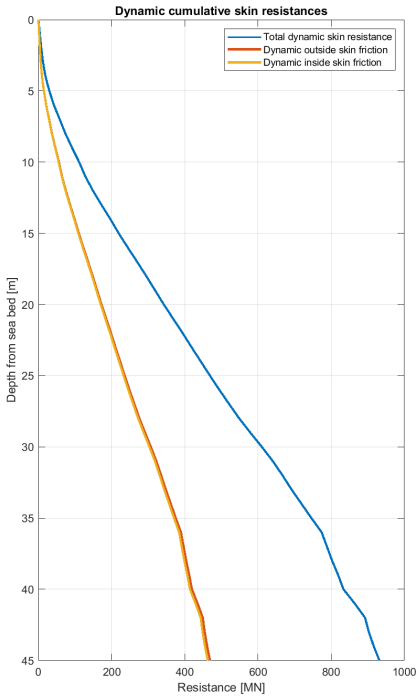

Figure 3.7: The outside and inside dynamic skin resistance in MN. Note that the shown inside resistance is only applicable in vertical direction, due to the rotating of the plug inside the monopile. The total dynamic resistance is the sum of the inside and outside resistance.

Refusal mechanism It is essential to understand the refusal mechanism of the monopile. Since the resistance essentially is made up of the skin and base resistance, we have to find what influence they both have. As the monopile will be screwed into the ground, it does not only have a vertical motion, but also a rotational one. We therefore have to distinguish the vertical and rotational resistances. Ultimately, when the monopile is fitted with helicals, the direction of movement is assumed to be in the same direction as the helicals. That means that we divide the resistances in horizontal and vertical components.

Outside skin resistance The outside skin resistance of the monopile is in essence independent of the direction of movement. This means that we can draw a force diagram when a torque is added onto the monopile. With an applied torque the resultant force becomes larger. Eventually it needs to become bigger than the resistance in order for the monopile to move. In fig. 3.8 this is schematically shown. At the left the situation with only vertical forces is shown, the skin resistance and the own weight force of the monopile. At the right a tangential force is added, resulting in a larger resultant force. Since the wall of the monopile is travelling in the direction of the helicals, the resistances can also be divided into components. This has as a result that an applied tangential force which is large enough to overcome the skin resistance, will cause the monopile not only to rotate, but also to move downward.

The horizontal and vertical components of the resistance are depending on the angle of attack of the helicals and can be quantified by

$$R_{soh} = R_{so}cos(\alpha) \tag{3.12}$$

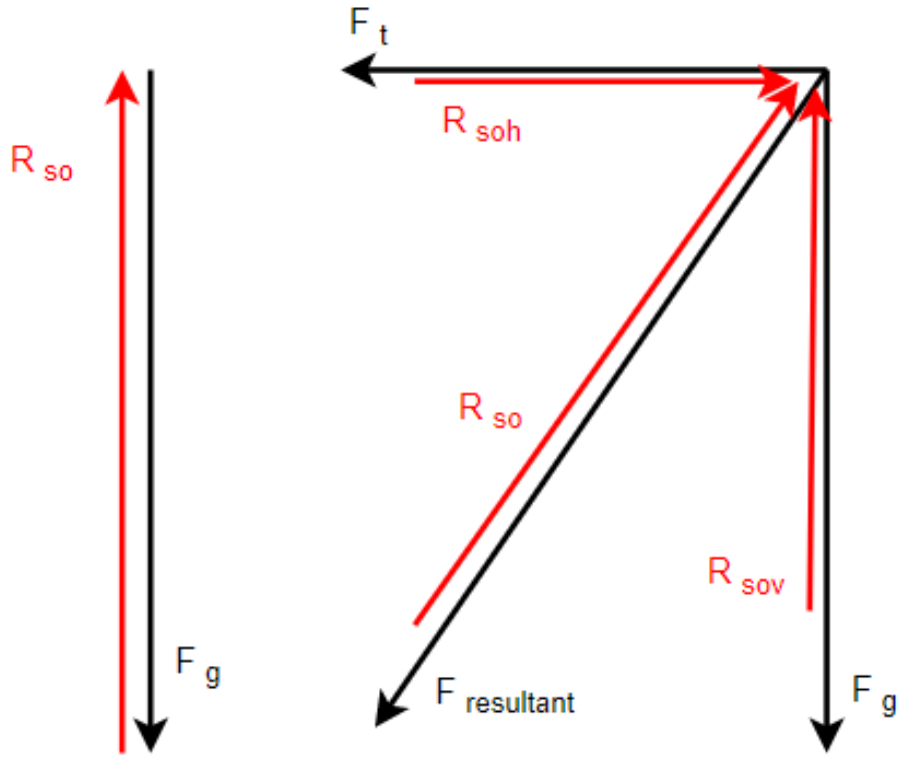

Figure 3.8: Principal of increased resultant force when adding a torque on the monopile. The resistance force kept the same amplitude.

$$R_{sov} = R_{so} sin(\alpha) \tag{3.13}$$

where R_{soh} is the horizontal outside skin resistance, R_{sov} is the vertical skin resistance and α is the angle of attack of the helicals, and therefore also the assumed direction of movement.

An important condition for equations 3.12 and 3.13 to be correct, is that the soil at the outside of the monopile is not moved by the monopile or helicals. That is, the soil surrounding the monopile is assumed to not rotate along with the monopile. Since the soil is part of the semi-infinite ground this is a safe assumption.

Inside skin resistance In the above paragraph the outside skin resistance of the monopile is determined. However, the outside and inside soil of the monopile might have a different behaviour. Firstly there is a probability that the soil on the inside will rotate along with monopile. If that is the case, the skin resistance does not act independently on the direction the wall of the monopile is moving. Secondly, it must be determined whether the soil on the inside will move vertically along with the monopile, or stays stationary. If the inside is static with respect to the monopile, i.e. it moves along with the monopile, it is said to be plugged. If the inside soil remains stationary with respect to the sea bed it is un-plugged. This behaviour can influence the resistance the monopile encounters while driving it into the sea bed.

As the penetration depth varies over time, it might be possible that the soil inside the monopile changes from plugged to un-plugged, or vice versa. The inside soil, from here on called the plug, is modelled as a solid cylinder with a diameter equal to the inside diameter of the monopile D_i and a length equal to the penetration depth z. This assumption makes that it has a contact surface with the inner side of the monopile and at the bottom with the always stationary ground underneath. At the upper side it is in contact with the sea water, which exerts a pressure but has a negligible friction. The friction between the plug and the monopile is calculated using f as described in eq. (3.8). Between the plug and soil underneath the angle of repose is used to determine the friction. In fig. 3.9 the plug is schematically shown.

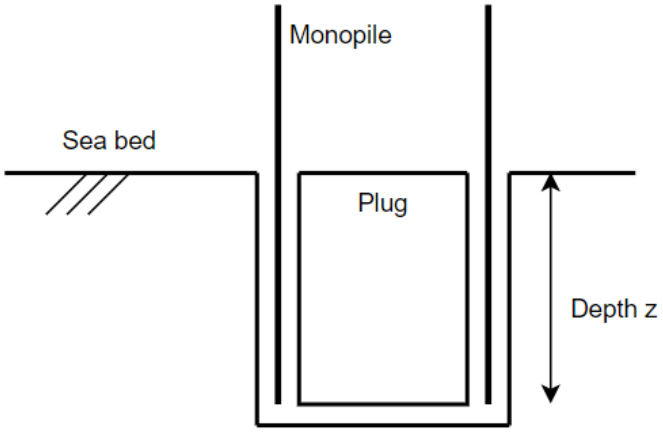

Figure 3.9: Schematic depiction of the plug inside the monopile.

To determine the behaviour of the plug a balance is set up. Since the ultimate goal is to screw the monopile into the ground, the plug could have both a rotational, as a vertical speed. Therefore two conditions must be met in order to make the plug move, where in both conditions the only driving force is the skin resistance from the inside of the monopile which acts on the plug. For the plug to move in a vertical direction the force due to the skin resistance must be larger than the base resistance of the plug. For the plug to rotate along with the monopile, the skin resistance must overcome the rotational resistance between the plug and the soil underneath. The following two balances are therefore set up

$$R_{si} \leftrightarrow q_c A_{plug} \tag{3.14}$$

$$T_{si} \leftrightarrow R_p \tag{3.15}$$

where A_{plug} is the area at the underside of the plug, determined with the inner diameter of the monopile D_i, while the inner skin resistance R_{si} is calculated using eq. (3.10) for the inner diameter.

In eq. (3.15) the T_{si} is derived by

$$T_{si} = F_{sin}\frac{1}{2}D_i \tag{3.16}$$

to obtain the torque exerted onto the plug. R_p is calculated with

$$R_p = \frac{2}{3}tan(\varphi)A_{plug}p_{soil} \tag{3.17}$$

where the right term gives the rotational resistance the plug experiences due to the friction with the soil underneath, with p_{soil} the effective soil pressure at depth z and φ the angle of repose, which is here 35°. Both the balances are a function of the depth z.

Eq. 3.14 gives the balance for the vertical direction of the plug. In fig. 3.10 this balance is graphically shown at the left. It can be seen that the vertical resistance of the plug is greater than the exerted vertical force on the plug, indicating that the plug stays stationary in vertical direction. eq. (3.15) gives the rotational balance between the monopile and the plug. Since the plug only can resist the torque at the contact area at the underside, the torque exerted by the monopile quickly becomes larger than the torque resistance. This means that the plug will rotate along with the monopile once a significant depth is reached. Here, with a significant depth is meant a depth where the torque exerted on the soil plug is much larger than the rotational resistance underside plug, as shown in the right side graph in fig. 3.10. We can therefore conclude that the inner skin resistance in vertical direction is

$$R_{siv} = R_{si} \tag{3.18}$$

and in the rotational direction is

$$R_{sih} = \frac{2}{3}tan(\varphi)A_{plug}p_{soil} \tag{3.19}$$

It must be noted that for the above calculations, the monopile is theoretically forced to rotate, in this case independent of the actual resistance or driving mechanisms.

Note that here, the plug is assumed as a solid cylinder, whereas in realty the behaviour of the soil inside can be much more complex. For example, the upper part might turn with the monopile while the lower part stays stationary. However, it is save to assume that the failure mechanism in this case occurs at the underside of the cylinder since this is the shape with the least contact area with the underneath ground. Furthermore, the soil inside experiences extra soil pressure because the monopile pushes it against the underneath soil. This might cause the soil the exert a increasing pressure to the walls of the monopiles due to the Poisson effect. Lastly, we only looked at potential dynamic soil at the inside, while at the outside it is assumed stationary. Given the fact that the outside soil is also supported by the semi-infinte sea bed, rather than only at the underside as with the plug, this is save to assume. The results as shown in fig. 3.10 and experiences in the field also give no reason to believe otherwise. For the purpose of this research therefore, the calculations with the given assumptions give a sufficient understanding of the behaviour of the soil inside the plug.

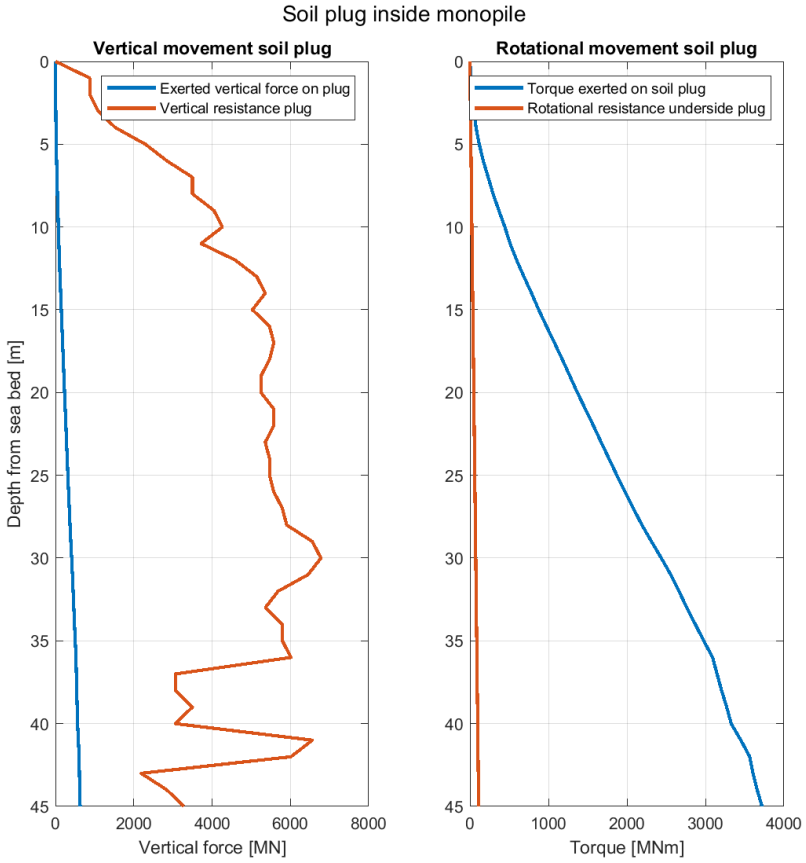

Figure 3.10: Graph to determine the behaviour of the plug. Left: the vertical resistance exceeds the vertical force exerted on the plug, thus the plug stays stationary in vertical direction. Right: the torque exerted on the plug is far greater than the rotational resistance, causing the plug to rotate along with the monopile.

Vertical and tangential base resistance The base resistance occurs at the bottom of the pile. As established above we can consider a plugged situation, so we can approximate the monopile as an open ended cylinder.

The base resistance in vertical direction R_{bv} for non-cohesive soils is approximated with

$$R_{bv} = q_b A_{tip} \tag{3.20}$$

where R_{bv} is the vertical base resistance, q_b the cone resistance from the CPT and A_{tip} the area of the tip of the monopile. In fig. 3.11 the end bearing resistance is shown.

Since the ultimate goal is to screw the monopile, the bottom will experience a torque resistance due to the rotation as well. The tangential base resistance R_{bt} is obtained by

$$R_{bt} = Q_{b,ver} tan(\alpha)\beta \tag{3.21}$$

where R_{bt} is the vertical base resistance, $tan(\alpha)$ the friction coefficient between the bottom of the monopile and the soil, and β the dynamic coefficient. R_{bt} as a function of the depth is shown in fig. 3.11.

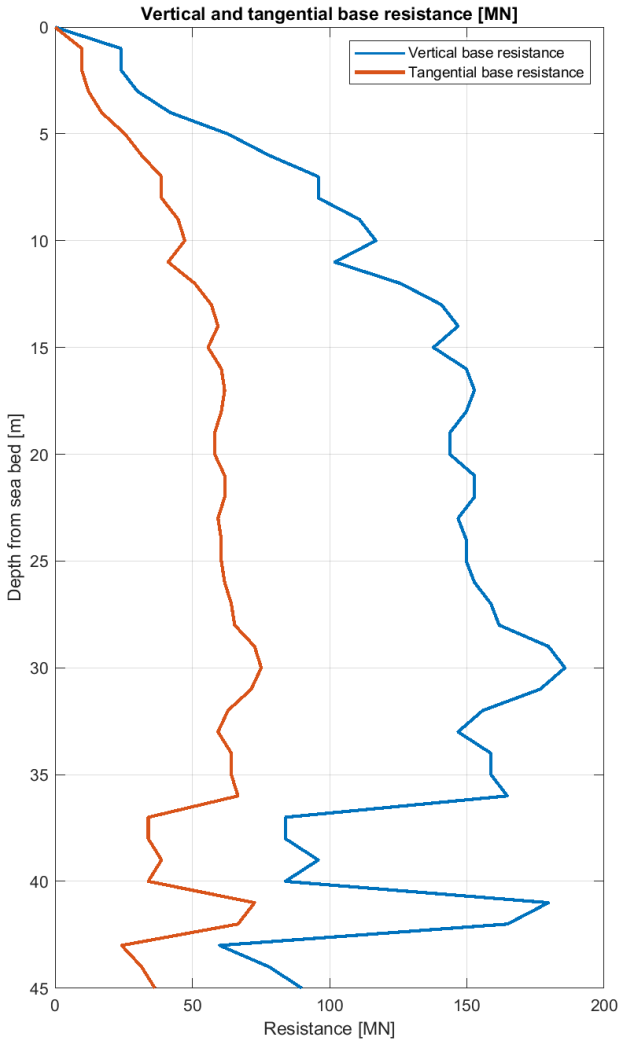

Figure 3.11: Vertical and tangential components of the base resistance, expressed in MN.

Self penetration depth Under its own weight, the monopile sinks into the soil up until a certain depth, the so called self penetration depth. To determine this depth the downward force of the monopile is plotted against the total vertical resistance. The point where the lines intersect corresponds to the self penetration depth. The force that the monopile exerts onto the ground is derived by

$$F_g = (m_{mp} - (\rho_{water} V_{water} + \gamma V_{soil}))g \tag{3.22}$$

where F_g is the own weight force corrected for the buoyancy caused by the water and soil, $m_m p$ is the mass of the monopile and g the gravity acceleration. To correct for the buoyancy, V_{water} and V_{soil} are vectors ranging from 0 to the water depth and 0 from the sea bed to the penetration depth respectively. Multiplied with the density of water ρ and effective density of the soil γ, this gives the buoyant mass which is subtracted from the mass of the monopile. In fig. 3.12 the self penetration is plotted. It can be seen that with found soil conditions, the self penetration depth is only in the order of 1 meter.

Furthermore, it can be seen that the buoyancy of the monopile is insignificant with respect of its own weight. It must be noted that here the monopile does not have helicals. In case of threaded monopile, the situation might occur that the monopile is resting on the helicals, reducing the self penetration depth. Lastly, in practice the self penetration depth is often in the order of a few meters, unlike what the model shows. An explanation for this is that the model does not take into account the curling up of the soil at the top. This might have a reducing effect on the resistance in reality, but is not incorporated in the model. Since we want to determine a minimum torque requirement it is safe to ignore the effect. In further research it could be explored whether it is beneficious to take it into account.

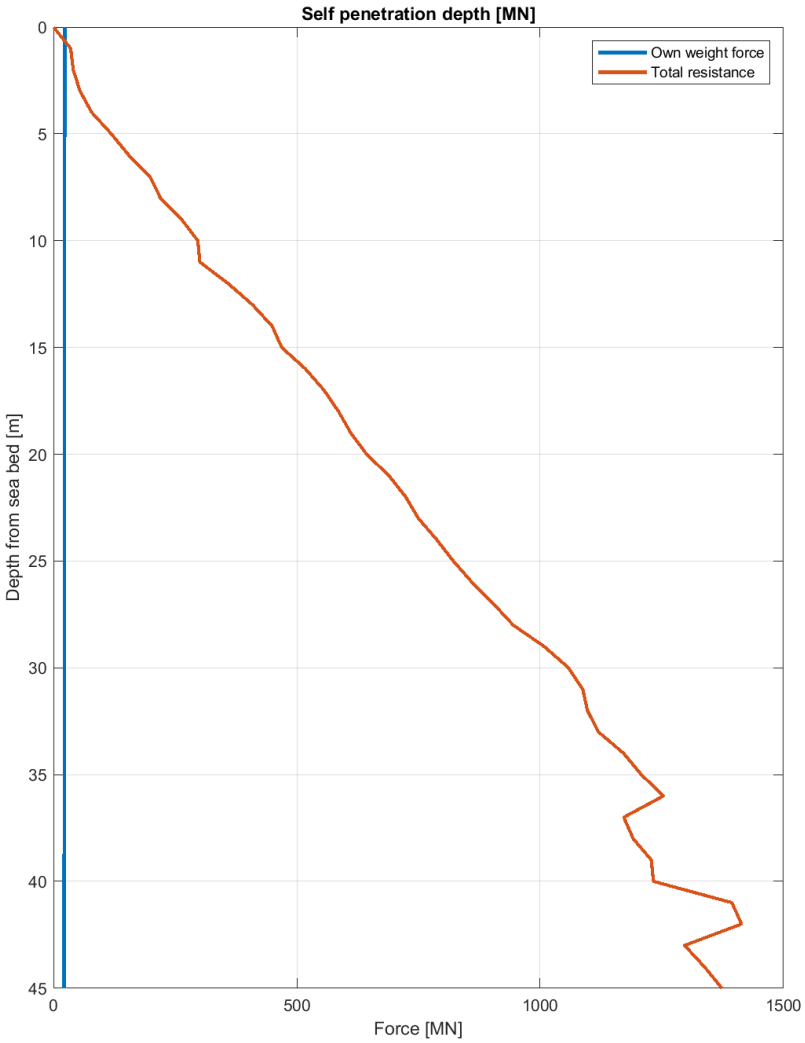

Figure 3.12: Self penetration of the monopile due to its own weight.

4. Design of the screw thread

Based on the graph shown in fig. 3.12, it is evident that a driving mechanism is necessary in order to get the monopile into the ground. To determine whether screwing the monopile will be effective, we first look at rotating the monopile without the helicals. This will give an indication of the required performance of the helicals. After that, we present a model of the monopile with the helicals and search for an optimization to derive the optimal design.

4.1 Rotation of the monopile

Resistance independent of helicals If we consider the monopile without the helicals, we can distinguish between the horizontal and vertical driving force and resistance. The skin and base resistance are assumed to be independent on the helicals. We can therefore make a graph what the required magnitude of the force is, to make the monopile move at all. Since the outside skin resistance is depending on the angle of attack as expressed in eq. (3.13), we have put multiple values of α in the graph. Here α ranges from 0 to 30 degree, since those are probable values the angle of attack could attain. The total rotational and vertical resistance without the helicals R_{tr} and R_{tv} are given by respectively

$$R_{tr} = R_{soh} + R_p + R_{bt} \tag{4.1}$$

$$R_{tv} = R_{sov} + R_{siv} + R_{bt} \tag{4.2}$$

where R_{soh} and R_{sov} are a function of the angle α. In fig. 4.1 the results of equations 4.1 and 4.2 are printed. It shows that the minimum torque that is required must be capable of creating a tangential force in the order of 500 MN. With a diameter of 12 meter this translates into a torque of 3000 MNm. Note that with this figure we only reach an equilibrium, and that therefore a higher torque is necessary. The total vertical resistance learns that the effective downward force of the helicals that is required, varies in the order of 500 to 800 MN. For both of these figures applies that the screw thread itself has its own resistance, so ultimately the required torque figures will become larger.

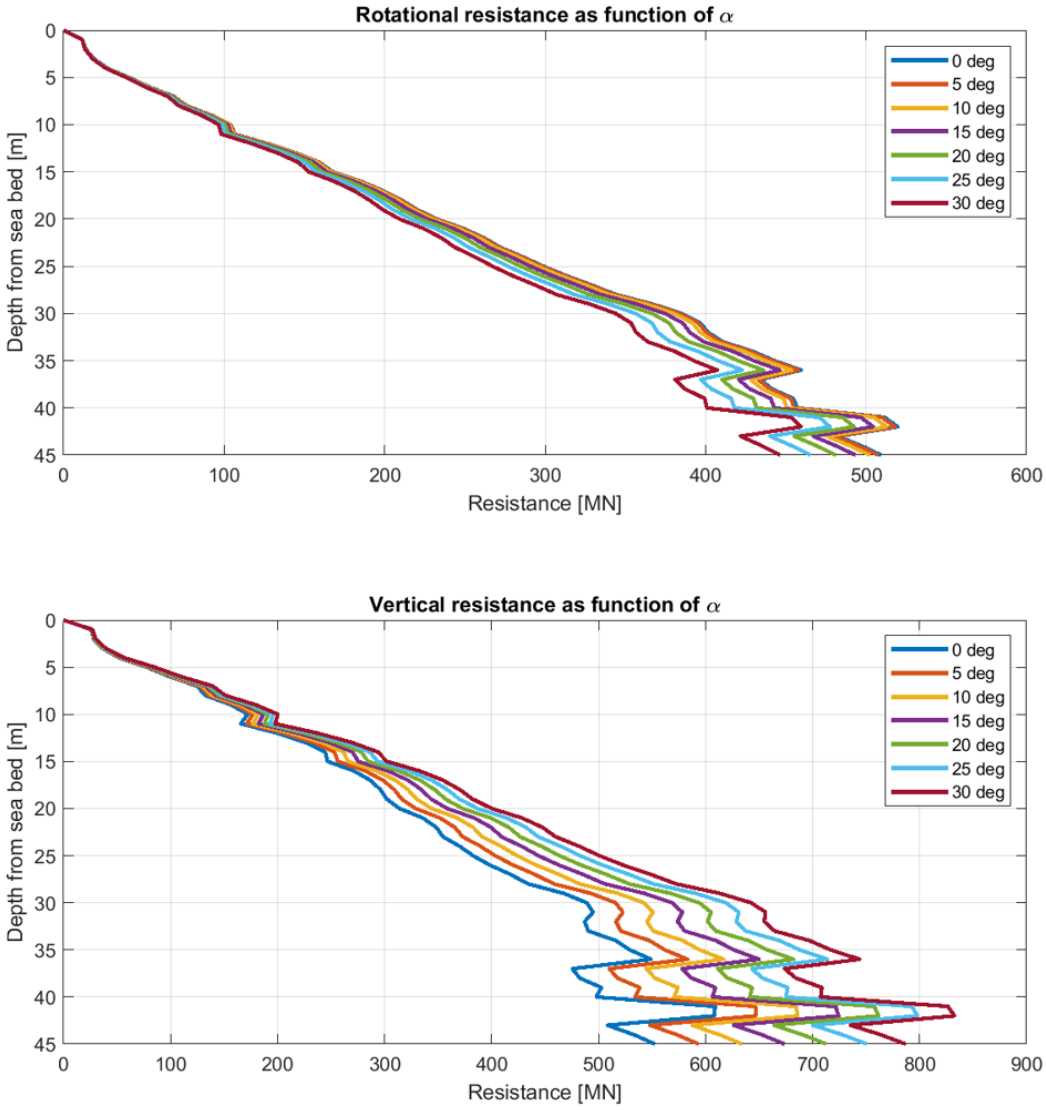

Figure 4.1: Rotational and vertical resistance of the monopile without helicals as a function of α, ranging from 0 to 30 degree.

4.2 Screw-thread helicals

Model of the helical-soil interaction The principle of the helicals driving the monopile downwards, functions because the upper side of the helicals pushes against the soil with the angle of attack α. Figure 4.2 shows an FBD of the soil-helical interaction with all the relevant forces. In this research we consider the interaction between the underside of the helical and the soil as negligible given the direction of rotation. With the FBD equations can be set up that give the relation between the force caused by the torque and the downward force, and the corresponding resistances.

$$\sum F_x = F_t - F_N sin(\alpha) - \mu F_N cos(\alpha) = 0 \tag{4.3}$$

$$\sum F_y = -F_h + F_N cos(\alpha) - \mu F_N sin(\alpha) = 0 \tag{4.4}$$

$$R_f = \mu F_N \tag{4.5}$$

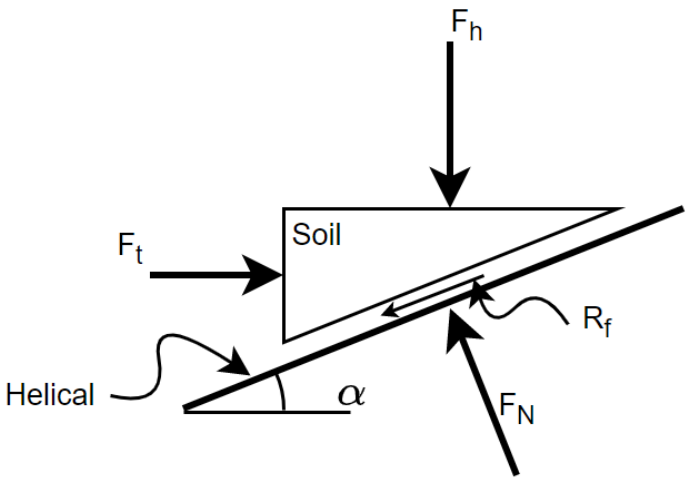

Figure 4.2: Free body diagram of the helical and the involved forces.

Equations (4.3) and (4.4) relate the tangential force F_t and vertical force excited by the helicals F_h via the normal force F_N and the angle of attack α. The friction coefficient μ is given by $tan(\delta)$. If we eliminate the normal force F_N we get

$$F_t = \frac{sin(\alpha) + \mu cos(\alpha)}{cos(\alpha) - \mu sin(\alpha)} F_h \tag{4.6}$$

where F_t and F_h are directly related to each other. Eq (4.6) essentially gives a ratio as a function of the angle α and the friction coefficient μ. In fig. 4.3 this ratio is plotted with a maximum angle of 35 degree. The ratio at 0 degree is equal to the friction coefficient. At 10 degree and higher the ratio becomes larger than 1, meaning that it requires more tangential force than the helicals push the monopile downwards.

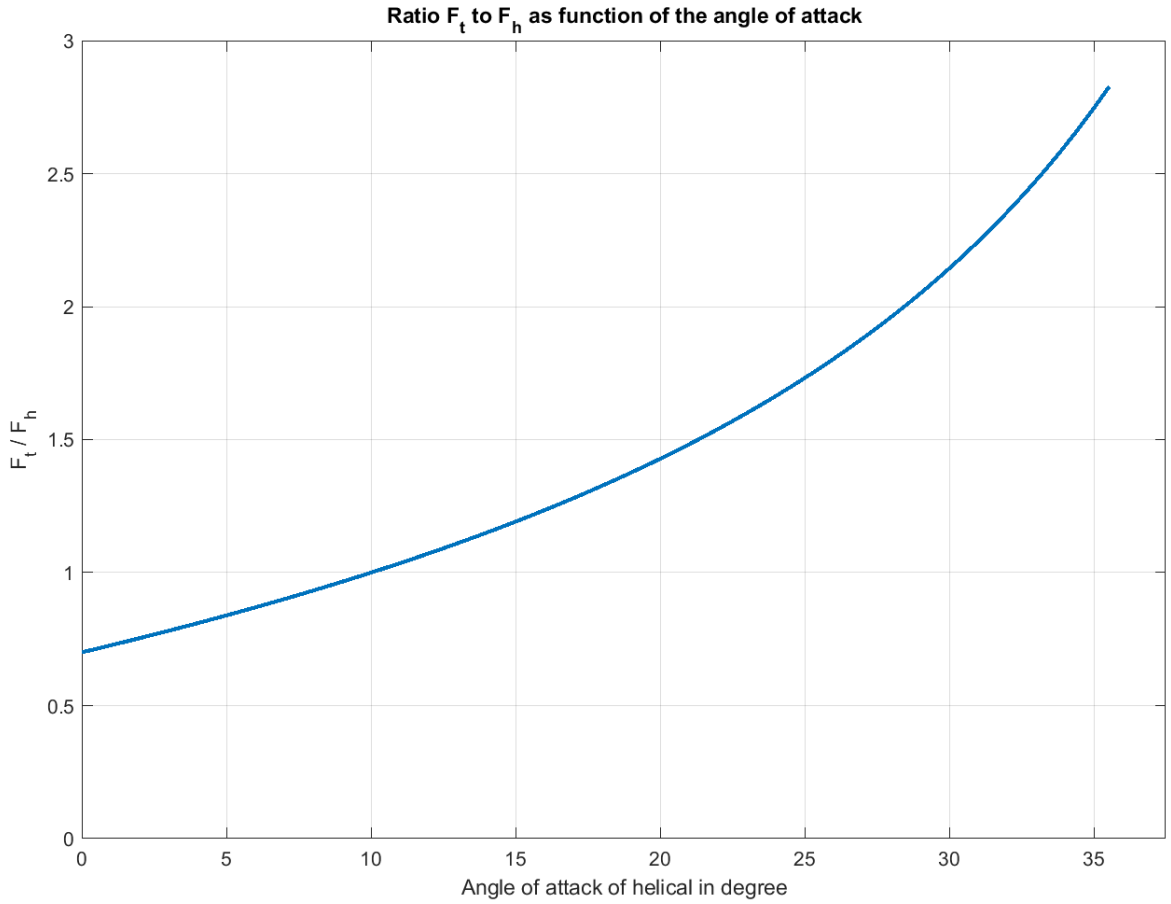

Figure 4.3: Plot of the ratio between the tangential and helical force as a function of angle α and a friction coefficient of 0.7.

4.3 Helical performance

Helical performance requirements Ultimately, the effective downward force F_h must be larger than the total vertical resistance R_{tv}. In fig. 4.1 it can be seen that the F_h must be in the order of 600 to 800 MN, depending on the angle of attack of the helicals. Fig. 4.3 shows that with an angle of 10 degree the ratio in eq. (4.6) becomes 1, meaning that the magnitude of the tangential force and helical force are equal. If we combine the vertical resistance R_{tv} and the ratio of eq. (4.6), we can determine the required tangential force F_t. The total required torque as a function of α can then be computed by taking the sum of the rotational resistance R_{tr} and F_t. Fig. (4.4) shows the results of this computation. It is clearly visible that smaller angles require a smaller tangential force, and thus torque. The downside however is, that a monopile with a smaller angle needs more revolutions to reach the desired depth. It must be noted that it is a theoretical helical performance still, Later in this chapter we will consider the design of the helical itself.

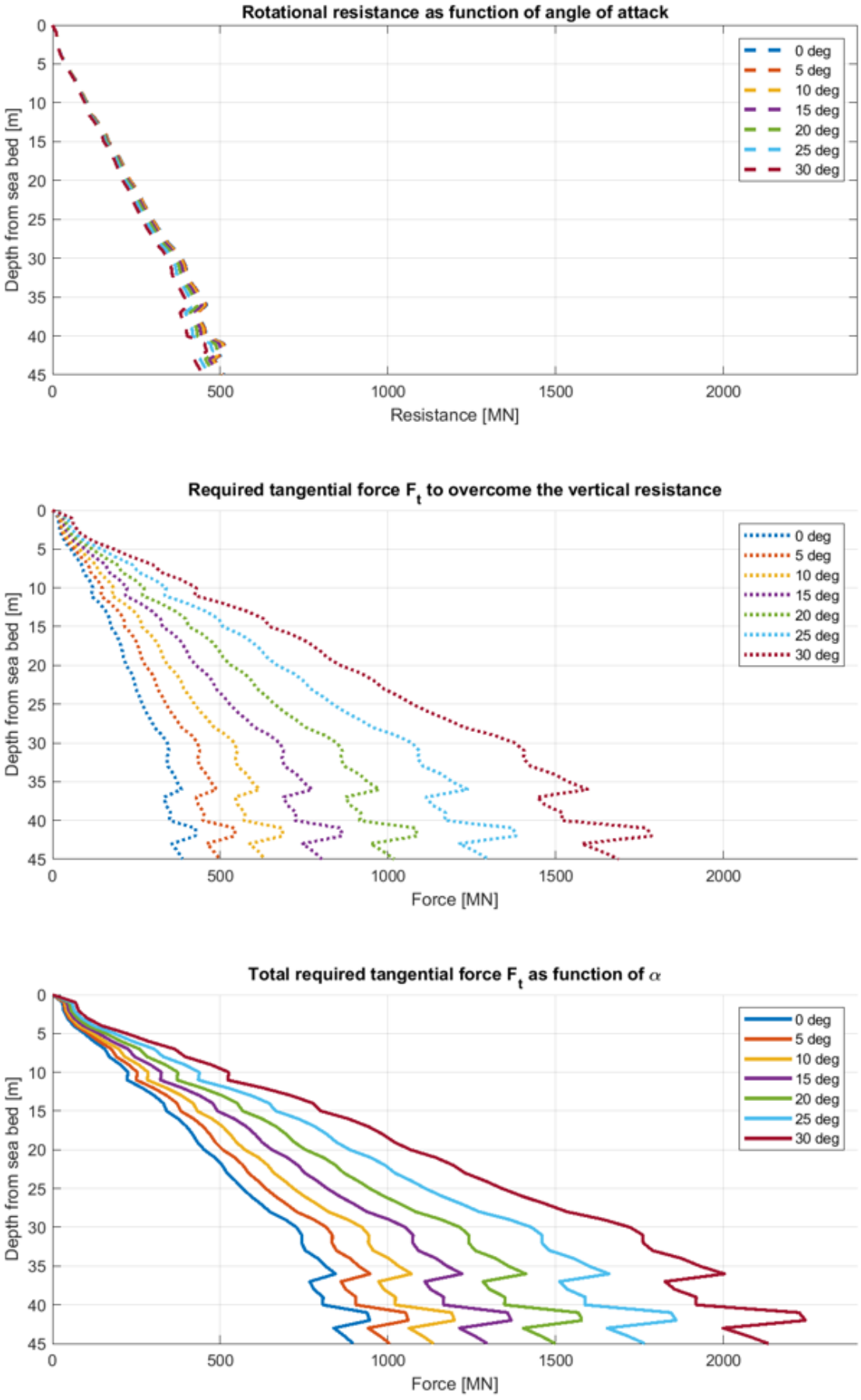

Figure 4.4: The minimum torque requirements to screw the monopile into the soil, as a function of the angle of attack of the helicals α

Based on the results as showed in fig. 4.4 the minimum torque that must be delivered by the equipment, must be able to excite a tangential force reaching from 1100 to 2000 MN, depending on the angle and the safety factor. Expressed in tonnes-force, this would mean that far over 100.000 tonnes of force are required to screw the monopile. This causes not only challenges for the driving equipment, but also for the monopile itself. To put his amount of force in perspective, the heaviest crane is rated to lift 20.000 tonnes, more than five times less.

4.4 Boundary conditions

In the previous sections we explored the possibilities of screwing a monopile by only considering the force balance. However, in reality several factors need to be considered as well. The stresses inside the monopile and helicals must stay within safety limits and the soil around the monopile has to stay stationary. In this section we explore the limitations given by these aspects.

Allowable stress monopile Monopiles are manufactured using S355 steel. S355 means that the material has a yielding stress of 355 MPa. Evidently the stresses need to stay under that limit. However, safety factors exist that lower the limit. These factors are based on the load cycles and risk of failures and are set at 1.13, 1.3 and 1.5. Since a monopile is mechanically a relatively simple object and the applied forces are strictly monitored and controlled, a low safety factor of 1.13 can be applied. Furthermore, the monopile only experiences these high stresses once, so fatigue does not occur due to the driving.

The maximum stress occurs at the upper part of the monopile, since it has a smaller diameter. The stress is predominantly shear stress and is calculated with

$$\tau = \frac{F_t}{A} \tag{4.7}$$

where F_t is the tangential driving force and A is the area cross sectional area of the upper part. Given that we can use a safety factor of 1.13 and a yielding stress of 355 MPa, the stress has to stay below 314 MPa. Using eq. (4.7) this gives an maximum allowable force of 625 MN for an upper diameter of 8 m and a thickness of 80 mm. However, this is the maximum force to be applied at a radius of 4 m, while the calculated tangential force in fig. 4.4 is applied at a radius of 6 m. This has as a consequence that if the driving force is applied directly to the upper side of the monopile, it has to be a factor 1.5 larger than the required force at the lower part. With the initial dimensions this would mean that a maximum lower force can be excited of 416 MN. Given the results as shown in fig. 4.4, this seems to be on the lower side. If we assume the the driving force is applied at the flange of the monopile, we can calculate what the influence of a larger diameter and thickness is. The results are given in table 4.1. The allowable upper force is dictated by a maximum stress of 314 MPa. The resultant lower tangential force is the tangential force that interacts with the soil at the lower part of the monopile, as also shown in fig. 4.4. The values in table 4.1 show that it with increasing diameter and thickness, the allowable upper and resultant lower force indeed increase as well. These values will be used in section 4.5 to determine the final driving force.

Diameter [m]	Thickness [m]	Allowable upper force [MN]	Resultant lower tangential force [MN]
8	0.08	625	416
8	0.10	780	519
8	0.12	933	622
10	0.08	783	652
10	0.10	978	814
10	0.12	1170	975
12	0.08	941	941
12	0.10	1174	1147
12	0.12	1406	1406

Table 4.1: Parameter study of various upper diameter and thickness

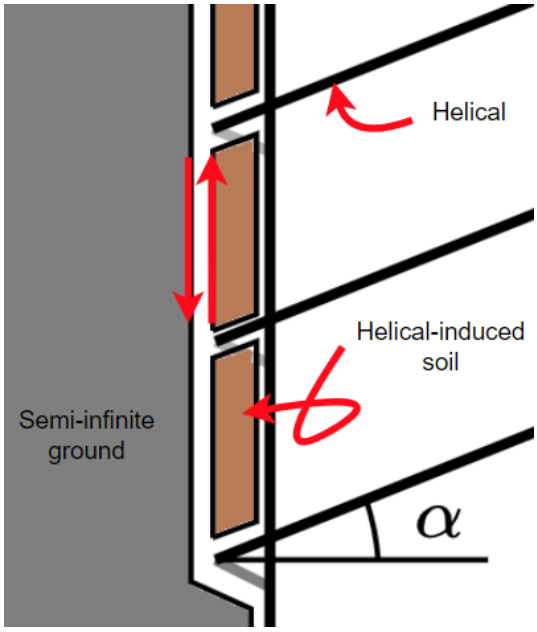

Figure 4.5: schematic interaction between the soil between the helicals and the semi-infinte ground. The vertical red arrows indicate the force interaction.

Soil-ground interaction We model the soil above the helicals as a hollow cylinder between the outside of the monopile and the outer edge of the helicals. At the distance equal to the with w of the helical, the soil cylinder has a contact area with the semi infinite ground. Essentially through this contact area the the force of the helicals is transmitted. This means that the resistance between this soil and the ground should be larger than the force required to push the monopile down. This situation is illustrated in fig. 4.5.

In order for the screwing principle to work, the helical must not push the soil upwards. To determine whether this is the case, we will plot the soil-ground resistance R_{sg} and the helical induced soil force F_i. The induced force F_i is derived by

$$F_i = \sqrt{R_{tr}^2 + R_{tv}^2} \tag{4.8}$$

where R_{tr} and R_{tr} are given in eq. (4.1) and (4.2). The soil-ground resistance is given by

$$R_{sg} = tan(\theta) p A_{sg} \tag{4.9}$$

where $tan(\theta)$ is the internal friction of the soil, p is the pressure and Asg is the contact area of soil and semi-infinite ground. The results are shown in fig. 4.6. It is can be seen that the two forces are of equal magnitude, meaning that it is not evident the soil will remain unaffected of the helical forces.

The collapse mechanism as shown in fig. 4.5 considers shear in the plane parallel to the wall of the monopile. However, the soil could also be pushed outwards. To determine whether this will happen we use the horizontal passive earth pressure coefficient which is given by eq. (3.6). With the angle of repose $\theta = 35°$, this gives a K_p of 3.6. This means that the soil capacity in horizontal direction is 3.6 times that of the soil in vertical direction. This implies that the failure mechanism of the soil in vertical direction acts before that in the horizontal direction. We can therefore assume that as long as the vertical soil pressure is not exceeded, the horizontal pressure is neither.

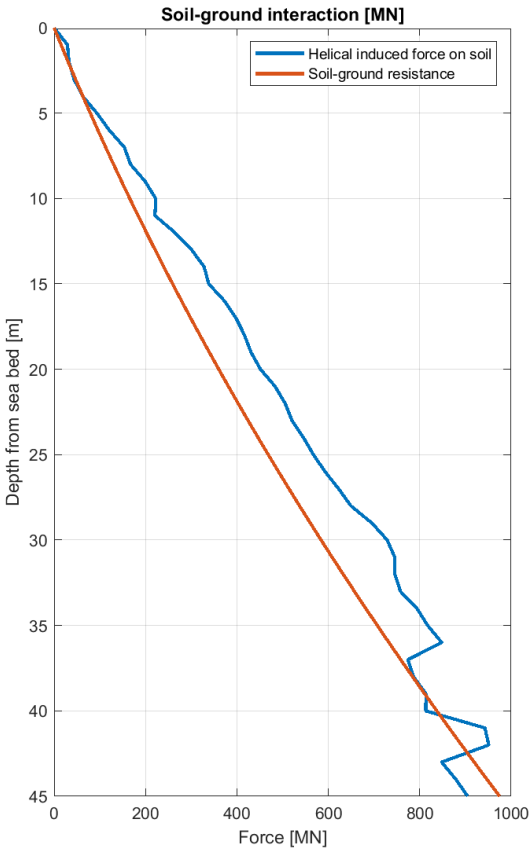

Figure 4.6: The ratio between the force applied by the helicals in blue, and the soil-ground resistance in red. In order for the soil to resist disturbance, the blue line must stay left of the red line.

Lastly, we assume an advance ratio (AR) of 1. The AR is defined by

$$AR = \frac{\Delta z_{mp}}{p} \tag{4.10}$$

where Δz_{mp} is the vertical displacement of the monopile during one revolution and p the pitch of the helicals [56]. An ratio of 1 therefore means that the direction of the wall of the monopile is parallel to the helicals. An AR lower than 1 indicates a disturbance of the soil around the monopile. In this research we assume a pitch matched installation. For the purpose of determining the feasibility an AR of 1 is acceptable, and it prevents the model becoming overly complex.

4.5 Optimization driving conditions

In the above sections we presented the required torque figures and the conditions needed in order to make the screwing principle work. It proves to be challenging at the least and on the edge of what is feasible. In this section we will therefore examine under what conditions it becomes feasible. To come to the above conclusion, we used quite conservative values. This approach follows from the fact that we want to be sure that it works in conditions where vibrating is not an option. The parameters that we will change to examine their influence are, among others, the diameter, friction of the walls, helicals and base. We express the results in certain key performance values that indicate whether a modification results in a feasible situation. In table 4.2 the parameter variation and the results are shown.

Parameters							Feasibility indicators	
Diameter	Skin friction	Helical friction	Base resistance	CPT	Angle of attack	Angle of repose	Required driving force x10^3 MN	Soil-ground resistance
12	1	1	1	1	10	35	1.20	0.96
6	-	-	-	-	-	-	0.63	0.98
8	-	-	-	-	-	-	0.82	0.98
10	-	-	-	-	-	-	1.01	0.97
-	0.8	-	-	-	-	-	1.00	0.81
-	0.6	-	-	-	-	-	0.81	0.65
-	0.4	-	-	-	-	-	0.62	0.50
-	-	0.8	-	-	-	-	1.07	0.96
-	-	0.6	-	-	-	-	0.95	0.96
-	-	0.4	-	-	-	-	0.84	0.96
-	-	-	0.8	-	-	-	1.17	0.93
-	-	-	0.6	-	-	-	1.13	0.90
-	-	-	0.4	-	-	-	1.10	0.87
-	-	-	-	0.8	-	-	0.96	0.77
-	-	-	-	0.6	-	-	0.72	0.58
-	-	-	-	0.4	-	-	0.48	0.39
-	-	-	-	-	5	-	1.06	0.93
-	-	-	-	-	10	-	1.20	0.96
-	-	-	-	-	15	-	1.37	0.99
-	-	-	-	-	20	-	1.58	1.02
-	-	-	-	-	25	-	1.86	1.04
-	-	-	-	-	30	-	2.24	1.07
-	-	-	-	-	-	40	1.84	1.11
-	-	-	-	-	-	30	0.77	0.84
-	-	-	-	-	-	25	0.48	0.74
-	-	-	-	-	-	20	0.29	0.68

Table 4.2: Parameter study of the driving conditions. If a dash is shown, the value of the top row applies.

The skin friction, helical friction, base resistance and CPT are expressed as a fraction of the original values as established in chapter 3. So a value of 0.8 means that the original is multiplied with 0.8. The diameter is in m and the angle of attack and angle of repose are given in degree. The value in the column of the soil-ground resistance is a fraction of the helical induced force over the soil-ground resistance at a depth of 42 m. These values are also shown for the original case in fig. 4.6. It can be seen there that the helical force is not smooth over the depth and has a maximum at 42 m. Therefore this value is given shown for a depth of 42 m. The value if this ratio determine whether the soil around

the monopile gets disturbed by the helicals. A values of 1 means that the force and the resistance are of equal magnitude, a value lower than 1 indicates that the resistance is larger than the exerted force. We have here arbitrarily chosen 0.95 as a boundary of the feasibility. The original value of the lower diameter is 12 m, the angle of attack 10 degree and the angle of repose 35.

If we examine the results as shown in table 4.2 we see that with the original values the principle of screwing is hardly feasible. Not only does it require an extreme driving force, but there is also a change of disturbance of the soil. The table indicates that reducing the magnitude of the CPT and angle of repose has a dramatic effect on the feasibility. In this research we based our conditions on a challenging CPT. The angle of repose can also be considered on the high side; a value of 28 degree for example is not uncommon. Since those parameters are initially chosen conservatively, we now explore the effects on decreasing them together.

Parameters		Feasibility indicators	
CPT	Angle of repose	Required driving force x10^3 MN	Soil-ground resistance
1	35	1.20	0.96
0.9	35	1.0	0.88
0.8	35	1.01	0.81
0.7	35	0.91	0.73
0.6	35	0.813	0.66
1	32.5	0.96	0.90
0.9	32.5	0.89	0.83
0.8	32.5	0.81	0.76
0.7	32.5	0.74	0.69
0.6	32.5	0.66	0.62
1	30	0.77	0.84
0.9	30	0.71	0.78
0.8	30	0.65	0.71
0.7	30	0.60	0.65
0.6	30	0.58	0.60
1	27.5	0.614	0.79
0.9	27.5	0.57	0.73
0.8	27.5	0.52	0.68
0.7	27.5	0.48	0.62
0.6	27.5	0.43	0.57
1	25	0.48	0.74
0.9	25	0.45	0.69
0.8	25	0.42	0.65
0.7	25	0.38	0.60
0.6	25	0.35	0.55

Table 4.3: Parameter study by various combinations of the CPT and the angle of repose

Table 4.3 gives the results for both varying the CPT-values and the angle of repose. In section 4.4, table 4.1 we established the allowable driving forces for various diameters and thickness. For the original upper diameter of 8 m and thickness of 80 mm, we read that the maximum driving force is 416 MN. According to the required driving force in table 4.3, this turns out to be only feasible with an considerable reduction of both the CPT-values and the angle of repose. We can also read in table 4.1 that an increase of the upper diameter to 10 m while keeping the thickness of 80 mm, causes the maximum lower tangential force to be 652 MN. If we compare this value to those in table 4.3, we see that a moderately small reduction of CPT-values and angle of repose enables the monopile to reach the desired

depth, while keeping the stresses within the limits of the monopile and the soil. Therefore we will modify the monopile by increasing the upper diameter to 10 m, while the thickness remains 80 mm. This adds 95 tons of mass to monopile, which is an increase of 4 percent. For terms of manufacturability this increase is technically straightforward, since the maximum diameter stays the same. It can therefore be applied rather effortlessly into the production process. The two major design changes are the stands where the monopile rests on during transit and the flange and upending tool, which all are to be adjusted to the bigger size. Since dimensions of monopiles vary currently as well for different locations, this will not lead to major technical implications. The largest consequence however, is not the monopile itself, but the TP and the tower of the wind turbine. These need to connect to the monopile and therefore have to grow as well.

If we consider both the soil-ground resistance and the maximum allowable driving force, we read in table 4.3 that a 0.8CPT and an angle of repose of 25.7 gives a driving force in the order of 500 MN. Furthermore, the ratio between the soil and ground resistance is 0.68, well below the threshold of 1. However, if the ratio is plotted over the depth, it shows that only after a depth of 15 m, the induced force becomes smaller than the soil-ground resistance, as is shown in fig. 4.7. We aim to increase the soil-ground resistance with the design of the helicals, as will be discussed in section 4.6.

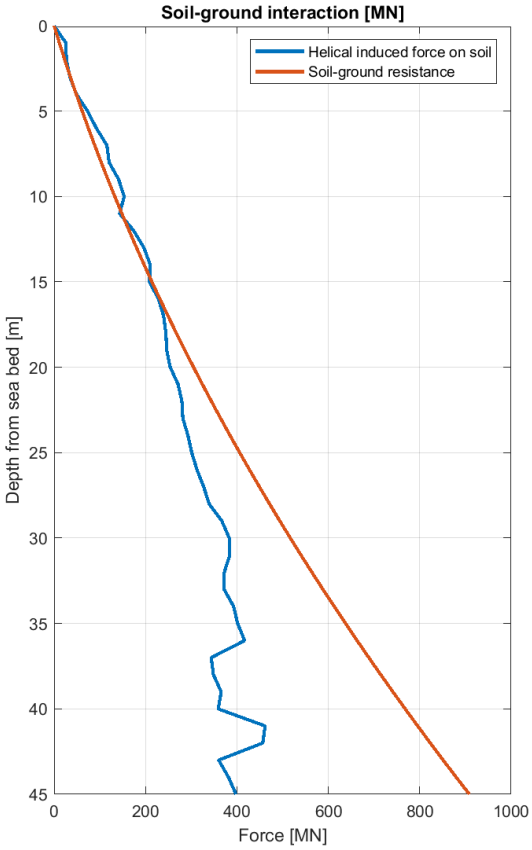

Figure 4.7: The ratio between the force applied by the helicals and the soil-ground resistance with the re-established soil conditions; a CPT of 0.8 and an angle of repose of 25.7 degree.

Further research would be required to determine what decrease of the CPT-values and angle of repose

are safe to assume. Since we already used conservative data and ultimately want to determine the feasibility, we will base our further design on a required driving force of 500 MN at a radius of 6 m. This would correspond to a decrease of the CPT-values of 0.8 and an angle of repose of 27.5 degree. Furthermore, it keeps the stress inside the monopile 20 percent under the determined allowable stress level without increasing the wall thickness.

4.6 Cross-sectional design

Up until now we have worked with a theoretical helical design and computed the results using eq. (4.6). In this section we will determine the final design of the individual helicals, and the placement of the screw thread on the monopile.

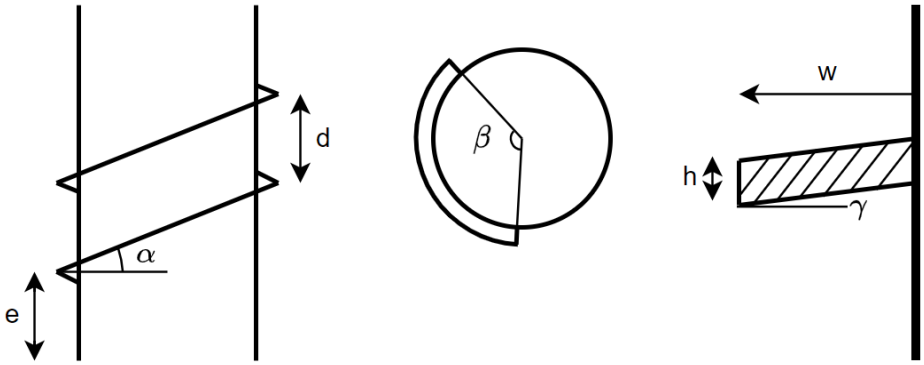

Figure 4.8: Schematic depiction of the helicals with the relevant parameters.

Parameter	Value	Description
e	0.4 m	Distance between the base and the first helical
α	15 deg	Angle between horizontal and helical
d	1.68 m	Distance between two helicals
β	714 deg	Contour of the helical
w	0.6 m	Width of the helical
h	80 mm	Height of the helicals
γ	20 deg	Bank angle of helical

Table 4.4: Description of the corresponding parameters in fig. 4.8.

Parameters helicals In fig. 4.7 we showed that the ratio between the force applied by the helicals and the resistance the ground can cope with, is in the order of 1 for the first 15 m. This indicates that there is a reasonable chance that the soil will be disturbed. However, if the helical is placed under an angle γ with respect of the wall of the monopile as is shown in fig. 4.8, it will push the soil slightly outwards and thus creating a stiffer soil-ground interaction. This will increase the resistance between the soil and the ground, and therefore decrease the ratio to acceptable values. Based on the results as shown in fig. 4.7, which are obtained using eq. (4.6), we can use superposition to calculate the influence of the angle γ. The outward pushing soil-ground-force F_{sg} is calculated with

$$F_{sg} = F_h tan(\gamma) \tag{4.11}$$

where F_h is the force that is excited by the helicals onto the ground and γ is the angle between the cross section of the helical and the horizontal plane. Then F_{sg} is added to R_{sg}, which results in a larger soil-ground resistance. fig. 4.9 shows the results for angles of 5 to 20 degree. It can be seen that with an angle of 20 degree the force that is applied on the soil, is less than the resistance between the soil and the ground, indicating that the soil will not be disturbed.

For this principle we assume that because of the passive pressure coefficient, the soil is not pushed outwards. Furthermore, this additional soil-ground resistance does not come free. It increases the rotational resistance. However, since the angle is comparatively small and in principle does not do

work in the direction of rotation, we assume that the contribution to the resistance is small compared with the tangential force of 500 MN as established earlier. Lastly, the vertical force that the helicals are required to apply remains the same since the angle has no effect on the vertical resistance.

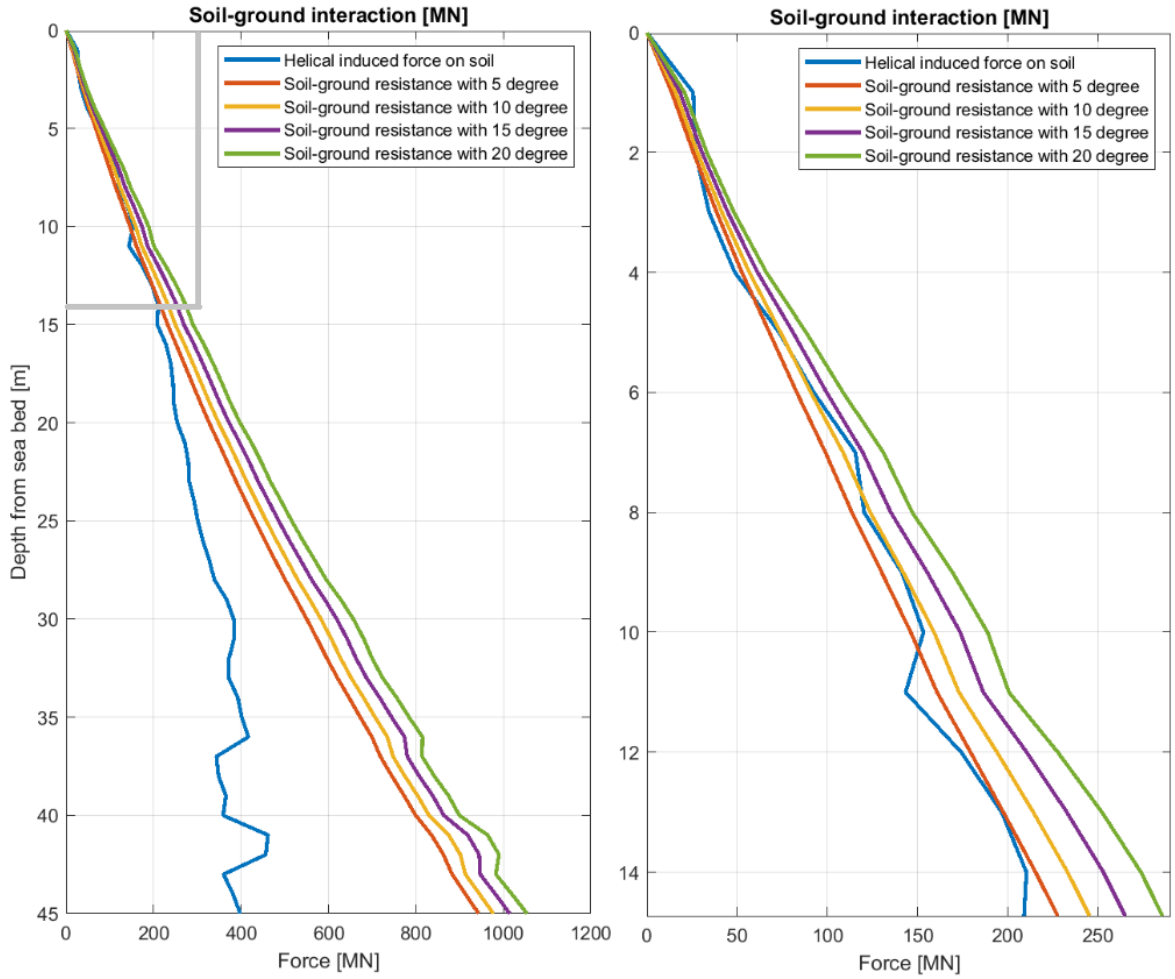

Figure 4.9: Graph of the soil-ground resistance for angles γ of 5 to 20 degree. At the right a close up of the first 15 m.

Helical induced force [MN]	Soil-ground resistance per meter [MN]	Sum of 15 m helicals [MN]	Sum of 17 m helicals [MN]	Sum of 20 m helicals [MN]
18	20	20	20	20
26	12	32	32	32
34	15	47	47	47
48	17	64	64	64
73	22	86	86	86
92	20	106	106	106
115	22	128	128	128
120	16	144	144	144
141	22	166	166	166
153	19	185	185	185
143	11	196	196	196
174	27	223	223	223
196	24	247	247	247
210	21	268	268	268
208	16	264	284	284
228	24	276	308	308
239	21	282	309	329
244	20	285	317	349
246	19	282	321	368
254	21	283	325	369
271	25	286	328	382
279	22	292	330	389
281	20	290	328	392
292	24	295	336	394
301	23	307	337	397
312	25	305	343	400
327	27	308	359	411
339	26	313	358	415
367	32	329	366	428
383	28	333	373	445
384	23	335	380	441
372	19	334	375	436
371	23	338	377	438
392	32	349	389	454
401	28	352	398	458
416	30	360	407	467
343	-1	339	381	446
348	27	342	386	454
365	32	351	398	465
359	24	350	398	464
461	64	387	439	506
456	25	386	439	511
360	-8	346	404	479
381	36	354	414	492
398	34	365	416	501

Table 4.5: Condition for determining the length of the screw thread over the monopile. When the sum of the soil-ground resistance with the lenght of the given screw thread is larger than the helical induced force, the soil will not be disturbed.

Length of the screw thread Determining the design is an iterative process based on the graphs as depicted in fig. 4.9. In essence the total helical force has to be smaller than the total soil-ground resistance. First we explore what portion of the length of the monopile requires helicals. In fig. 4.9 it

can be seen that till 15 m depth, the helical force is just slightly less than the soil-ground resistance. This means that at least 15 m of helicals is required. Deeper than 15 m though, the total helical force becomes significantly less than the soil resistance. This might mean that also at a larger depth, 15 m of helicals could be sufficient to transfer the helical force to the ground. To find out whether this hypothesis is correct, we have put the helical induced force, the soil-ground resistance per meter and the sum of the soil-ground resistance of the 15 m above in table 4.5. As long as the sum of the resistance is larger than the induced force, the helicals are indeed sufficiently placed over the monopile. With 15 m however, the soil could not cope with the helical force at certain depths. When we increase the length of the helicals to 17 m, all values of the total helical force are below the maximum force the soil can cope with. Still, with 17 m of helicals the difference is not always large. Given that we want to make sure that the principle works, we also explore a length of 20 m. With this length, all well below the maximum force. Therefore we are considering a screw thread length of 20 m from here on. To be able to handle the monopile during the welding of the helicals, the helicals start at 0.4 m from the bottom. This gives room for the rollers to support the monopile. It must be noted that the length of the screw thread is determined for the above established soil conditions. If those conditions change, this could have an influence on the screw thread length as well.

Design and spacing of the helicals For piles with a small diameter the ratio between the helical spacing and the helical diameter determines the design and placement of the helicals. However, with large, hollow piles such as monopiles, this theory does not hold anymore, because the inner soil must also be taken into account and the spacing will become too large, although it is not directly obvious what the boundary exactly is. The same principle holds however, that the design depends on the soil characteristics, which are for an important part determined by the angle of repose.

For determining the design of the helical we follow an iteration process. The first step is considering the force that is applied to soil by the helicals, as is depicted in fig. 4.9 as the helical induced force on soil. It can be seen that the largest force that must be delivered is 500 MN. With a screw thread of 20 m long, this is on average 25 MN per m screw thread length. If we assume now a beam structure of 1 m long along the wall of the monopile, it must cope with $25/\pi D = 0.66MN$. An impression of the beam structure is shown in fig. 4.10. The second step involves assuming that the force acts at the center of the beam so can use the beam model to determine the bending stress with $\sigma = My/I$. This gives the maximum stress, which must not exceed 355 MPa. Furthermore, the ratio of the spacing between the helicals and the width is kept in the order of three. This appears to be a ratio where the soil does not get stuck within the thread, but still maximizes the number of helicals. Although in principle we would want as little helicals as possible, we do need enough to prevent them from bending. After fitting the dimension to obtain the maximum allowable bending stress, we found that a helical height of 80 mm and a width of 0.6 m gives a bending stress of 335 MPa. The thickness is equal to the wall thickness of the monopile. Since the beam structure has an angle of 15 degree, it also adds to the integrity of the structure of the monopile. One disadvantage however, is that the individual helical does have a rather complex shape. With the width of 0.6 m the spacing is set at 1.8 m. The third step is to obtain the number of helicals. With a spacing of 1.8, the horizontal distance of the helicals can be derived by $1.8/tan(15deg) = 6.7m$. With a circumference of 37.7 m this gives us room for 5.6 helicals. Since only natural number are possible we will use 6 helicals that run 20 m high. The fourth and last step is to determine whether the dimension of the helicals can be optimized given the new spacing. With 6 helicals the horizontal distance is $37.7/6 = 6.28$ and the spacing becomes $6.28tan(15deg) = 1.68m$. With the smaller spacing, the ratio also decrease slightly to 2.8, so it stays in the order of three. The smaller spacing also has as a consequence that the individual helicals need to apply less force, resulting in a lower bending stress of 131 MPa. This reduction is however not enough to optimize the dimensions of the helicals.

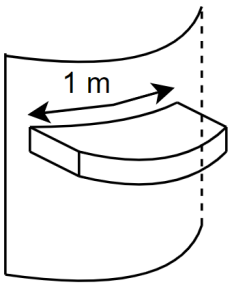

Figure 4.10: Schematic depiction of the beam structure of which the helicals are made of.

With the information we have established in the previous and this chapter we can make a final design of the monopile. In fig. 4.11 this monopile is presented.

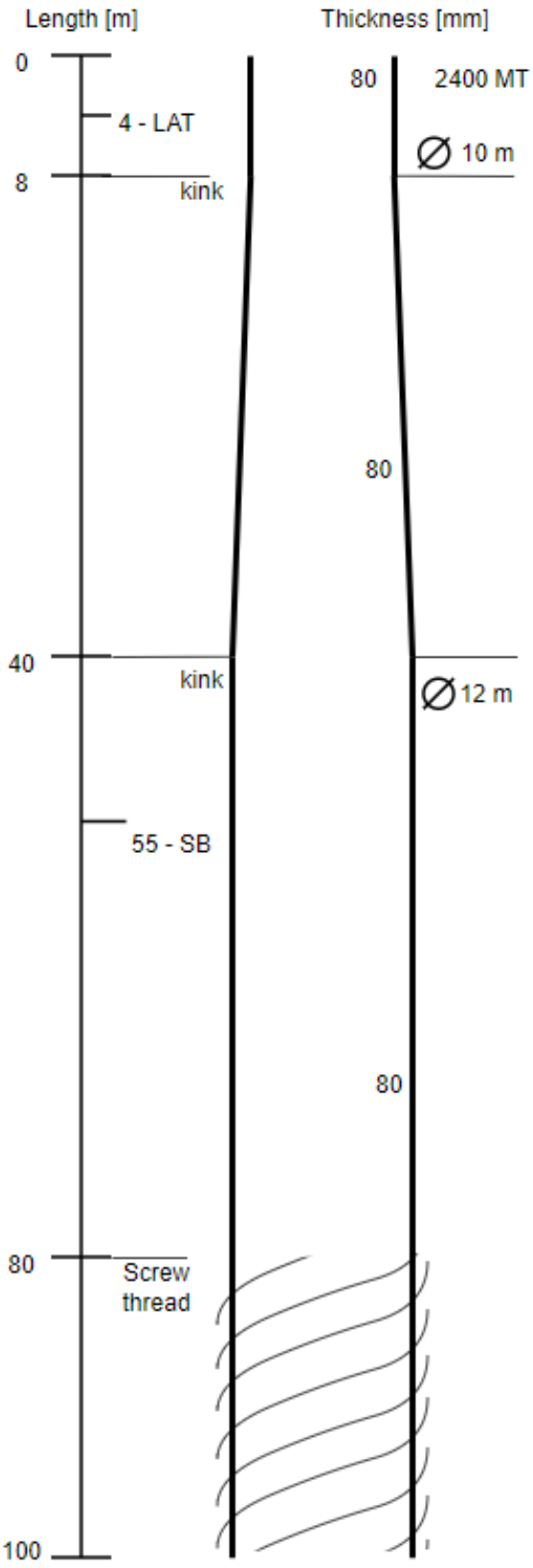

Figure 4.11: Final design of the monopile including the dimensions and the screw thread.

4.7 Conclusion

In this chapter we derived a model for the requirements of the helicals and subsequently the required tangential force acting on the lower part of the monopile. To determine the feasibility of the principle of screwing, we established design conditions for the monopile and soil. It turns out that with the original dimensions and soil data the principle of screwing is not feasible. The stresses inside the monopile are to high and the soil has a high probability of getting disturbed by the helicals. To investigate under what conditions the principle is feasible, we set up a parameter study where we vary both the design of the monopile and the values of the soil. We find that with a decrease of the CPT-values by a factor of 0.8 and an angle of repose of 27.5 degree, the monopile is able to penetrate the ground to the desired depth if it has an angle of attack of 10 degrees. An increase of the upper diameter to 10 m ensures that the stresses remain below the maximum allowable stress. The design of the monopile has thus changed, but since the largest diameter is still 12 m, it has relatively minor implications. The placement, spacing and design of the helicals are also derived and given in table 4.4. Finally, the design of the entire monopile with helicals is shown.

Although the design is based on soil mechanics, some assumptions are made. Further research would be required to determine what reduction of CPT-values and angle of repose are realistic and safe to assume. Furthermore, the behaviour of the soil around the helicals is simplified to enable the calculations. However, in reality the behaviour can by very complex around the helicals. This might have an consequence for the performance of the helicals, and thus for the driving requirements. Further research must be done at the this subject to determine these consequences. For validation of the model and assumptions, a real life test can be done with a smaller pile. However, one must be careful to scale the design the same in every direction. The validation is therefore also a topic for further research.

5. Driving mechanism

In this chapter we give an overview of what a driving mechanism could look like and what the critical boundaries and requirements are. Firstly we determine the required power demand for driving the monopile and discuss electric and hydraulic drive. Then we consider the connection between the ship and the monopile. This connection is challenging because the monopile has besides an angular velocity, also a vertical displacement. The connection therefore has to compensate for the height difference as well. Thereafter, we discuss two driving principles: a rack and pinion type and one with hydraulic cylinders. We focus on these principles because they can cope with the extreme forces that are required. The advantage of the geared principle is that it can continuously drive the monopile, whereas the cylinders can only rotate the monopile in steps. Lastly, we shortly analyse the reaction of the pile driving on the ship. We will consider a dynamic positioned vessel and a jack-up vessel. As concluded in chapter 4, we consider a required tangential force at the lower part of the monopile of 500 MN or 3000 MNm. Note that we discuss the above topics at a high level to determine feasibility, rather than to make a detailed design. In the final section we give an overview of the possibilities with their advantages and downsides.

5.1 Driving power

The required power to screw the monopile into the ground is derived as a function of the time it takes to reach the desired depth and the required force to do so. With the current installation methods of piling and vibrating, the driving time varies from 1.5 to 5 hours, depending on the size of the monopile and the conditions in the ground. Considering that we want an alternative for the current installation methods, we aim for a driving time within this range.

In chapter 4 the maximum tangential driving force is set at 500 MN at the maximum penetration depth of the monopile. We approximate the driving force over the depth by linearization of the required force, as shown in fig. 5.1.

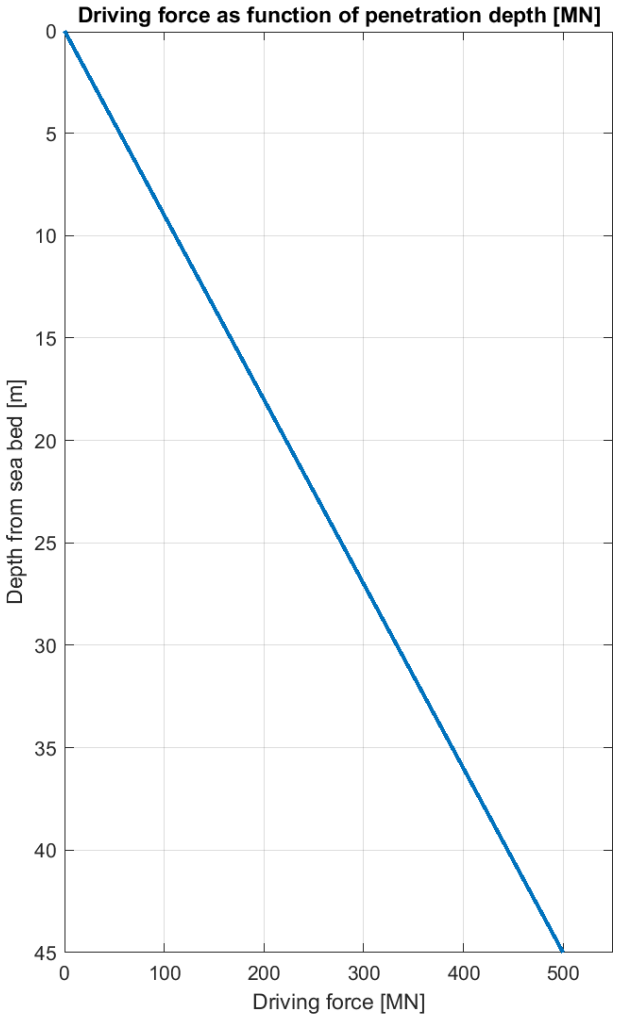

Figure 5.1: Linearized driving force as function of the penetration depth with a maximum of 500 MN.

With an angle of attack of 10 degrees and an assumed AR of 1 as described in section 4.4, the number of rotations is

$$r = \frac{d}{Dtan(\alpha)} \tag{5.1}$$

where d is the penetration depth, D is the lower diameter and α the angle of attack. With the dimensions of the monopile the number of rotations is 21,27. When we start by assuming a driving time of 1 hour, this would translate into an average angular velocity of 0.012 rad/s or a wall velocity of 0.07 m/s. The maximum power output is then calculated with

$$P_{0.012,45} = F_t r\omega = 500 \cdot 6 \cdot 0.012 = 35MW \tag{5.2}$$

where $P_{0.012,45}$ is the power at 45 m depth and 0.012 rad/s, F_t is the tangential force, r the radius and ω the rotational velocity. 35 MW is quite a large power requirement. To put it into perspective, a thruster of a ship typically has a power output of 5.5 MW and a bubble curtain consume about 5 MW. If we would use 10 MW of power supply for driving the monopile, i.e. using the power source of 2 thrusters, the

monopile would have a final rotational velocity of

$$\omega = \frac{P}{rF_t} = \frac{10}{6 \cdot 500} = 0.0033 rad/s. \tag{5.3}$$

We have to emphasize however, that this is the rotational velocity at the maximum depth and with the maximum resistance. At lesser depths, the resistance is considerably smaller. Because the model for the skin friction is built for slow movement and the equipment is not designed for high speed, we limit the rotational velocity at small depths. At a depth of 9 m and a power of 10 MW, the angular velocity is 0.017 rad/s, or a tangential velocity of 0.1 m/s. Although hard limits for the soil-pile-model are not defined, this velocity is small enough to be certain that the friction model will hold and the driving equipment can transfer the power. 0.017 rad/s is therefore set as the maximum angular velocity. To analyse the angular velocity for various power ratings, we used eq. (5.3) for 5 to 30 MW. The results are shown in fig. 5.2. Note that for all power outputs, the maximum angular velocity is thus 0.017 rad/s.

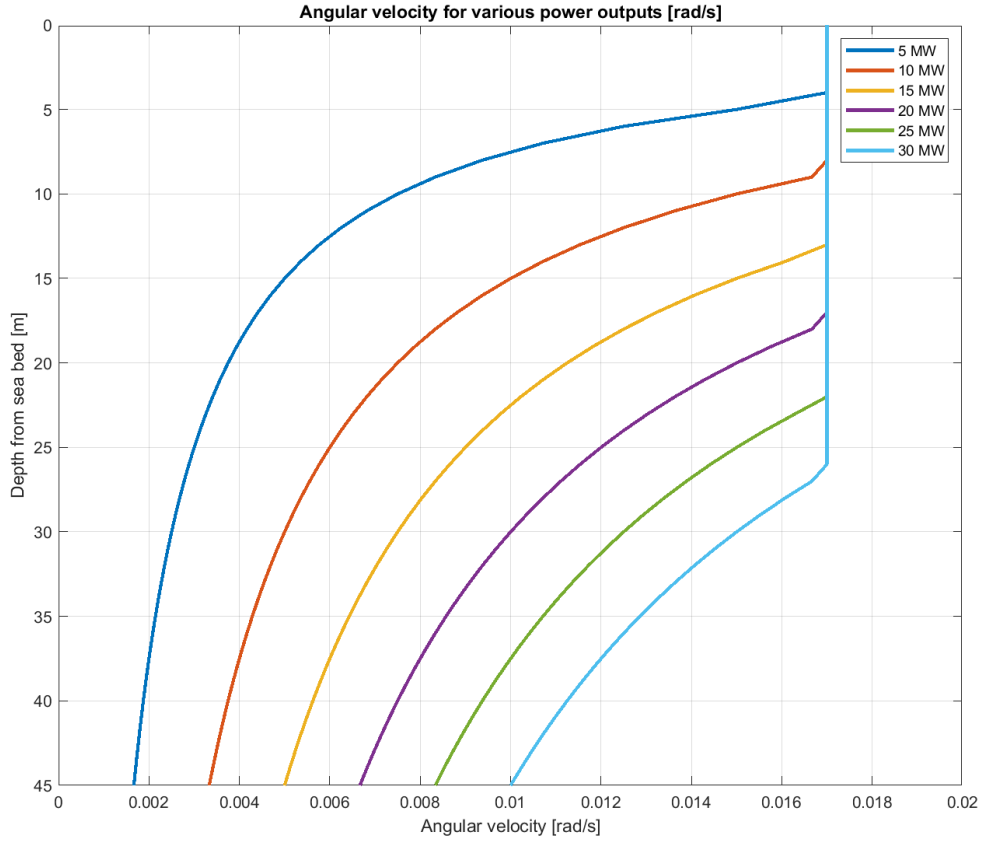

Figure 5.2: Profile of the angular velocity over the depth for power outputs of 5 to 30 MW.

The velocity profiles from fig. 5.2 are used to determine the piling duration. These are given in table 5.1. It shows that the duration drops quickly with increasing power output. Note the power output only reaches its maximum power when it can not drive the pile with a angular velocity of 0.017 rad/s. A power output of 15 MW is in the same order as is currently used for the installation of monopile. One thing that should be considered is the heat dissipation in the soil. In principle the energy that is put into the monopile, dissipates into the soil as heat. This could have an influence of the resistance and helical performance. It appears however, to only have a small contribution and is therefore not further

explored in this thesis.

In this section we considered a minimum theoretical power requirement regardless of possible driving mechanisms. However, in reality the power requirements and driving mechanism are depended on each other. In this feasibility study we look at electric and hydraulic driven equipment. Both are used for many years, so offshore installation companies are familiar with it. They are also reliable and operator friendly and, in this case most important, very efficient. Table 5.1 therefore only gives an order of magnitude for the required power, corresponding to the duration of installation as shown in fig. 5.2. If a final choice for a driving mechanism and for an electric or hydraulic drive is made, efficiencies and driving properties have to be considered to determine the ultimate power requirements. However, generally speaking one could estimate an efficiency in the order of 85 percent for hydraulic drive due to friction and leaks in the hoses and seals. For electric drive an efficiency of 95 percent of the electric motor and 99 percent for every gear can be reckoned.

Power output [MW]	Time [h]
5	2.1
10	1.3
15	1.1
20	0.9
25	0.8
30	0.7

Table 5.1: Piling duration per power output, ranging from 5 to 30 MW.

5.2 Connection

The torque must be transferred from the ship to the monopile. Since extreme forces are involved, this connection must be made extremely heavy. A further factor which makes this challenging is that the monopile has a vertical displacement of 45 m with respect to the ship. To cope with this height difference, we look at first at the principle of a pile driver lead, and then at a ball spline bearing principle.

Pile driver lead The principle of the pile drive lead has its origin at the onshore pile driving industry. It has a lead which travels via a guidance rail in vertical direction. At onshore piling equipment the lead contains the mechanism to lift the hammer that falls onto the pile. As the pile sinks into the ground, the lead goes down with it. In fig. 5.3 a regular piling rig is schematically shown.

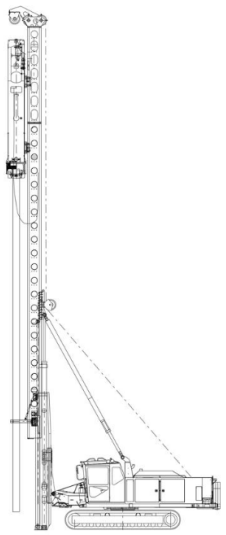

Figure 5.3: Schematic depiction of a onshore piling rig [7].

This type of rig also exists as a drilling rig. Instead of piling equipment, the lead contains drilling equipment. In essence the pile driver lead is an upscaled version of the same principle. In fig. 5.4 such a principle for offshore application is shown. In this case the monopile is driven from the side of the ship. From the back is also possible, but it is common that the crane is placed at the stern. It is clearly visible that a massive construction has to be build on the deck to accommodate the lead. This construction has to be able to cope with the forces to drive the monopile. A fortunate advantage however is, that the maximum force occurs at the lower depth, and thus at the lower part of the construction. This allows for a efficient design which prevents a top heavy construction on board.

Lastly, one of the main advantages of the pile driver lead principle is that the driving mechanism can be connected via the flange of the monopile. Unlike the other connection types as described in the next paragraphs, no additional tools or appendages are necessary to connect the monopile. Furthermore, the lead function thus also as the gripper. Normally the gripper holds the monopile in place and upright, until it penetrated enough to stand on its own. Since the driver lead keeps the monopile in place, the gripper is not required when this connection type is used.

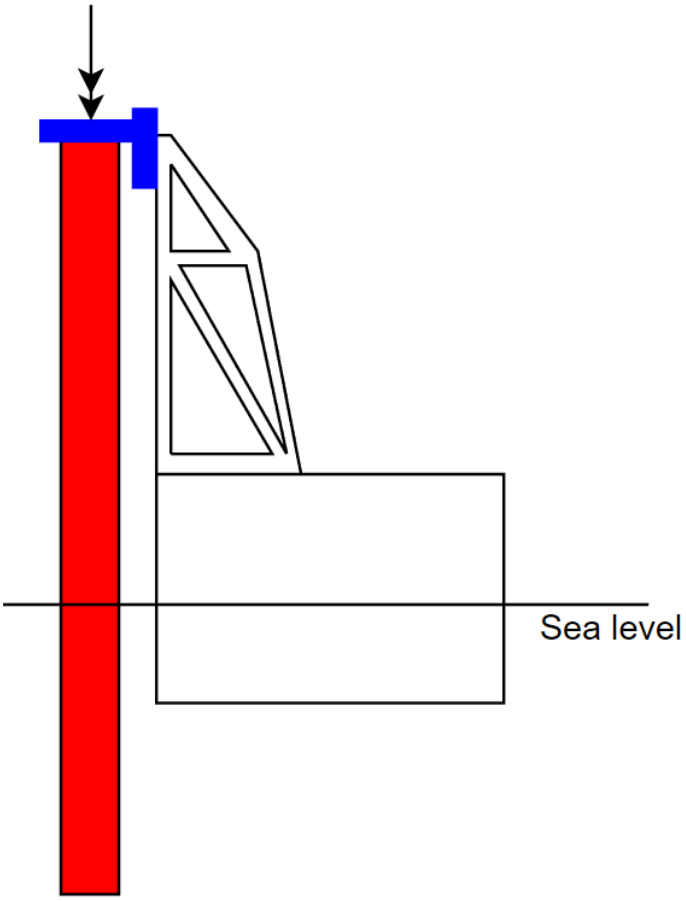

Figure 5.4: Schematic principle pile driver lead.

A possible contender for this principle is the Svanen hefschip. It currently has a hoisting height of 72 m above deck. That does not necessary mean that a lead could reach the same height, however, with the model monopile, a lead height of 55 meter would be sufficient. If indeed the Svanen would be used, the monopiles need to be brought floated since it has no deck space, nor a movable crane.

Figure 5.5: The Svanen has a construction that enables the pile driver lead principle [8].

Gripper-sleeve The gripper-sleeve principle uses a classic pile gripper, but between the monopile and the gripper is a sleeve located. In the next paragraph the same principle is used without a sleeve.

The function of the sleeve is to transfer the torque. It does that with splines that fall into the ring that applies the torque to the pile. With roller bearings the ring can apply the torque, while allowing vertical displacement as well. This means that a regular sized gripper can be used. In fig. 5.6 this principle is schematically shown. The sleeve is depicted in red, and is connected to the flange of the monopile. This connection is shown in yellow. The sleeve is pre-equipped with bolts that fall into the flange. Since the flange only has to transfer a torque, it might not be necessary to fasten the bolts. The reason a sleeve is used, is to avoid appendages on the monopile, other than the helicals.

The main disadvantage of the sleeve-principle is that the tapered section of the pile is higher than the gripper if it stands on the sea bed. Normally the rollers of the gripper can adjust for the varying diameter. To incorporate such a principle into the driving mechanism would be highly complex. A solution is to keep the rollers to guide the monopile while installing the sleeve. Once the sleeve is connected the rollers can retract to allow the monopile to rotate.

To avoid having to vary the diameter of the driving mechanism, a sleeve with a diameter that coincides with the diameter of the monopile could be used. Such a sleeve is shown in fig. 5.7.

Some last considerations are, that the sleeve is an extremely voluminous tool, which occupies valuable deck space, which other wise could have been used for the transport of monopiles. It also adds another time consuming step in the installation process, since the sleeve has to be hoisted over the monopile. Connecting the sleeve in advance would be to complex, since it has to be upended as well. To end with an advantage, the sleeve adds some extra weight to the monopile, in the order of 1000 ton depending on the design, although the contribution to the penetration ability might be small as shown in fig. 3.12.

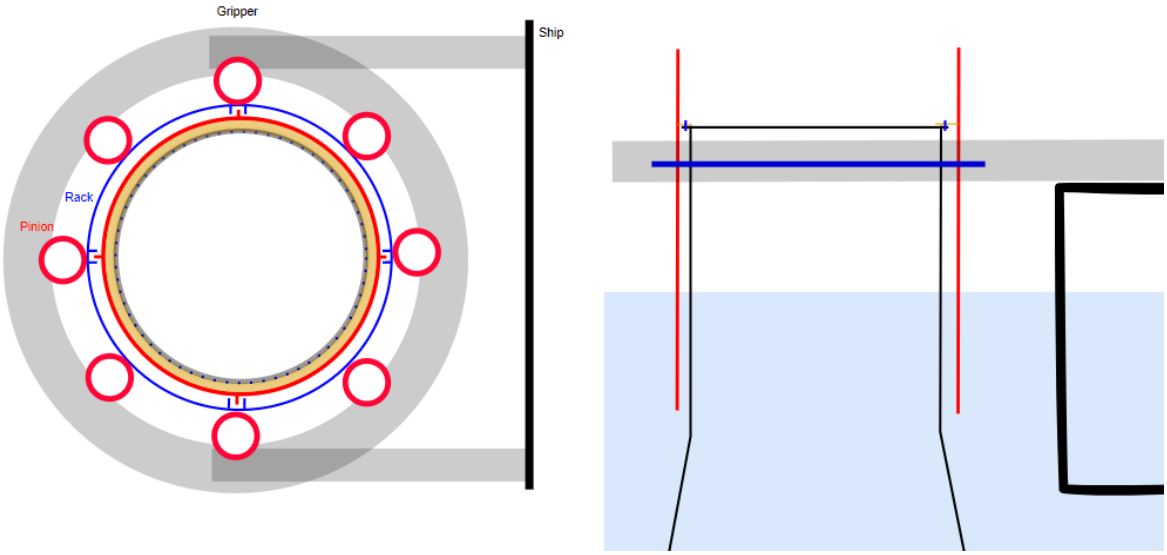

Figure 5.6: Principle of the gripper-sleeve connection. In this example driven by a geared driving mechanism. For explanatory reasons the dimensions are not to scale.

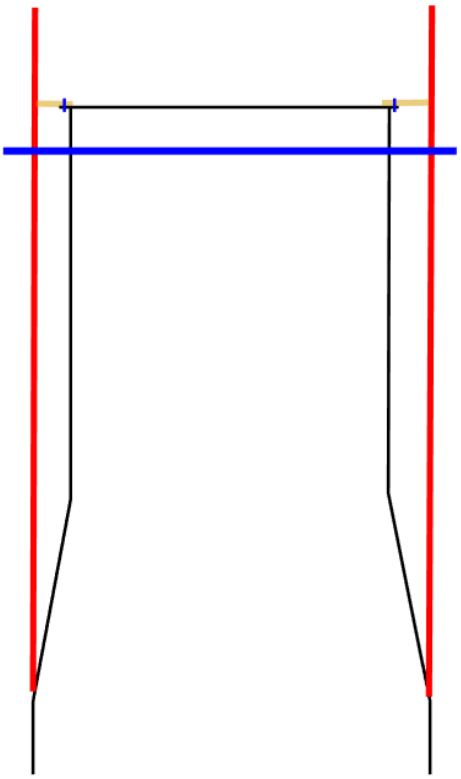

Figure 5.7: Sleeve with maximum diameter, equal to the lower part of the monopile.

Gripper-spline The gripper-spline principle functions similar to the gripper-sleeve principle, with the difference that the splines are welded directly onto the monopile, rather than onto the sleeve. This obviously has the downside that it adds complexity in the production process, as will be discussed in section 6.1. It also means that the initial design of the monopile has to be further modified to cope with the tapered section. Given the height of the monopile and the depth of the sea bed, the gripper encounters a varying diameter. With regular grippers it is conceptually easy to compensate for this, because the guiding rollers only have to allow for vertical displacement of the monopile. In this case however, the gripper also has to apply a torque onto the monopile, causing a tapered section to be too complex. Especially because with a increasingly narrower pile, the involved forces have to increase as well. This can be avoided in two ways. The first is to decrease the length of the tapered section such, that the gripper only encounters the upper part of the monopile. This does influence the bending resistance though, on which the monopile is predominantly loaded during operation. The second is to increase the upper diameter to coincide with the lower part. Not only is does this solve the driving problem, it also causes more resistance to buckling and bending. A downside however is that the tapered section has to be incorporated into the mast of the wind turbine. Furthermore, the smaller diameter at the upper part avoids unnecessary impact from waves. Increasing the diameter also increases the impact from the harsh environment. Lastly, adding appendages on the part of the monopile that is submerged in water can cause accelerated corrosion. Edges, such as those of the splines, are difficult to apply a proper layer of paint on so they are likely to corrode at first. Given that they need to be used only once, this might not lead to problems. Finally, welding splines onto the monopile will results in certain stress concentrations. The swaying of the turbine can subsequently cause fatigue in these points, either reducing the lifetime of the turbine, or making it necessary to increase the dimensions of the wall thickness.

5.3 Geared driving mechanism

For determining the requirements of a driving mechanism with gears, we assume a rack and pinion principle. The rack is located at the outside of the monopile while the gears are fixed to the ship. Since the rack has to fall over the monopile, we assume a diameter of 10.5 m, 0.5 m larger than the upper part op the monopile. This gives room for the rack. In fig. 5.8 the principle is schematically shown. The gripper is depicted in grey, the pinion gears in red and the rack in blue. This figure shows the gear driven principle together with a sleeve, which is here red, with a yellow connection to the flange where the bolts are shown as dots.

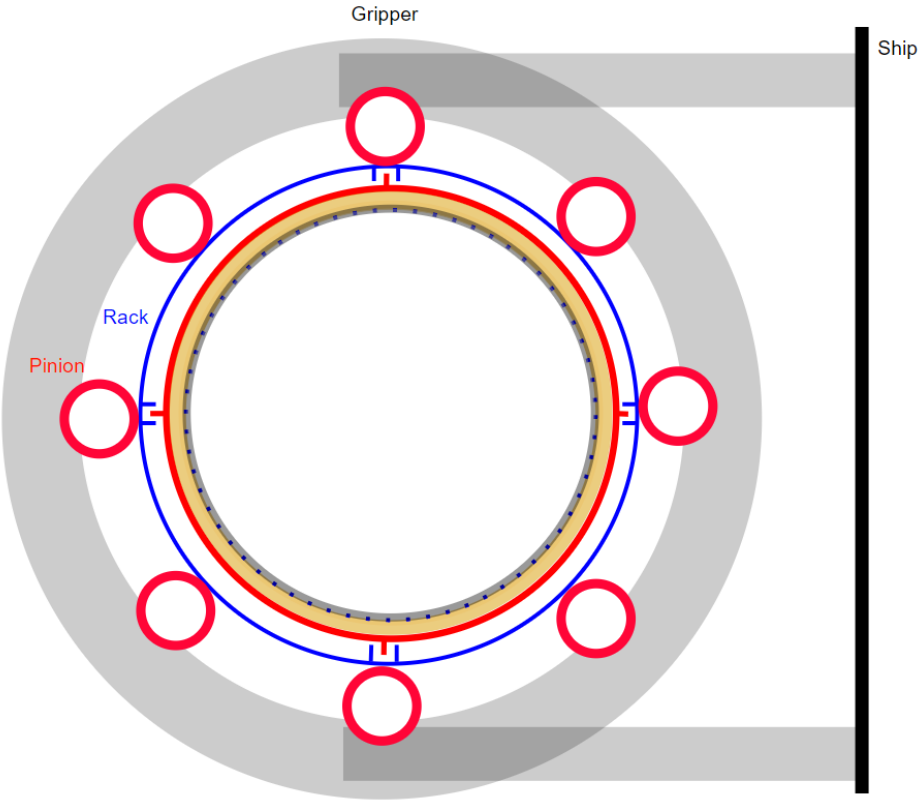

Figure 5.8: Schematic principle of the geared driving mechanism.

As discussed in the previous section, the diameter at which the force to the monopile is applied, varies depending on the connection type. For the power consumption this variance in diameter does in principle not matter, but for the force that has to be applied it does. To cope with the different connection types we have calculated the maximum required tangential force for multiple diameters. These are listed in table 5.2.

Upper diameter [m]	Maximum force [MN]
10.5	571
11.5	522
12.5	480

Table 5.2: Maximum force as function of upper diameter.

One critical limitation of the geared principle is the maximum force a pinion gear can transfer to the rack. The maximum force is determined by the maximum stress. For a gear tooth the maximum stress

is derived by

$$\sigma_t = \frac{2.2F_t}{Mt_w} \tag{5.4}$$

where σ_t is the stress in the gear, F_t is the force that is acting on the gear, t_w is the width and M and 2.2 are the module and corresponding factor for the equivalent base of the gear.

The maximum allowable stress in the gears σ_t is $240MPa$. Heavy gears have an module of $M = 50mm$ with an maximum width of $8M = 400mm$. If we use these numbers we get an maximum gear force

$$F_t = \frac{\sigma_t M t_w}{2.2} = 2.2MN \tag{5.5}$$

Based on the values of the peak force in table 5.2, the required number of gears is 571/2.2=260 for 10.5 m diameter, or 237 and 218 for 11.5 and 12.5 m in diameter respectively. These are impractically high numbers.

If we assume the motor gear assembly to have a diameter of 1 m and an placement at 0.5 m from the rack, the theoretical maximum number of gear assemblies is 36, 39 or 42 for the upper diameter of 10.5, 11.5 and 12.5 respectively. If we would have an upper and lower rack, it could be upgraded to 72, 78 or 84. This means there is at least a factor of 3.6, 3.0 or 2.6 between the minimum required number of gears and the maximum of possible gears.

In fig. 5.8 a schematic top view of the pinion-rack principle is given. In the shown configuration the gear-engine assemblies are placed vertically, with a maximum of 42 if the largest diameter is considered. This vertical configuration allows for a top and lower placement of the assemblies as well. Note that this drawing is made such, that it indicates the theoretical limits of a gear driven mechanism and is therefore not on scale. Based on the space around the monopile and the mechanical properties of the gears, this principle is not able to deliver the required force to rotate the monopile to the final penetration depth. Furthermore, apart from the above issues, 42 or even 84 gear-engine assemblies have a massive weight on the gripper and will be extremely expensive.

The final remark on the geared driving mechanism is the upending of the monopile. When a monopile is upended, it is tilted such that the lower part is directly lowered into the sea. This prevents costly lifting time. The gripper then opens and grabs the monopile. With the gear rack however, this is not possible. Given the required robustness of the rack it is preferably manufactured into a solid piece. An unfolding rack would be tedious since the enormous forces acting on it, and, in contrast to the gripper, it rotates along with the monopile. This makes fitting and controlling actuators practically impossible. This means that with the pinion-rack principle the must be hoisted into the gripper. With this procedures however, the gripper has to have a diameter large enough to let the lower part of the monopile through. If a splined monopile would be used, driven by hydraulic cylinders, one would avoid having the rack. Although the gripper must be extremely heavy, the method using hydraulic cylinders can be used with an openended gripper.

5.4 Hydraulic cylinders

To determine the feasibility of a hydraulically driven monopile, we consider the maximum force that can be applied by a hydraulic cylinder. This is given by

$$F_{hc} = \frac{\pi D^2 p}{4} = \frac{\pi \cdot 0.96^2 \cdot 32 \cdot 10^6}{4} = 32MN \tag{5.6}$$

where D is the diameter of the piston, with a max of 0.96 m and p is the hydraulic pressure which generally has a maximum value of 32 MPa. These are values of which is known that they are possible. If a diameter of 10.5 is assumed, a maximum force of 571 MN must be applied, as given in table 5.2. This means that 18 cylinders are enough to drive the monopile to a depth of 45 m. In fig. 5.9 a schematic top view of a possible lay out of the gripper is shown. In this example 10 cylinders are shown, but we consider a double layer of cylinder, 20 in total. Every cylinder needs to be controlled and actuated in order to be placed onto the spline. Not only in the horizontal plane, but also vertically since it has to be able to allow for the vertical movement of the monopile as well.

The spline at which the cylinder apply their force, needs to be thick enough to be able to cope with the enormous forces. If an stress of 340 MPa is allowed, the minimum area through which this force must be transferred is given by

$$A_{spline} = \frac{F}{\sigma} = \frac{32}{340} = 0.9m^2 \tag{5.7}$$

where F is the maximum force the a cylinder can deliver and σ the maximum stress. At the maximum depth the spline has to have base of $0.9m^2$. These are serious dimensions for a spline. If we assume that the cylinder has a foot of 1 m long, the spline needs to be 9 cm wide. Note that this is only for the top side of the monopile, since that would correspond to the maximum penetration depth.

If the pile drive lead principle is used, a transfer tool can be connected to the flange. Because it is not a one time use product, it can be made strong enough that it can cope with the extreme forces. Another advantage is that the speed can be higher in the beginning due to the smaller torque.

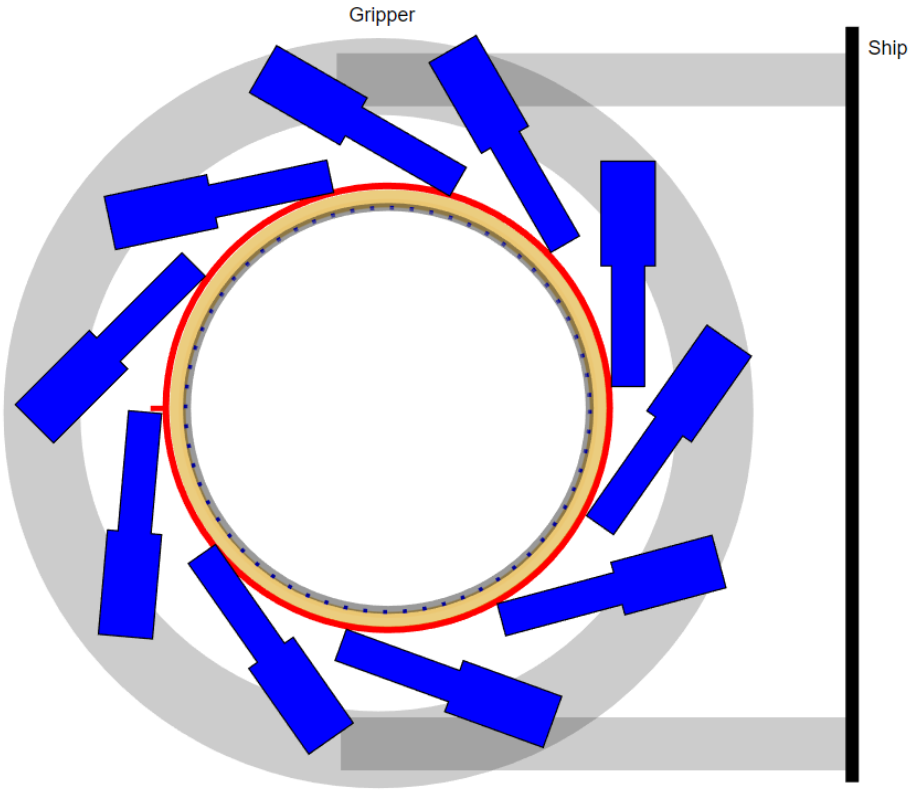

Figure 5.9: Schematic principle of the hydraulic driving mechanism.

5.5 Reaction on ship

In the off shore two types of installation vessels are common; jack-up vessels and dynamically positioned vessels (DP-vessels). If the screwing method would be used, it is therefore probable that the industry will use one of these methods, since these vessels already exist and they offer great flexibility and experience. To determine the feasibility we will look at the reaction on the vessels due to the torque applied on the monopile. We will base the calculations on two vessels which have representative dimensions to be adequate as a model for the whole installation field.

Jack-up vessel For the jack-up vessel we consider the Jan de Nul Voltaire [57]. This installation vessel is 170 m long and 60 m wide. The legs have a distance of 80 m from heart to heart. In fig. 5.10 a schematic top and side view of a jack-up vessel installing a monopile is shown.

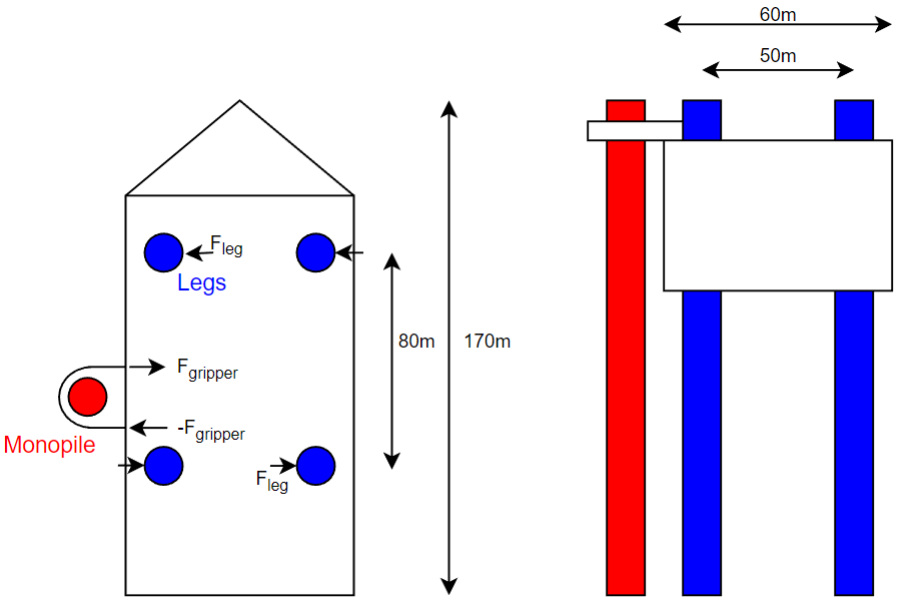

Figure 5.10: Schematic depiction of a jack-up vessel.

Although the ship is statically indeterminate, due to the dimensions it has some structural flexibility. Together with the fact that it is a relatively simple situation, we can assume that both front and rear legs experience equal lateral force. Given that the maximum torque on the monopile is 3000 MNm and the distance between the legs 80 m, the lateral force for each leg is $F_{leg} = 19MN$. This is a considerable force, especially if one considers that the legs are clamped in the hull of the ship. It can thus cause a substantial bending moment on the legs.

DP-vessel Calculations for the DP-vessel will be based on the DEME Orion [58]. This is a modern ship which is currently being used for the installation of wind farms. The length of the ship is 216 m and the thrusters are located at the very front and rear of the ship, with 180 m distance between them. In fig. 5.11 a top view of the ship with the locations of the thrusters is shown.

With a maximum torque of 3000 MNm and a distance of 180 m between the thrusters, a thrust of 16.7 MN has to be delivered if the monopile reaches the maximum depth. This is equivalent to 1600 ton. Thrusters have a wide variety of power outputs, with a maximum in the order of 140 ton bollard pull and a power of 7.5 MW. If we assume that each thruster can deliver 100 ton pull we are 1300 ton short at the bow, ignoring the power required by the DP-system. Since the bow has three thrusters with a maximum thrust of 1.3 MN and the distance between the bow and stern thrusters is 180 m, the maximum torque that can be applied on the monopile without lateral force is 700 MNm. This torque is enough to let the monopile penetrate to a depth in the order of 13 m. This torque figure is larger if lateral force on the monopile is allowed. This might be allowed when the monopile has already penetrated a substantial amount. Another way this figure can be enlarged, is when the inertia of the ship can be used. It takes time for the pistons to retract and push again against the monopile. If the thrusters keep applying the thrust during that time, the ship will turn against the rotational direction of the monopile. Using the inertia and the added mass of the water around the ship, a larger torque can be applied momentarily.

With a DP-vessel a considerable amount of power is drawn by the DP-system. The Orion is equipped with a DP3-system. This is a level of DP that enables a ship to continue its operations when a partial system failure occurs. This means that although it is equipped with numerous thrusters, it also needs a reserve for the situation if one would fail.

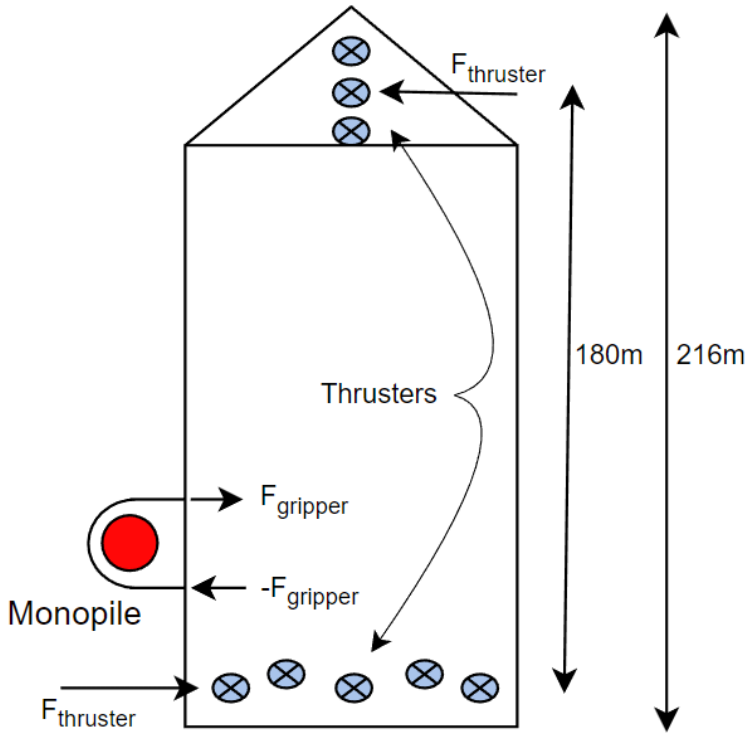

Figure 5.11: Schematic top view of a DP-vessel including its dimensions.

Apart from how the ship is hold in position, an important difference between a jack-up and DP-vessel is that a jack-up vessel is rigid while a DP-vessel moves about through the waves. Although it is able to stay on the same location within small tolerances, waves still cause the ship to heave, roll and pitch. In case of a DP-vessel the connection must therefore allow for movement in the vertical direction and rotation around the horizontal axes. Since the pile driver lead principle has a construction that towers high above the deck, the movement caused by rolling of the ship is large. Especially because at large heights the penetration depth is only small, and thus a non-wobbling monopile is desired. It is however particularly suitable to compensate for the vertical movement via the lead. The gripper-sleeve and gripper-spline principles are similar in that they both share the same type of gripper. The spline connection already allows for a vertical degree of freedom. The gripper therefore needs to be designed such, that it can rotate a few degrees around the x and y-axis. This adds another layer on the already complex design of the gripper.

5.6 Conclusion

In this chapter we explored possible connection types and driving mechanisms. It shows that due to the extreme forces that are required, not every option will work. The geared rack and pinion driving mechanism is limited by the force a tooth of a gear can transfer. It turns out that the number of gear-engine assemblies is so large that they can not be accommodated around the monopile. Also the use of a DP-vessel is ruled out since the DP-system can not deliver the thrust required to let the vessel stationary, especially since the system needs to position the ship itself as well. In table 5.3 an overview of the connection types and driving mechanism is given with their advantages and disadvantages.

If the connection and driving mechanism is robust enough, the driving duration is determined by the

	Advantages	Disadvantages
Lead pile driver	Regular upending Flange connection	Construction on deck Large sway when vessel rolls
Gripper-sleeve	Driving gear in gripper Integration in current vessel design	Extra (voluminous) tool
Gripper-spline	Driving gear in gripper Integration in current vessel design	Extra appendages on monopile Adapted monopile design
Rack and pinion	Electric and hydraulic	Inadequate maximum force Complex gripper design
Hydraulic cylinders	Relatively simple design Large force output	Only hydraulic Slower at greater depths due to retractiion of pistons

Table 5.3: Overview of the connection types and drive systems

power output. With a power output of 10 MW the duration will be in the order of 1.5 hour, depending on the driving mechanism. The hydraulic cylinders for example, need time to retract, prolonging the driving duration. In industry there is a slight preference for electric drive and DP, however it seems that it is not possible due to the extreme forces. Note that this also indicates what enormous forces are involved. In the chapter we have determined the possibilities using critical points in the design, such as the tooth of a gear. However, if a gripper is used to screw the monopile, it must have a considerable heavier construction than current grippers. And this applies for everything involved at the installation, making screwing a quite challenging driving method.

6. Logistics of the screwpile

Although with ordinary monopiles the logistics is well thought out, always is sought for improvements. For example the travel time from the port to the wind farm is a factor to be taken into consideration when designing an installation ship. However, this chapter will focus on the implications the helicals and the accessory equipment have with respect to the current logistics. We first look at the production of the monopiles, then at the transshipment and transport. Lastly we consider the installation itself.

6.1 Production

In essence the monopile is a rather simple product; a tube with a tapered end and a flange. The production process however is highly optimized. Only then the price can be kept relatively low. The design of the monopile itself is kept essentially the same in this research. However, at the lower part helicals are welded and, depending on the connection type as discussed in chapter 5, a spline at the upper part. The current production process does not take these appendages into account. The streamlined manufacturing must therefore be adapted, so to make production of the helicals possible, while keeping the efficiency.

As shown in section 2.4, the monopile is manufactured in one production hall in steps. From rings, to sections, to one monopile. Since the helicals and splines are intersecting multiple rings, at least the sections have to be made first. If designed such, that the appendages are placed at one section, the final assembly can be done after welding the appendages. However, the monopile lies on rollers, so at the support point the whole circumference needs to be free of appendages. In fig. 6.1 the side profile of a monopile is shown while it lays on rollers while in fig. 6.2 a monopile on rollers is shown in a factory. In this example it also has splines, although the upper part is also supported by a roller. It is also visible that the helicals do not start at the very bottom of the pile, but slightly up, to give room for the roller stands.

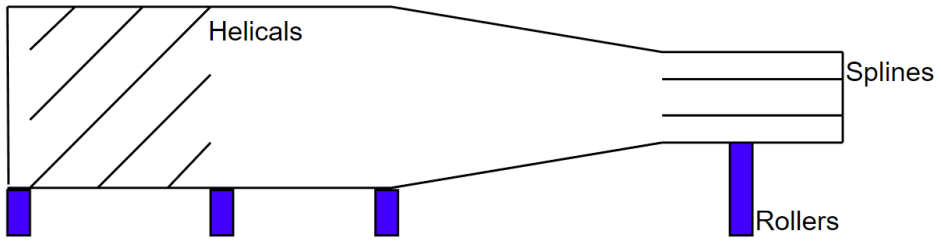

Figure 6.1: Profile of a monopile on rollers.

The production process of monopile is highly optimized. A helical is a however a rather complex shape which has to be rolled in the factory. Then it must be placed and welded onto the monopile. The rings and sections are welded by rotating them and keeping the welding machine stationary on the ground. For the helicals however, the welding machine can be guided by the helicals to move horizontally. It does require multiple passes and is therefore a time consuming process. Welding the helicals will thus be time consuming and therefore conflicting with the efficient production process.

Figure 6.2: Monopile on rollers in the production hall.

6.2 Transshipment and transport

One of the advantages of monopiles over jackets, is that they have a comparatively simple shape. This makes it possible to plainly lay them on a sandbank for storage, and on support stands during transport. It also enables easy transshipment because they can be easily picked up by a self propelled modular transporter (SPMT). Helicals and potentially splines can make this rather simple process very laborious. The monopile stands must therefore be designed to fit the specific monopile, such that no weight is put on any of the appendages. Normally monopiles are tailor made for a specific location. With the helical-monopile however, it is advantageous to keep the support points at the same location, so the same stands on the vessel can be used for an entire wind farm. Because the broad design of the monopile is essentially unchanged, the only critical point is that the appendages do not interact with the support structures during transport and transshipment. In fig. 6.3 a monopile is shown during transshipment. The space between the monopile and the SPMT must be larger than 0.6 m, due to the width of the helicals. The shown monopile is supported by two stands, and it can be seen that it sticks out more than 20 m, so this would be enough to avoid interference with the screw thread.

Figure 6.3: A monopile on a SPMT during transshipment. The circular support stands are clearly visible. It also can be seen that it stick out more than 20 m.

6.3 Installation

The helicals can prevent the monopile from lying in the gripper as with current practice. Similar to the monopile stands, the upending tool must be designed such, that it does not interfere with the appendages. In fig. 6.4 a monopile is shown lying down in the upending tool. It is supported by pads, which need to be placed such, that they avoid contact with the appendages. Given a spacing of 1.68 m, this should be enough to accomadate sufficient support. Since every monopile has a flange on top where the TP, or in case of a TP-less mp the mast of the turbine, is placed, this is also where the upending tool can hold the monopile. Apart from avoiding putting weight on the appendages, the installation process until the pile driving is equal to the current process.

Normally the monopile is rotated in the direction that is most ideal for the connection of the electricity cable to the grid. If one would screw a monopile, the desired direction might not coincide with the desired depth. Given that the correct height has a larger priority than the direction, it may be that the cable has to make a slight detour around the monopile. However, if one considers a broad detour of twice the monopile diameter, i.e. 24 m, and the distance to the next connection in the order of a few hundred meter, it is a relatively small price to pay, if a loud installation can be avoided.

Figure 6.4: A monopile lying down in the upending tool. The support pads need to avoid contact with the appendages.

7. Conclusion and recommendations

The increasing demand of offshore wind energy has an enormous impact on the sea life around the wind farms. Current installation techniques produce noise levels that are too high for fish and marine mammals. With the ever increasing size of wind turbines, and therefore the foundations as well, this is seen as one of the biggest challenges for the offshore wind industry. Since monopiles are the most popular foundation, and expected to stay so in the foreseen future, we will explore the possibility of reducing the sound levels during installation. We do this by assessing the feasibility of the installation method of screwing for monopiles.

To asses the feasibility of the method of screwing monopiles for offshore wind turbines, an extensive model of the soil-pile interaction is set up. The soil data is based on CPT-data from the wind farm Hollandse Kust West (HKW). Specifically from a location of which it is known to be challenging to install monopiles. This CPT-data is used to derive the skin resistance of the monopile using the ICP-05 method. A model is subsequently build to quantify all resistances the monopile encounters during installation, including those of the helicals. Based on this quantification the helical performance can be determined. It turns out that it is technically not possible to screw the monopile into the ground with the considered soil data and monopile design. A tangential force ranging from 1100 to 2000 MN is required to rotate the monopile. This is above the maximum stress level and close to what the ground itself can transfer, risking disturbance of the soil directly around the monopile.

With this knowledge we looked at what conditions would allow the screwing method to work. Initially we have chosen a difficult location and a maximum size monopile. Decreasing the monopile size also decrease the required driving force, but there is still a chance of soil disturbance. Decreasing the values of the CPT and the angle of repose however, made the outcome lies well within all the limits of the soil-pile interaction. Since we have started with a challenging location, we have multiplied the CPT-values by a factor 0.8 and reduced the angle of repose to 27.5 degree. This is a significant decrease with respect to the initial values. However, those initial values were conservative. Furthermore, with those values it is not possible, and the new values allow us to further explore the possibilities of screwing monopiles. As a result, a required driving force of 500 NM at a radius of 6 m, or 3000 MNm, is established. It must be noted though, that further research is necessary to determine whether this decrease in CPT-values is justified and if they are still accurate for real life piling locations. Lastly the design of the monopile must be changed such, that the stresses do not exceed the maximum allowable stresses. Therefore the diameter of the upper part of the monopile is increased to 10 m in diameter with a wall thickness of 80 mm.

The design of the screw thread consists of helicals that are welded onto the monopile. They are placed on the monopile from 0.4 m from the bottom, till 20 m from the bottom. They are 0.6 m wide and 80 mm thick. They also have a bank angle of 20 degree, to push the soil slightly against the ground, for higher soil-ground resistance. The angle of attack is 15 degree, which ensure a well balance between drivability and penetration speed.

With the design change and the torque requirements a review of possible driving mechanisms is made. At first the power requirement is established. With 10 MW the driving time is 1.3 hour, if the maximum and a continuous angular velocity is achieved. The explored connections between the vessel and the monopile are a lead driver type and a gripper type. For both holds that they add a significant layer of complexity with respect to the current equipment that is involved in pile driving. The lead driver requires a massive construction on deck, and therefore also a massive investment in equipment. However, the monopile itself does not need any appendages or extra tools. The gripper types however, are dependent on splines on the monopile, which can either be welded onto the monopile itself, or fixed by

an sleeve. The modifications on the deck of the ship on the other hand are minor, all the modifications are embedded in the gripper itself.

For the driving mechanism a comparison between a geared drive and hydraulic cylinders is made. These two mechanisms can apply the most force which is necessary given the driving requirements. Even so, the geared rack and pinion is not able to drive the monopile to the desired depth of 45 m within its specification. The maximum allowable force that the teeth can handle is lower than the required force. The hydraulic cylinders however are able to deliver this force. With the established requirements a tandem of 20 hydraulic cylinders can drive the monopile up to depth. Lastly a comparison between a jack-up vessel and a DP-vessel is made. Although the DP-vessel has a large distance between its thrusters, they are not able to withstand the torque that the monopile acts on the ship. The jack-up however is able to withstand the lateral force on the legs. It must be investigated though, what the consequence is for the weather conditions the ship can operate in. Choosing a jack-up also avoids making the connection able to allow rotations due to rolling of the ship.

At last the logistics of the monopile is explored. The most significant change lies within the production of the monopile. Welding the helical and possible splines, interferes with the efficient production process. Extra steps and production facilities must be introduced to make this possible. Considering the transport, transshipment and installation up until the actual driving, only the avoiding contact with the appendages is required. The essential shape of the monopile is still the same, so the same sort of stands can be used, as long as the pads can avoid the appendages.

In this thesis the method of screwing of a monopile is explored. It is a feasible option. Given that the speed of rotational is relatively slow, it is a silent alternative for hammer piling. However, it turns out that it is likely not possible on difficult locations, that is, locations where vibratory piling is not an option either. If the conditions are changed such, that it is possible, it might also be possible for vibratory piling. Further research must be done to specify the soil conditions more accurately. Furthermore, if drivable conditions are assumed, the force that are required push the equipment and the monopile itself to the limit. Lastly, the essence of the monopile is its simplicity, adding appendages nullifies that property. All things considered, it is possible to screw a monopile into the ground, but not at challenging locations and it comes at a great cost.

Bibliography

[1] "DEME builds on turbine job with deal to install foundations at giant Vineyard Wind 1 off US | Recharge." [Online]. Available: https://www.rechargenews.com/wind/deme-builds-on-turbine-job-with-deal-to-install-foundations-at-giant-vineyard-wind-1-off-us/2-1-1079939

[2] "XL Monopiles." [Online]. Available: http://www.esru.strath.ac.uk/EandE/Websites/14-15/XLMonopiles/technical.html

[3] "Monopiles | Transition Pieces." [Online]. Available: https://www.geminiwindpark.nl/monopiles–transition-pieces.html

[4] "Riviera - Opinion - US foundations face multiple challenges." [Online]. Available: https://www.rivieramm.com/opinion/opinion/us-foundations-face-multiple-challenges-22879

[5] "Cone Penetration Test - AMERICAN GEOSERVICES." [Online]. Available: http://americangeoservices.com/cone-penetration.html

[6] "Soll Hollandse Kust (west) · Offshorewind RVO." [Online]. Available: https://offshorewind.rvo.nl/cms/view/f4f39d87-68f8-4925-97c4-c49f6a07a001/soll-hollandse-kust-west

[7] "PM20LC - Pile Driving Rig - Junttan." [Online]. Available: https://junttan.com/product/pm20lc/

[8] "Den stora kranen Svenen lämnade Malmö hamn vid 16-tiden i dag - PPPress.se." [Online]. Available: https://www.pppress.se/nyhet/den-stora-kranen-svenen-lamnade-malmo-hamn-vid-16-tiden-i-dag/

[9] "Global Wind Report 2021 - Global Wind Energy Council." [Online]. Available: https://gwec.net/global-wind-report-2021/

[10] K. A. Schmoor, M. Achmus, A. Foglia, and M. Wefer, "Reliability of design approaches for axially loaded offshore piles and its consequences with respect to the North Sea," *Journal of Rock Mechanics and Geotechnical Engineering*, vol. 10, no. 6, pp. 1112–1121, 12 2018.

[11] I. Energy Agency, "Offshore Wind Outlook 2019: World Energy Outlook Special Report," *IEA*, 2019. [Online]. Available: www.iea.org/tc/

[12] "Offshore wind technical potential and electricity demand, 2018 – Charts – Data & Statistics - IEA." [Online]. Available: https://www.iea.org/data-and-statistics/charts/offshore-wind-technical-potential-and-electricity-demand-2018

[13] "Global Offshore Renewable Map | 4C Offshore." [Online]. Available: https://www.4coffshore.com/offshorewind/

[14] Golightly C, "Technical Paper: Tilting of monopiles Long, heavy and stiff; pushed beyond their limits ," 2014. [Online]. Available: https://www.geplus.co.uk/technical-paper/technical-paper-tilting-of-monopiles-long-heavy-and-stiff-pushed-beyond-their-limits-20-12-2013/

[15] Y. Liu, "Monopile Forever Overcoming the Technical Boundaries of Monopile Foundations in Deep Waters," Ph.D. dissertation, TU Delft, 2021.

[16] M. Asgarpour, "Assembly, transportation, installation and commissioning of offshore wind farms," *Offshore Wind Farms: Technologies, Design and Operation*, pp. 527–541, 1 2016.

[17] M. U. Rentschler, F. Adam, P. Chainho, K. Krügel, and P. C. Vicente, "Parametric study of dynamic inter-array cable systems for floating offshore wind turbines," *Marine Systems and Ocean Technology*, vol. 15, no. 1, pp. 16–25, 3 2020.

[18] Greedy and Lyndon, "TENNET, NL OFFSHORE WIND FARM TRANSMISSION SYSTEMS 66 kV Systems for Offshore Wind Farms," *TenneT*, 2015. [Online]. Available: www.dnvgl.com

[19] W. J. Richardson, C. R. Greene, C. I. Malme, D. H. Thomson, S. E. Moore, and B. Wiirsig, "Marine Mammals and Noise," *Marine Mammals and Noise*, pp. 1–576, 10 2013.

[20] L. L. Mazzuca, "Potential Effects of Low Frequency Sound (LFS) from Commercial Vessels on Large Whales," *Master of Marine Affairs*, 2001.

[21] H. Bailey, B. Senior, D. Simmons, J. Rusin, G. Picken, and P. M. Thompson, "Assessing underwater noise levels during pile-driving at an offshore windfarm and its potential effects on marine mammals," *Marine Pollution Bulletin*, vol. 60, no. 6, pp. 888–897, 6 2010.

[22] S. Robinson, P. Theobald, G. Hayman, L. Wang, P. A. Lepper, V. Humphrey, S. Mumford, and F. Report, "Measurement of underwater noise arising from marine aggregate dredging operations," *MALSF Report 09/P108*, no. February, p. 2011, 2011.

[23] C. McKenzie-Maxon and O. Nielsen, "Offshore Pile Driving Underwater and Above water. Noise Measurements and Analysis," Odegaard and Danneskiold-Samsoe, Tech. Rep., 2000.

[24] S. Lippert, M. Nijhof, T. Lippert, D. Wilkes, A. Gavrilov, K. Heitmann, M. Ruhnau, O. Von Estorff, A. Schäfke, I. Schäfer, J. Ehrlich, A. MacGillivray, J. Park, W. Seong, M. A. Ainslie, C. De Jong, M. Wood, L. Wang, and P. Theobald, "COMPILE - A Generic Benchmark Case for Predictions of Marine Pile-Driving Noise," *IEEE Journal of Oceanic Engineering*, vol. 41, no. 4, pp. 1061–1071, 10 2016.

[25] A. Tsouvalas and A. V. Metrikine, "A three-dimensional vibroacoustic model for the prediction of underwater noise from offshore pile driving," *Journal of Sound and Vibration*, vol. 333, no. 8, pp. 2283–2311, 4 2014.

[26] N. Fisheries, "UNITED STATES DEPARTMENT OF COMMERCE National Oceanic and Atmospheric Administration NATIONAL MARINE FISHERIES SERVICE Northwest Region," *NOAA*, 2012.

[27] M. Zampolli, M. J. J. Nijhof, C. A. F. De Jong, M. A. Ainslie, . Erwin, H. W. Jansen, and B. A. J. Quesson, "Validation of finite element computations for the quantitative prediction of underwater noise from impact pile driving," *The Journal of the Acoustical Society of America*, vol. 133, no. 1, p. 72, 1 2013. [Online]. Available: https://asa-scitation-org.tudelft.idm.oclc.org/doi/abs/10.1121/1.4768886

[28] T. Lippert, M. A. Ainslie, and O. v. Estorff, "Pile driving acoustics made simple: Damped cylindrical spreading model," *The Journal of the Acoustical Society of America*, vol. 143, no. 1, p. 310, 1 2018. [Online]. Available: https://asa-scitation-org.tudelft.idm.oclc.org/doi/abs/10.1121/1.5011158

[29] J. A. David, "Likely sensitivity of bottlenose dolphins to pile-driving noise," *Water and Environment Journal*, vol. 20, no. 1, pp. 48–54, 3 2006.

[30] P. T. Madsen, M. Wahlberg, J. Tougaard, K. Lucke, and P. Tyack, "Wind turbine underwater noise and marine mammals: Implications of current knowledge and data needs," *Marine Ecology Progress Series*, vol. 309, pp. 279–295, 3 2006. [Online]. Available: https://www.researchgate.net/publication/236156710_Wind_turbine_underwater_noise_and_marine_ mammals_Implications_of_current_knowledge_and_data_needs

[31] D. P. Woodbury and J. H. Stadler, "A PROPOSED METHOD TO ASSESS PHYSICAL INJURY TO FISHES FROM UNDERWATER SOUND PRODUCED DURING PILE DRIVING," *http://dx.doi.org.tudelft.idm.oclc.org/10.1080/09524622.2008.9753852*, vol. 17, no. 1-3, pp. 289–291, 2012. [Online]. Available: https://www-tandfonline-com.tudelft.idm.oclc.org/doi/abs/10.1080/09524622.2008.9753852

[32] S. H. Ridgway and W. W. Au, "Hearing and Echolocation in Dolphins," *Encyclopedia of Neuroscience*, pp. 1031–1039, 2009. [Online]. Available: https://www.researchgate.net/publication/286597329_Hearing_and_Echolocation_in_Dolphins

[33] D. R. Ketten, "The Marine Mammal Ear: Specializations for Aquatic Audition and Echolocation," *The Evolutionary Biology of Hearing*, 1992.

[34] C. R. Greene, "Characteristics of oil industry dredge and drilling sounds in the Beaufort Sea," *The Journal of the Acoustical Society of America*, vol. 82, no. 4, p. 1315, 6 1998. [Online]. Available: https://asa-scitation-org.tudelft.idm.oclc.org/doi/abs/10.1121/1.395265

[35] C. Peng, X. Zhao, and G. Liu, "Noise in the Sea and Its Impacts on Marine Organisms," *undefined*, vol. 12, no. 10, pp. 12 304–12 323, 9 2015. [Online]. Available: www.mdpi.com/journal/ijerph

[36] M. Defingou, F. Bils, B. Horchler, T. Liesenjohann, and G. Nehls, "PHAROS4MPAS - Safeguarding marine protected areas in the growing Mediterranean blue economy. Capitalization report for the offshore wind energy sector." 1 2019.

[37] C. W. Clark, W. T. Ellison, B. L. Southall, L. Hatch, S. M. Van Parijs, A. Frankel, and D. Ponirakis, "Acoustic masking in marine ecosystems: intuitions, analysis, and implication," *Marine Ecology Progress Series*, vol. 395, pp. 201–222, 12 2009. [Online]. Available: https://www.int-res.com/abstracts/meps/v395/p201-222/

[38] J. Carstensen, O. D. Henriksen, and J. Teilmann, "Impacts of offshore wind farm construction on harbour porpoises: Acoustic monitoring of echolocation activity using porpoise detectors (T-PODs)," *Marine Ecology Progress Series*, vol. 321, pp. 295–308, 9 2006. [Online]. Available: https://www.researchgate.net/publication/250218741_Impacts_of_offshore_wind_farm_construction_on_harbour_porpoises_Acoustic_monitoring_of_echolocation_activity_using_porpoise_detectors_T-PODs

[39] P. M. Thompson, D. Lusseau, T. Barton, D. Simmons, J. Rusin, and H. Bailey, "Assessing the responses of coastal cetaceans to the construction of offshore wind turbines," *Marine Pollution Bulletin*, vol. 60, no. 8, pp. 1200–1208, 8 2010. [Online]. Available: https://abdn.pure.elsevier.com/en/publications/assessing-the-responses-of-coastal-cetaceans-to-the-construction-

[40] A. A. Y. H. Chan, P. Giraldo-Perez, S. Smith, and D. T. Blumstein, "Anthropogenic noise affects risk assessment and attention: the distracted prey hypothesis," *Biology Letters*, vol. 6, no. 4, p. 458, 8 2010. [Online]. Available: /pmc/articles/PMC2936217/ /pmc/articles/PMC2936217/?report=abstract https://www-ncbi-nlm-nih-gov.tudelft.idm.oclc.org/pmc/articles/PMC2936217/

[41] W. T. Ellison, B. L. Southall, C. W. Clark, and A. S. Frankel, "A New Context-Based Approach to Assess Marine Mammal Behavioral Responses to Anthropogenic Sounds," *Conservation Biology*, vol. 26, no. 1, pp. 21–28, 2 2012. [Online]. Available: https://www.researchgate.net/publication/51900547_A_New_Context-Based_Approach_to_Assess_Marine_Mammal_Behavioral_Responses_to_Anthropogenic_Sounds

[42] R. P. A. Dekeling (a), M. L. Tasker, A. J. Van der Graaf, M. A. Ainslie, M. H. Andersson, M. Andre, J. F. Borsani, K. Brensing, M. Castellote, D. Cronin, J. Dalen, T. Folegot, R. Leaper, J. Pajala, P. Redman, S. P. Robinson, P. Sigray, G. Sutton, F. Thomsen, S. Werner, D. Wittekind,

and J. V. Young, "Monitoring guidance for underwater noise in European seas- Part I. Executive summary." *JRC Scientific and Policy Reports EUR 26557 EN*, pp. 1–13, 2014. [Online]. Available: https://mcc.jrc.ec.europa.eu/documents/OSPAR/MonitoringGuidanceforUnderwaterNoiseinEuropean.pdf

[43] W. Strietman, R. Michels, and E. Leemans, "Measures to reduce underwater noise and beach litter : an assessment of potential additional measures for the Netherlands," -, 2018. [Online]. Available: https://doi.org/10.18174/457443

[44] T. Bohne, T. Grießmann, and R. Rolfes, "Modeling the noise mitigation of a bubble curtain," *The Journal of the Acoustical Society of America*, vol. 146, no. 4, pp. 2212–2223, 10 2019.

[45] N. England, "Statutory nature conservation agency protocol for minimising the risk of injury to marine mammals from piling noise," *JNCC*, 2010.

[46] "Offshore Wind in Europe Key trends and statistics 2019," 2019.

[47] C. Mone, M. Hand, M. Bolinger, J. Rand, D. Heimiller, and J. Ho, "2015 Cost of Wind Energy Review," *NREL*, 2015. [Online]. Available: www.nrel.gov/publications.

[48] "Sif studying expansion plans to capture offshore wind market growth - Egeria." [Online]. Available: https://egeriagroup.com/nl/nieuws/sif-studying-expansion-plans-to-capture-offshore-wind-market-growth/

[49] "Beyond XXL – Slim Monopiles for Deep-Water Wind Farms | Offshore Wind." [Online]. Available: https://www.offshorewind.biz/2020/05/11/beyond-xxl-slim-monopiles-for-deep-water-wind-farms/

[50] "SAL Ships Monopiles for Japanese OWF - BBN | Breakbulk.News™." [Online]. Available: https://breakbulk.news/sal-ships-monopiles-for-japanese-owf/

[51] "Dillinger continues to invest in monopile production – Baltic Wind." [Online]. Available: https://balticwind.eu/dillinger-continues-to-invest-in-monopile-production/

[52] M. A. El-Reedy, "Soil Investigation and Pile Design," *Onshore Structural Design Calculations*, pp. 345–385, 1 2017.

[53] P. Robertson, R. Campanella, D. Gillespie, and J. Greig, "Use of Piezometer Cone Data," *undefined*, 1986.

[54] G. Mesri and T. M. Hayat, "The coefficient of earth pressure at rest," *Canadian Geotechnical Journal*, vol. 30, no. 4, pp. 647–666, 1993.

[55] S. Lacasse, F. Nadim, T. Langford, S. Knudsen, G. L. Yetginer, T. R. Guttormsen, and A. Eide, "Model Uncertainty in Axial Pile Capacity Design Methods," *One Petro*, 5 2013.

[56] B. Cerfontaine, M. Ciantia, M. J. Brown, and Y. U. Sharif, "DEM study of particle scale and penetration rate on the installation mechanisms of screw piles in sand," *Computers and Geotechnics*, vol. 139, p. 104380, 11 2021.

[57] Voltaire, "J A N D E N U L. C O M."

[58] "Orion | DEME Group." [Online]. Available: https://www.deme-group.com/technologies/orion

Assessing the feasibility of the installation method of screwing for monopiles for offshore wind turbines

E.P. Jongkees[a], Dr. J. Javanova[a], Dr. H. Polinder[a], ir. E. Romeijn[b]

[a]*Department of Maritime and Transport Technology, Faculty Mechanical, Maritime and Materials Engineering, Delft University of Technology, Delft, The Netherlands*
[b]*Huisman Equipment B.V., Admiraal Trompstraat 2, 3115 HH, Schiedam, The Netherlands*

Abstract

The installation method of screwing is proposed as an alternative for hammer and vibratory piling for monopiles. Based on a location at wind farm HKZ soil conditions are determined. Then a model is build to approximate the resistance of the monopile and the helicals during piling. Based on this model a proposal for a helical design is shown. This ultimately results in driving requirements, which are the basis for determining the driving equipment. The required power output is determined to be between 5 to 20 MW. For the connection a driver lead and gripper type are discussed, together with the driving method, a geared rack and pinion or hydraulic cylinders. Finally the implications on the logistics are considered.

Keywords: Offshore wind, Monopile, Screw thread, Helicals, Soil-pile interaction

1. Introduction

Wind energy has become an ever-increasing market. Due to climate agreements, there is a growing demand for electricity produced by wind turbines. The worldwide wind power capacity will multiple in size the coming decades. Furthermore, it is expected by the global wind energy council (GWEC) that most wind power capacity will be installed in the second half of the decade (1). Although these numbers are an estimation, the trend of an increase in installed wind power is obvious. Offshore wind energy has a large share in this increase. While at the moment responsible for no more than 13 per cent of the total wind energy capacity, it does see the biggest growth with a potential annual installation of 40 GW in 2030 according to the GWEC.

The international energy agency, IEA, estimates the technical potential of offshore wind power at 36.000 TWh per year for installations in water less than 60 m deep and within 60 km from shore (2). These water depths and distances to shore are ideal for bottom fixed wind turbines, such as monopile based wind turbines. It is clear that particularly Europe and China have great ambitions for offshore wind power. Although China has less technical potential, they still are the country with the most planned wind energy. The big potential in Europe is mainly due to the North Sea. Therefore countries as England, Denmark, Germany and Norway are planning to build large wind farms in the coming decades.

Despite all the potential and plans however, exploiting offshore wind energy is a major challenge. The easy locations at sea were used at first, causing every next location to be more challenging to install offshore wind turbines (OWTs). The difficulty herein is mainly due to water depth, soil condition and the distance to shore, which make them economically less feasible to exploit. These challenges arise for example from difficulties with the ever growing weight and dimensions of the equipment and components, the logistics, sound production under water caused by pile driving and the connection to the main grid.

In industry one of the biggest foreseen challenges is the sound radiation under water caused by impact piling of the monopile. Legislation forbids exceeding certain sound levels. Currently sound mitigation measures have to be taken to stay under the sound limits. However, as monopiles become larger, the radiated sound levels increase as well. There is therefore a strive to develop low noise methods to install monopiles.

In the search for a silent method to install monopiles, we find that screwing is a method which is not yet explored, but has great potential. In this paper we explore the method of screwing for monopiles.

2. Soil-monopile interaction

At first the soil properties are determined, based on CPT-data. With the soil properties the skin and base resistance can be calculated for a monopile without a screw thread. Then the force balance around the helicals is discussed. These aspects can then be combined to calculate the drivability, and consequently the torque requirements.

The monopile encounters friction from the soil it eventually needs to penetrate. In order to determine all the relevant force, we start with a free body diagram, FBD, of the monopile inserted in the soil. In figure 1 the FBD is shown and in table 1 the various components are described. For convenience, the signs of the driving forces are given with an F, while the resistances are referred to with an R. Ultimately, all the components listed in 1 need to be analysed to determine whether the principle of screwing works, and what the torque requirements are.

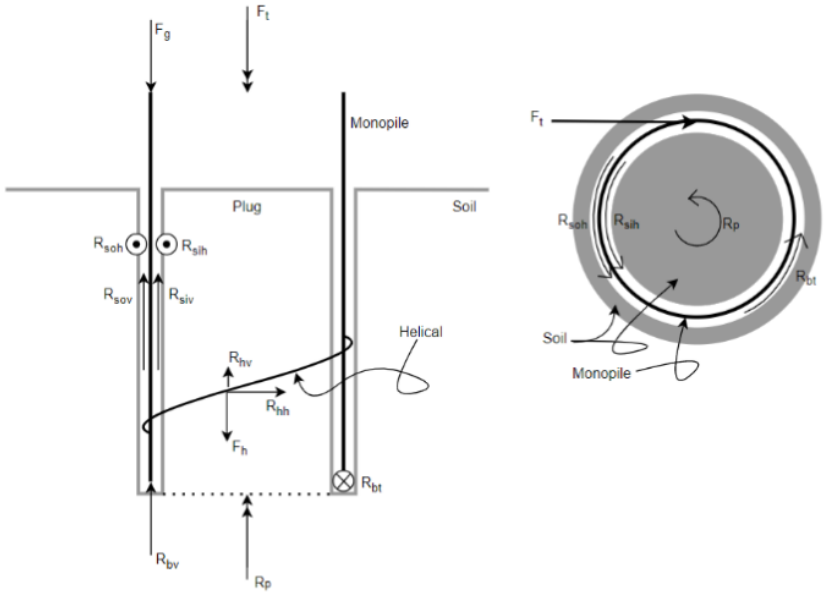

Figure 1: Free body diagram of the monopile as it is inserted into the ground. At the left the side view and on the right the top view. In table 1 the drawn components are described.

	Description	Sign
2*Independent on helicals	Own weight	F_g
	Tangential driving force	F_t
	Outside horizontal skin resistance	R_{soh}
	Outside vertical skin resistance	R_{sov}
	Inside horizontal skin resistance	R_{sih}
	Inside vertical skin resistance	R_{siv}
	Vertical base resistance	R_{bv}
	Tangential base resistance	R_{bt}
	Rotational resistance plug	R_p
Dependent on helicals	Helical driving force	F_h
	Horizontal helical resistance	R_{hh}
	Vertical helical resistance	R_{hv}

Table 1: Description of the forces acting at the monopile and their signs as used in mpfbd

For determining the skin friction, the ICP-05 method is used which has the general formula $f(z)$, which gives the skin friction as a function of the depth z in $[Pa]$. $f(z)$ is denoted by

$$f(z) = uq_c(\frac{\sigma'_v}{p_a})^a A_r^b [max(\frac{L-z}{D_0}, v)]^{-c} (tan\varphi)^d \tag{1}$$

with q_c the measured cone tip resistance, σ'_v the vertical pressure, p_a the atmospheric pressure, φ the angle of repose and A_r the pile displacement ratio, defined by

$$A_r = 1 - (\frac{D_i}{D_0})^2 \tag{2}$$

where D_i is the inner diameter and D_o the outer diameter. Furthermore, L is the length of the monopile and z the penetration depth.

With the skin friction f as described in equation (1) the force that the monopile encounters due to skin friction can be calculated with

$$R_s = \sum_{z=1}^{d} f(z) A_{mp} \tag{3}$$

where z is the depth the monopile is inserted in the sea bed and A_{mp} the area of the monopile per meter height.

In the above paragraph the static skin friction is obtained. In reality however, there is a difference between the static and dynamic resistance. In industry the dynamic resistance is derived by multiplying the static friction with a β-factor. The β-factor is calculated by

$$\beta = tan\delta \tag{4}$$

where δ represents the friction angle between sand and steel, and is equal to $\delta = \theta - 5$ with θ the angle of repose 35°. This makes $\beta = 0.58$.

The horizontal and vertical components of the resistance are depending on the angle of attack of the helicals and can be quantified by

$$R_{soh} = R_{so} cos(\alpha) \tag{5}$$

$$R_{sov} = R_{so} sin(\alpha) \tag{6}$$

where R_{soh} is the horizontal outside skin resistance, R_{sov} is the vertical skin resistance and α is the angle of attack of the helicals, and therefore also the assumed direction of movement.

The base resistance occurs at the bottom of the pile. As established above we can consider a plugged situation, so we can approximate the monopile as an open ended cylinder.

The base resistance in vertical direction R_{bv} for non-cohesive soils is approximated with

$$R_{bv} = q_b A_{tip} \tag{7}$$

where R_{bv} is the vertical base resistance, q_b the cone resistance from the CPT and A_{tip} the area of the tip of the monopile.

Since the ultimate goal is to screw the monopile, the bottom will experience a torque resistance due to the rotation as well. The tangential base resistance R_{bt} is obtained by

$$R_{bt} = Q_{b,ver} tan(\alpha)\beta \tag{8}$$

where R_{bt} is the vertical base resistance, $tan(\alpha)$ the friction coefficient between the bottom of the monopile and the soil, and β the dynamic coefficient.

3. Design of the screw thread

If we consider the monopile without the helicals, we can distinguish between the horizontal and vertical driving force and resistance. The skin and base resistance are assumed to be independent on the helicals. We can therefore make a graph what the required magnitude of the force is, to make the monopile move at all. Since the outside skin resistance is depending on the angle of attack as expressed in (6), we have put multiple values of α in the graph. Here α ranges from 0 to 30 degree, since those are probable values the angle of attack could attain. The total rotational and vertical resistance without the helicals R_{tr} and R_{tv} are given by respectively

$$R_{tr} = R_{soh} + R_p + R_{bt} \tag{9}$$

$$R_{tv} = R_{sov} + R_{siv} + R_{bt} \tag{10}$$

where R_{soh} and R_{sov} are a function of the angle α. In rotver the results of equations 9 and 10 are printed. It shows that the minimum torque that is required must be capable of creating a tangential force in the order of 500 MN. With a diameter of 12 meter this translates into a torque of 3000 MNm. Note that with this figure we only reach an equilibrium, and that therefore a higher torque is necessary. The total vertical resistance learns that the effective downward force of the helicals that is required, varies in the order of 500 to 800 MN. For both of these figures applies that the screw thread itself has its own resistance, so ultimately the required torque figures will become larger.

With the FBD equations can be set up that give the relation between the force caused by the torque and the downward force, and the corresponding resistances. If we eliminate the normal force F_N we get

$$F_t = \frac{sin(\alpha) + \mu cos(\alpha)}{cos(\alpha) - \mu sin(\alpha)} F_h \tag{11}$$

where F_t and F_h are directly related to each other. Eq (11) essentially gives a ratio as a function of the angle α and the friction coefficient μ.

Based on the above results a proposed design for a monopile is presented in figure 4.

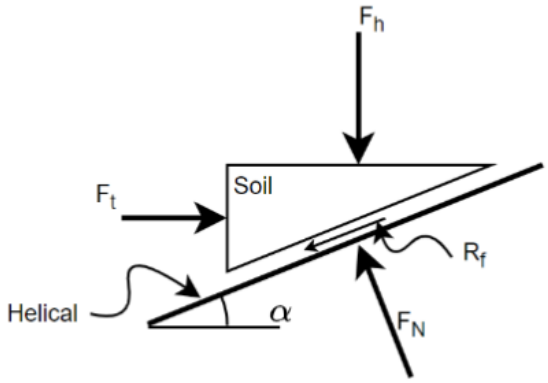

Figure 2: Free body diagram of the helical and the involved forces

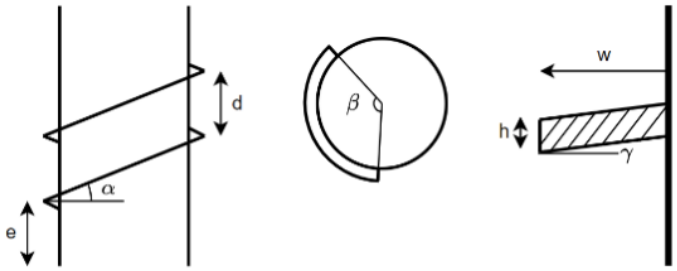

Figure 3: Schematic depiction of the helicals with the relevant parameters

4. Driving mechanism

To drive the monopile the following range of power outputs is established as is given in table 3. With the design change and the torque requirements a review of possible driving mechanisms is made. At first the power requirement is established. With 10 MW the driving time is 1.3 hour, if the maximum and a continuous angular velocity is achieved. The explored connections between the vessel and the monopile are a lead driver type and a gripper type. For both holds that they add a significant layer of complexity with respect to the current equipment that is involved in pile driving. The lead driver requires a massive construction on deck, and therefore also a massive investment in equipment. However, the monopile itself does not need any appendages or extra tools. The gripper types however, are dependent on splines on the monopile, which can either be welded onto the monopile itself, or fixed by an sleeve. The modifica-

Parameter	Value	Description
e	0.4 m	Distance between the base and the first helical
α	15 deg	Angle between horizontal and helical
d	1.68 m	Distance between two helicals
β	714 deg	Contour of the helical
w	0.6 m	Width of the helical
h	80 mm	Height of the helicals
γ	20 deg	Bank angle of helical

Table 2: Description of the corresponding parameters in figure 3.

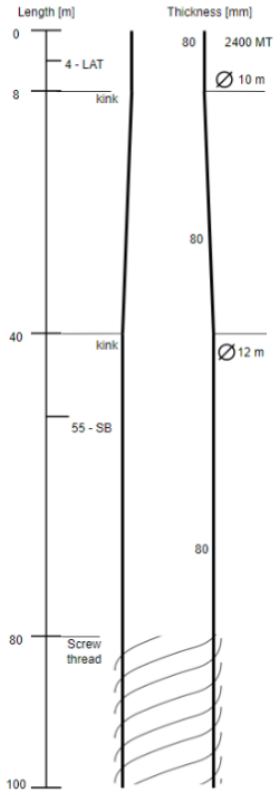

Figure 4: Final design of the monopile including the dimensions and the screw thread.

Power output [MW]	Time [h]
5	2.1
10	1.3
15	1.1
20	0.9
25	0.8
30	0.7

Table 3: Piling duration per power output, ranging from 5 to 30 MW.

tions on the deck of the ship on the other hand are minor, all the modifications are embedded in the gripper itself. The pile driver lead principle and the gripper principle are shown in figures 5 and 6.

For determining the requirements of a driving mechanism with gears, we assume a rack and pinion principle. The rack is located at the outside of the monopile while the gears are fixed to the ship. Since the rack has to fall over the monopile, we assume a diameter of 10.5 m, 0.5 m larger than the upper part op the monopile. This gives room for the rack. In figure 7 the principle is schematically shown. The gripper is depicted in grey, the pinion gears in red and the rack in blue. This figure shows the gear driven principle together with a sleeve, which is here red, with a yellow connection to the flange where the bolts are shown as dots.

If we assume the motor gear assembly to have a diameter of 1 m and an placement at 0.5 m from the rack, the theoretical maximum number of gear assemblies is 36, 39 or 42 for the upper diameter of 10.5, 11.5 and 12.5 respectively. If we would have an upper and lower rack, it could be upgraded to 72, 78 or 84. This means there is at least a factor of 3.6, 3.0 or 2.6 between the minimum required number of gears and the maximum of possible gears. This makes the principle of the geared type not feasible.

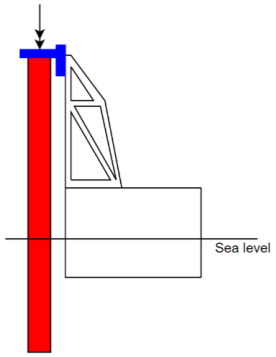

Figure 5: Schematic principle pile driver lead.

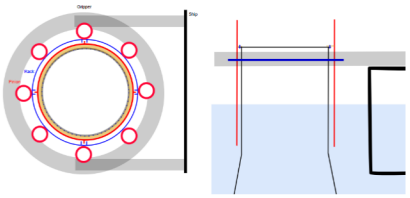

Figure 6: Principle of the gripper-sleeve connection. In this example driven by a geared driving mechanism. For explanatory reasons the dimensions are not to scale.

To determine the feasibility of a hydraulically driven monopile, we consider the maximum force that can be applied by a hydraulic cylinder. This is given by

$$F_{hc} = \frac{\pi D^2 p}{4} = \frac{\pi \cdot 0.96^2 \cdot 32 \cdot 10^6}{4} = 32MN \qquad (12)$$

where D is the diameter of the piston, with a max of 0.96 m and p is the hydraulic pressure which generally has a maximum value of 32 MPa. These are values of which is known that they are possible. In figure 8 this principle is showed.

The spline at which the cylinder apply their force, needs to be thick enough to be able to cope with the enormous forces. If an stress of 340 MPa is allowed, the minimum area through which this force must be transferred is given by

$$A_{spline} = \frac{F}{\sigma} = \frac{32}{340} = 0.9m^2 \qquad (13)$$

where F is the maximum force the a cylinder can deliver and σ the maximum stress. At the maximum depth the spline has to have base of $0.9m^2$. These are serious dimensions for a spline. If we assume that the cylinder has a foot of 1 m long, the spline needs to be 9 cm wide. Note that this is only for the top side of the monopile, since that would correspond to the maximum penetration depth.

If the pile drive lead principle is used, a transfer tool can be connected to the flange. Because it is not a one time use

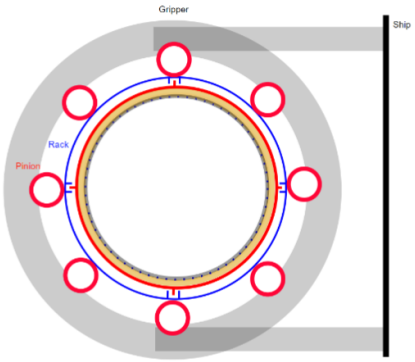

Figure 7: Schematic principle pile driver lead.

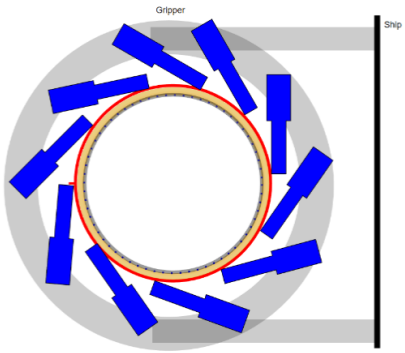

Figure 8: Schematic principle of the hydraulic driving mechanism.

product, it can be made strong enough that it can cope with the extreme forces. Another advantage is that the speed can be higher in the beginning due to the smaller torque.

In the off shore two types of installation vessels are common; jack-up vessels and dynamically positioned vessels (DP-vessels). If the screwing method would be used, it is therefore probable that the industry will use one of these methods, since these vessels already exist and they offer great flexibility and experience. To determine the feasibility we will look at the reaction on the vessels due to the torque applied on the monopile. We will base the calculations on two vessels which have representative dimensions to be adequate as a model for the whole installation field. For the jack-up vessel we consider the Jan de Nul Voltaire (3). This installation vessel is 170 m long and 60 m wide. The legs have a distance of 80 m from heart to heart. In figure 9 a schematic top and side view of a jack-up vessel installing a monopile is shown.

Although the ship is statically indeterminate, due to the dimensions it has some structural flexibility. Together with the fact that it is a relatively simple situation, we can assume that both front and rear legs experience equal lateral force. Given that the maximum torque on the monopile is 3000 MNm and the distance between the legs 80 m, the lateral force for each leg is $F_{leg} = 19MN$. This is a considerable force, especially if one considers that the legs are clamped in the hull of the ship. It can thus cause a substantial bending moment on the legs.

Calculations for the DP-vessel will be based on the DEME Orion (4). This is a modern ship which is currently being used

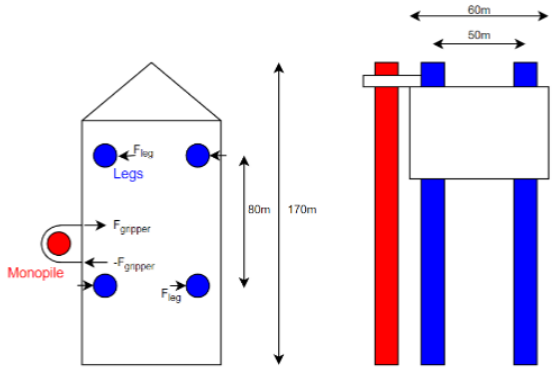

Figure 9: Schematic depiction of a jack-up vessel.

for the installation of wind farms. The length of the ship is 216 m and the thrusters are located at the very front and rear of the ship, with 180 m distance between them. In dp a top view of the ship with the locations of the thrusters is shown.

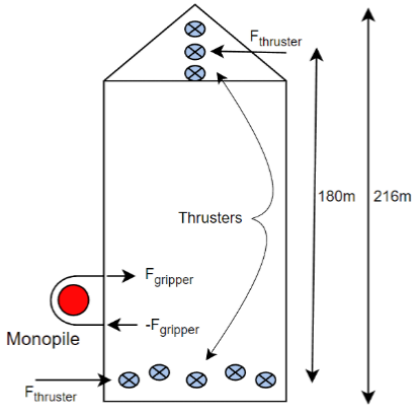

Figure 10: Schematic top view of a DP-vessel including its dimensions.

With a maximum torque of 3000 MNm and a distance of 180 m between the thrusters, a thrust of 16.7 MN has to be delivered if the monopile reaches the maximum depth. This is equivalent to 1600 ton. Thrusters have a wide variety of power outputs, with a maximum in the order of 140 ton bollard pull and a power of 7.5 MW. If we assume that each thruster can deliver 100 ton pull we are 1300 ton short at the bow, ignoring the power required by the DP-system. Since the bow has three thrusters with a maximum thrust of 1.3 MN and the distance between the bow and stern thrusters is 180 m, the maximum torque that can be applied on the monopile without lateral force is 700 MNm. This torque is enough to let the monopile penetrate to a depth in the order of 13 m.

5. Logistics

At last the logistics of the monopile is explored. The most significant change lies within the production of the monopile. Welding the helical and possible splines, interferes with the efficient production process. Extra steps and production facil-

ities must be introduced to make this possible. Considering the transport, transshipment and installation up until the actual driving, only the avoiding contact with the appendages is required. The essential shape of the monopile is still the same, so the same sort of stands can be used, as long as the pads can avoid the appendages.

6. Summary and conclusions

To asses the feasibility of the method of screwing monopiles for offshore wind turbines, an extensive model of the soil-pile interaction is set up. The soil data is based on CPT-data from the wind farm Hollandse Kust West (HKW). Specifically from a location of which it is known to be challenging to install monopiles. This CPT-data is used to derive the skin resistance of the monopile using the ICP-05 method. A model is subsequently build to quantify all resistances the monopile encounters during installation, including those of the helicals. Based on this quantification the helical performance can be determined. It turns out that it is technically not possible to screw the monopile into the ground with the considered soil data and monopile design. A tangential force ranging from 1100 to 2000 MN is required to rotate the monopile. This is above the maximum stress level and close to what the ground itself can transfer, risking disturbance of the soil directly around the monopile.

With this knowledge we looked at what conditions would allow the screwing method to work. Initially we have chosen a difficult location and a maximum size monopile. Decreasing the monopile size also decrease the required driving force, but there is still a chance of soil disturbance. Decreasing the values of the CPT and the angle of repose however, made the outcome lies well within all the limits of the soil-pile interaction. Since we have started with a challenging location, we have multiplied the CPT-values by a factor 0.8 and reduced the angle of repose to 27.5 degree. This is a significant decrease with respect to the initial values. However, those initial values were conservative. Furthermore, with those values it is not possible, and the new values allow us to further explore the possibilities of screwing monopiles. As a result, a required driving force of 500 NM at a radius of 6 m, or 3000 MNm, is established. It must be noted though, that further research is necessary to determine whether this decrease in CPT-values is justified and if they are still accurate for real life piling locations. Lastly the design of the monopile must be changed such, that the stresses do not exceed the maximum allowable stresses. Therefore the diameter of the upper part of the monopile is increased to 10 m in diameter with a wall thickness of 80 mm.

The design of the screw thread consists of helicals that are welded onto the monopile. They are placed on the monopile from 0.4 m from the bottom, till 20 m from the bottom. They are 0.6 m wide and 80 mm thick. They also have a bank angle of 20 degree, to push the soil slightly against the ground, for higher soil-ground resistance. The angle of attack is 15 degree, which ensure a well balance between drivability and penetration speed.

With the design change and the torque requirements a review of possible driving mechanisms is made. At first the power requirement is established. With 10 MW the driving time is 1.3 hour, if the maximum and a continuous angular velocity is achieved. The explored connections between the vessel and the monopile are a lead driver type and a gripper type. For both holds that they add a significant layer of complexity with respect to the current equipment that is involved in pile driving. The lead driver requires a massive construction on deck, and therefore also a massive investment in equipment. However, the monopile itself does not need any appendages or extra tools. The gripper types however, are dependent on splines on the monopile, which can either be welded onto the monopile itself, or fixed by an sleeve. The modifications on the deck of the ship on the other hand are minor, all the modifications are embedded in the gripper itself.

For the driving mechanism a comparison between a geared drive and hydraulic cylinders is made. These two mechanisms can apply the most force which is necessary given the driving requirements. Even so, the geared rack and pinion is not able to drive the monopile to the desired depth of 45 m within its specification. The maximum allowable force that the teeth can handle is lower than the required force. The hydraulic cylinders however are able to deliver this force. With the established requirements a tandem of 20 hydraulic cylinders can drive the monopile up to depth. Lastly a comparison between a jack-up vessel and a DP-vessel is made. Although the DP-vessel has a large distance between its thrusters, they are not able to withstand the torque that the monopile acts on the ship. The jack-up however is able to withstand the lateral force on the legs. It must be investigated though, what the consequence is for the weather conditions the ship can operate in. Choosing a jack-up also avoids making the connection able to allow rotations due to rolling of the ship.

In this paper the method of screwing of a monopile is explored. It is a feasible option. Given that the speed of rotational is relatively slow, it is a silent alternative for hammer piling. However, it turns out that it is likely not possible on difficult locations, that is, locations where vibratory piling is not an option either. If the conditions are changed such, that it is possible, it might also be possible for vibratory piling. Further research must be done to specify the soil conditions more accurately. Furthermore, if drivable conditions are assumed, the force that are required push the equipment and the monopile itself to the limit. Lastly, the essence of the monopile is its simplicity, adding appendages nullifies that property. All things considered, it is possible to screw a monopile into the ground, but not at challenging locations and it comes at a great cost.

References

[1] "Global Wind Report 2021 - Global Wind Energy Council." [Online]. Available: https://gwec.net/global-wind-report-2021/

[2] I. Energy Agency, "Offshore Wind Outlook 2019: World Energy Outlook Special Report," *IEA*, 2019. [Online]. Available: www.iea.org/tc/

[3] Voltaire, "J A N D E N U L. C O M."

[4] "Orion — DEME Group." [Online]. Available: https://www.deme-group.com/technologies/orion

B. CPT-data

The following pages give the CPT-data on which the soil conditions are based. Table B.1 gives the initial values for the model. These values are obtained from the CPT-data from Fugro shown below [6]. Per meter one data point is entered. Figure fig. B.1 shows the same values graphically.

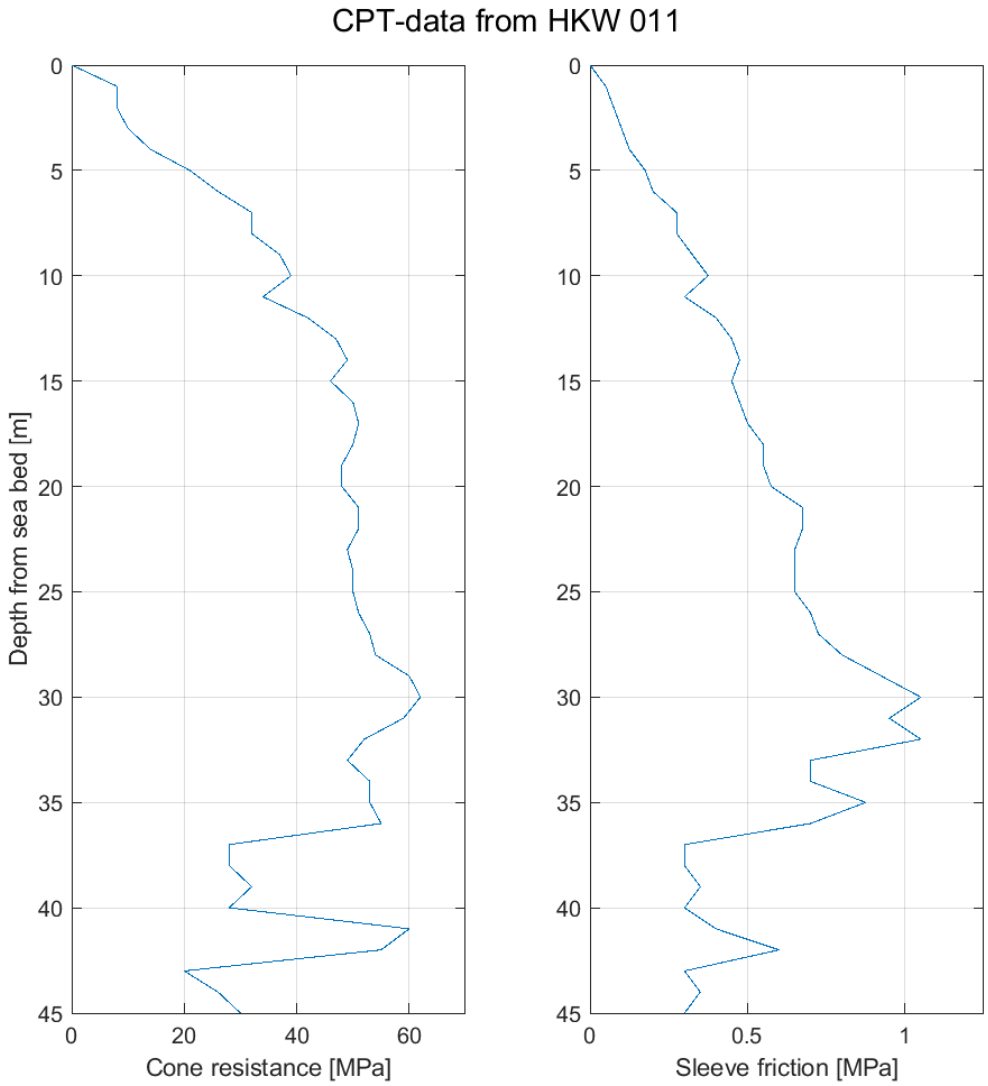

Figure B.1: CPT

Depth [m]	Cone resistance q_c [MPa]	Sleeve friction f_s [MPa]
1	8	2
2	8	3
3	10	4
4	14	5
5	21	7
6	26	8
7	32	11
8	32	11
9	37	13
10	39	15
11	34	12
12	42	16
13	47	18
14	49	19
15	46	18
16	50	19
17	51	20
18	50	22
19	48	22
20	48	23
21	51	27
22	51	27
23	49	26
24	50	26
25	50	26
26	51	28
27	53	29
28	54	32
29	60	37
30	62	42
31	59	38
32	52	42
33	49	28
34	53	28
35	53	35
36	55	28
37	28	12
38	28	12
39	32	14
40	28	12
41	60	16
42	55	24
43	20	12
44	26	14
45	30	12

Table B.1: Discretized data from CPT

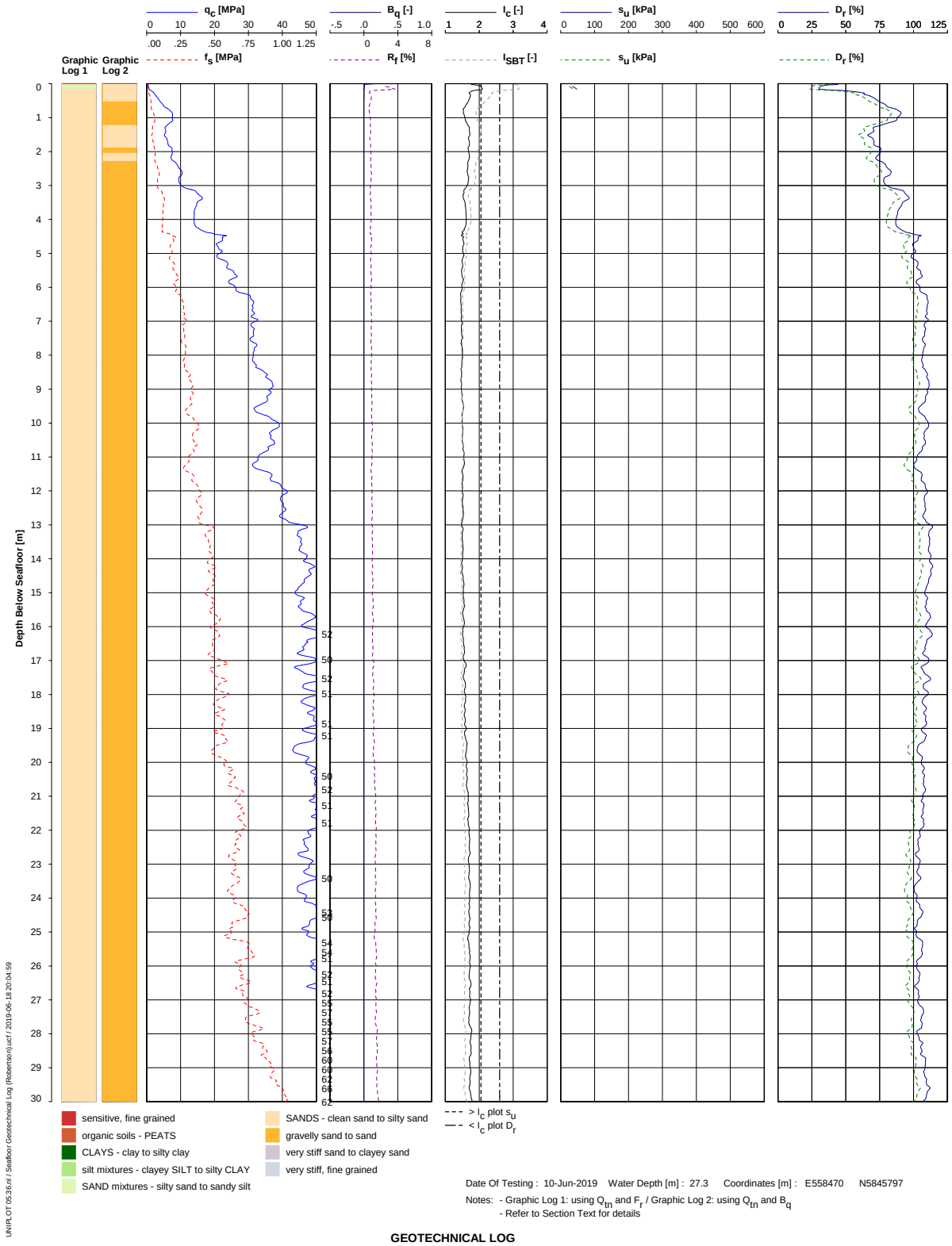

Date Of Testing : 10-Jun-2019 Water Depth [m] : 27.3 Coordinates [m] : E558470 N5845797

Notes: - Graphic Log 1: using Q_{tn} and F_r / Graphic Log 2: using Q_{tn} and B_q
- Refer to Section Text for details

GEOTECHNICAL LOG
HKW011-PCPT

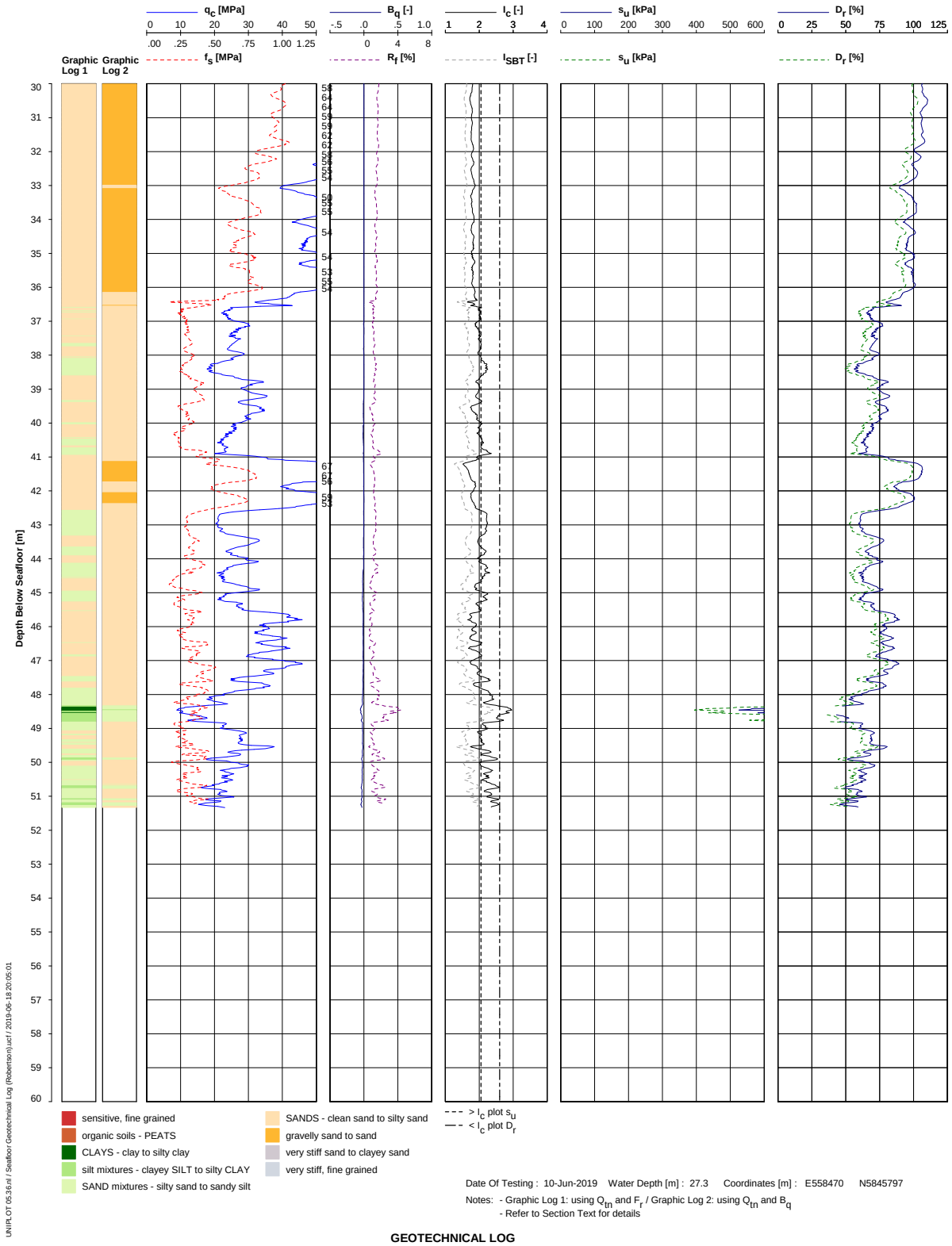

Date Of Testing : 10-Jun-2019 Water Depth [m] : 27.3 Coordinates [m] : E558470 N5845797

Notes: - Graphic Log 1: using Q_{tn} and F_r / Graphic Log 2: using Q_{tn} and B_q
- Refer to Section Text for details

GEOTECHNICAL LOG
HKW011-PCPT